8-2018

CHARACTERIZING THE MOLECULAR MECHANISMS FOR THE BACTERIAL TRANSFORMATION OF RECALCITRANT ORGANIC MATTER IN COASTAL SALT MARSHES

Lauren Nicole Quigley
University of Tennessee

To the Graduate Council:

I am submitting herewith a dissertation written by Lauren Nicole Quigley entitled "CHARACTERIZING THE MOLECULAR MECHANISMS FOR THE BACTERIAL TRANSFORMATION OF RECALCITRANT ORGANIC MATTER IN COASTAL SALT MARSHES." I have examined the final electronic copy of this dissertation for form and content and recommend that it be accepted in partial fulfillment of the requirements for the degree of Doctor of Philosophy, with a major in Microbiology.

Alison Buchan, Major Professor

We have read this dissertation and recommend its acceptance:

Sarah L. Lebeis, Andrew D. Steen, Erik R. Zinser

Accepted for the Council:
Dixie L. Thompson

Vice Provost and Dean of the Graduate School

(Original signatures are on file with official student records.)

CHARACTERIZING THE MOLECULAR MECHANISMS FOR THE BACTERIAL TRANSFORMATION OF RECALCITRANT ORGANIC MATTER IN COASTAL SALT MARSHES

A Dissertation Presented for the
Doctor of Philosophy
Degree
The University of Tennessee, Knoxville

Lauren Nicole Mach Quigley
August 2018

ACKNOWLEDGEMENTS

I would like to thank my friends and family who have supported me throughout my life and in particular during the past five and a half years of graduate school. I'd especially like to thank my parents Tim and Kim who have supported me both emotionally and financially for the past 28 years. They have been in my corner every step of the way even if they don't totally understand exactly what it is I've been doing for the past five years. I'd also like to thank my sisters Marla and Noelle who have been very supportive and are my biggest cheerleaders. Additionally, I have made some of the most incredible friends in graduate school who have been so helpful every step of the way as they went through the same trials and tribulations of graduate school. They have gone above and beyond to be supportive even driving the 500 miles to South Bend, IN (in December no less) to celebrate my wedding.

I would be remiss if I did not thank my wonderful husband, Kevin, who has gracefully and calmly dealt with me coming home frustrated from long days in the lab (looking at you, RNA extractions and respirometer). His impulse is always to identify the problem and troubleshoot to find a solution as quickly as possible even if it is something he's unfamiliar with. In addition to being a calming influence Kevin has done everything imaginable to help me through graduate school including but not limited to making 95% of our meals, only being slightly repulsed when I would bring plates home to count while watching TV, and formatting the table of contents in this document. Without his love and support I would not be where I am today.

I would also like to thank Drew Steen for making me use R. When I started my rotation project in Alison's lab Drew insisted that all of the data be visualized in R. At the time I was convinced that I was not capable and never would be of programming after struggling immensely in a biostatistics course my senior year at Notre Dame, a large component of which was running analyses in R. Drew worked with me, was very patient, and refused to

accept for one second that I was not capable. Thanks in large part to Drew's efforts every figure in this dissertation was generated in R.

Lastly, I need to thank my advisor Alison Buchan who had been incredibly supportive over the past five years. Alison's positive attitude and encouragement have been instrumental in my success in graduate school. Additionally, Alison has been exceedingly patient with me has I learned what it means to be scientist, and always gave me the benefit of the doubt when lab work was not going to plan. This gave me the space and independence to develop into the best scientist I could be for which I am exceedingly thankful.

ABSTRACT

Terrestrially-derived dissolved organic matter (t-DOM) is one of the largest reservoirs of reduced carbon on the planet with approximately $2.5x10^{14}$ g-C entering the global coastal oceans annually. This carbon pool is largely derived from the products of vascular plant degradation, such as humic and fulvic acids, which are recalcitrant due to their enrichment in aromatic moieties. As t-DOM travels through riverine systems to the coastal oceans it becomes increasingly refractory as riverine microbial communities preferentially oxidize the most bioavailable components. However, most chemical tracers diagnostic of t-DOM (e.g. lignin-derived phenols) are removed before reaching the open oceans, suggesting that this material is transformed in the coastal margins. Microbial transformations are expected to contribute to the disappearance of t-DOM in these systems, but the mediating factors and mechanisms are presently unknown. The work described in this dissertation aims to understand how coastal microbial communities degrade t-DOM. Within, I show that a concept well studied in soil systems, the priming effect (PE), may help explain the disappearance of t-DOM in these systems. PE occurs when the presence of a labile carbon source and/or nutrients stimulates the degradation of a recalcitrant carbon source. I focused my studies on coastal margins of the Southeastern United States. These systems represent a transition zone between riverine systems, carrying recalcitrant t-DOM, and marsh systems, which are sites of new production and contain small yet labile carbon pools. As such, they are ideal study sites in which to investigate whether coastal microbial communities can indeed be primed. A first study employed a mesocosm experiment to demonstrate that PE could be invoked in a natural coastal microbial community. A second study demonstrates that concentration and type of labile carbon influence the magnitude, timing and sign of PE in a species-specific manner. Finally, metatranscriptome-based field studies provide evidence that coastal marsh microbial communities are actively catabolizing aromatics and carbohydrates common to the systems. Collectively, these studies enhance our understanding of the mechanisms through which estuarine communities transform t-DOM and provide insights and future directions for continued study in the field.

TABLE OF CONTENTS

LIST OF TABLES

LIST OF FIGURES

CHAPTER ONE - INTRODUCTION

I. TERRESTRIALLY-DERIVED, DISSOLVED ORGANIC MATTER

Annually, $2.5x10^{14}$ g-C terrestrially-derived, dissolved organic matter (t-DOM) flows from riverine to marine systems (1, 2). Riverine microbial communities preferentially utilize the most labile components of t-DOM, resulting in an increasingly refractory carbon pool with increased residence time in the rivers (3, 4). However, there are vanishingly small traces of t-DOM in the open ocean, thus, this pool of carbon is disappearing in the coastal margins (1, 5). While abiotic processes such as photodegradation and burial account for some of the disappearance (6–8), t-DOM is being biodegraded by the microbial communities in the coastal margins. However, the mechanisms by which the microbial communities transform t-DOM are largely unknown (9). The work detailed in this dissertation focuses on the degradation of t-DOM by estuarine microbial communities. Accordingly, the sections below discuss the relevance of t-DOM to global carbon cycling and the composition and ecological importance of t-DOM to estuarine systems.

t-DOM in global carbon (C) cycling

t-DOM is one of the largest carbon pools on Earth. As t-DOM originates from vascular plant detritus it is enriched in lignin phenols which are among the most well studied and characterized biomarkers of terrestrially-derived C (*10*, *11*). However, these signatures are greatly reduced in marine DOM (*1*, *5*), suggesting that t-DOM is being transformed in the coastal margins. While patterns of delivery, reaction, and burial of t-DOM depend on transport-reaction properties within the source regions (*12*), some overarching trends are present. Dissolved organic matter (DOM) concentrations are more variable in the upper regions of estuaries than the mouth, and DOM composition is effected by river discharge levels and biological activity within the rivers themselves (*13*). Furthermore, the concentration of DOM decreases along a salinity gradient, with aromatic signatures and polyphenols being almost completely removed before this material reaches continental shelfs. These findings indicate that estuaries are hot spots in the removal of t-DOM, yet the mechanisms of the transformations leading to removal remain largely unknown.

The two major routes of t-DOM degradation are bio- and photodegradation. However, the role of photodegradation in t-DOM transformations is largely system-dependent and principally influenced by land-use practices (*14*). Rivers flowing through watersheds characterized by cropland carry DOM that is more photo-resistant, with less than 30% of riverine DOM being photodegraded and bio-available (due to an enrichment in nitrogen) compared to basins covered by forests and grasslands (*14*). Over the past 50 years, the rivers flowing into the coastal margins of the Southeastern United States have catchments which have seen a 50% decrease in agriculture and 65% increase in forest cover (*15*). The disappearance of t-DOM needs to be better characterized in order to be constrained in global carbon budget models (*16*, *17*). The importance of understanding the degradation dynamics and fate of t-DOM is becoming even more vital as average annual temperatures rise as increased temperatures lead to increased remineralization of recalcitrant C (*18*).

Composition of t-DOM

Vascular plant material constitutes a large component of t-DOM (*19*) and is particularly recalcitrant to biodegradation due to a key structural element, lignin, which is characterized by several interlinking aromatic moieties (*20*). As vascular plant detritus decays the t-DOM pool increases in the number of molecular formulae present, with estimates ranging between 1500-2000 unique molecular formulae (*19*, *21*); resulting in a highly heterogenous, recalcitrant carbon pool. Furthermore production and transformation of DOM by phytoplankton and bacteria have been shown to increase the richness and abundance of molecular formulae within DOM (*22*). Long-term incubation studies demonstrate that eventually bacteria will reduce the diversity of molecular formulae present in DOM (122 days according to Mentges et al., 20). However, the length of the incubation studies typically exceeds the residence time of DOM in most major river channels. These data suggest that while bacteria are capable of decreasing the functional diversity within DOM, they cannot do it on ecologically relevant time scales; however, this incubation study was performed in the dark which excludes the possibility of photodegradation.

Photodegradation is another important route of t-DOM decomposition and influences the bioavailability of molecules within the DOM pool. Chemical compounds which absorb UV like aromatic monomers as well as high unsaturated oxygen poor compounds are preferentially removed by photodegradation. In contrast, polyphenolic and polycyclic aromatics and dissolved black carbon are preserved (*23–25*). However, while these traditionally recalcitrant compounds are preserved during photodegradation, light does modify the chemical structure of DOM, increasing its bioavailability. A comprehensive study of the reactivity of DOM from ten major world rivers revealed that all aromatic signatures were removed after a coupled short (10 day) photodegradation and long (1 year) biodegradation incubation (*14*). These data demonstrate that biological action and photodegradation may act cooperatively to transform t-DOM, particularly the plant-derived components.

The polyphenolic and polycyclic aromatic moieties characteristic of lignin contributes greatly to the recalcitrance of t-DOM. As t-DOM flows through riverine systems the native microbial communities preferentially use aliphatic residues, thus enriching t-DOM in aromaticity (*26*). Increased residence time in the river results in an increase of lignin, humic and fulvic acids resulting in increased recalcitrance (*26*). Traditionally, initial biological oxidation of lignin occurs under aerobic conditions and is mediated by Basidiomycetes (white and brown rot fungi) and a few species of bacteria (*27*, *28*). Ligninolytic enzymes play a critical role in delignifying t-DOM but have only been extensively studied in fungi (*29*, *30*). These enzymes fall into two broad categories: lignin-modifying peroxidases and laccases. Laccases are generally considered the more important enzyme in delignification (*31*, *32*). With mounting evidence for the presence of both lignin-modifying peroxidases and laccases in bacterial genomes further work needs to be done to characterize bacterial lignin peroxidases and laccases in order to understand how the entire microbial community functions to remove plant-derived C from t-DOM.

Ecological importance of t-DOM

Historically, t-DOM was thought to be biologically inert, specifically the humic and fulvic acid components, which constitute a large portion of the chemical moieties within t-DOM (*33*, *34*). This idea was bolstered by observations that bacterial production and respiration are carbon limited in the mainstream of the Amazon river, indicating that the majority of the particulate and dissolved organic carbon is of limited bioavailability (*35*). Reports suggest that 11-22% of the humic substance pool is bioavailable to the microbial community (*36–38*), suggesting that while humic and fulvic acids are not biologically inert, they are resistant to biological degradation.

Other factors that may influence the degradation of humic and fulvic acids by microbes include the presence of autochthonous C from phytoplankton primary production as well as photodegradation. Studies using ^{13}C-labeled phytoplankton have shown that microbial communities preferentially use autochthonous phytoplankton biomass over allochthonous t-DOM (*39–41*). A whole lake experiment revealed that although autochthonous C made up only 13% of the DOM pool, bacterial biomass was composed of 35-70% allochthonous C. These results simultaneously show that while bacteria preferentially degrade autochthonous C they are capable of using humic DOM to support growth (*39*). Another freshwater lake-based study demonstrated that bacterial communities use algal-derived DOC at rates ten times greater than terrestrial DOC. However, because the total amount of terrestrial DOC is much higher than the algal DOC there is actually four times more labile C in terrestrial DOC than algal DOC and the lake community processes both pools of C in parallel (*41*). Further, a five hour photo-irradiation of humic acids resulted in a 32% increase in bacterial growth efficiency (*42*). These data demonstrate that interactions between the microbial community, t-DOM, and other sources of C and abiotic factors can, in fact, enhance the ability of the microbial community to use t-DOM as a growth source.

As rivers carrying humic and fulvic acids reach the coastal ocean there is a shift in the microbial community composition (*43*, *44*), which may be responsible for the increased degradation of t-DOM at the land-sea interface. Marine and estuarine bacteria were capable

of degrading 40-60% of humic acids provided to them in a flow-through experiment within 21 days (*45*). This increase in t-DOM use in marine and estuarine bacteria compared to values reported in lakes suggests that the coastal microbial communities are more adept at degrading t-DOM. Additionally, a microbial community from the Chukchi Sea responded rapidly (4-6 days) to the addition of t-DOM from an Arctic river, both in terms of shifts in community composition and bacterial abundance (*46*). The addition of t-DOM shifted the marine community away from oligotrophic taxa and towards copiotrophic taxa. From these experiments, Sipler and colleagues identified indicator taxa for the presence and degradation of t-DOM. One of these taxa was the family Rhodobacteraceae, a well-studied family of marine bacteria characterized by their numerical dominance in coastal systems and generalist metabolic strategy (*47*). These results suggest that marine and estuarine bacteria may be more adept at degrading t-DOM than freshwater microbial communities, particularly generalist lineages within these communities. However, in order to understand how the microbial community process t-DOM it is necessary to link metabolic functions to active lineages.

II. PRIMING EFFECT

The priming effect (PE) occurs when the addition of labile substrates and/or nutrients influences the degradation of a more recalcitrant C source. Historically priming has been studied in soil systems with inconsistent results, generally believed to be due to the differential metabolic potential of microbial communities inhabiting different types of soil (*48–50*). However, some factors have been determined to be critical in eliciting a PE in soils: concentration and chemical composition of the labile substrate (*51*, *52*). Recently, PE has received increased interest for its applicability to aquatic systems. This dissertation aims to examine if PE is a potential mechanism for the biodegradation of t-DOM; consequently, the following sections discuss the mechanism of PE, the factors influencing PE, and the relevance of PE to aquatic systems.

Mechanisms of PE

The vast majority of priming studies seek to quantify the magnitude of PE with measurements of respiration, and do not actually assess the underlying microbial processes, which might lead to a mechanistic understanding of PE. Priming is measured by comparing the degradation of a recalcitrant C source in an unamended control to that of a treatment with added labile C and/or nutrients (*52*). While there are many methods of measuring PE, the most common methodology in soil studies apply a ^{13}C-labeled compound to the soil and monitor the respiration of labeled and unlabeled CO_2 (*51*). The unlabeled CO_2 is generated from remineralization of recalcitrant soil organic matter (real PE) or the turnover of microbial biomass (apparent PE). Disentangling real and apparent PE in soils is challenging as it is impossible to uniformly label the soil organic matter without also labeling microbial biomass (*50*). It is assumed that most of the unlabeled CO_2 respiration within the first couple of days is apparent PE and that the magnitude and duration of apparent PE increases with substrate availability (*51*). Apparent PE is then followed by real PE which can last months (*53*). Although real and apparent PE are difficult to differentiate in soils, overcoming this hurdle is less of a challenge in aquatic ecosystems where it is possible to both label recalcitrant C and separate the microbial community from the background recalcitrant C.

Mechanisms for the shift from apparent to real PE are unknown but, it has been postulated that the transition from labile C use to recalcitrant C is a result of a change in the microbial community from r-strategists to k-strategists (*54*). In soils, bacteria are assumed to be r-strategists because of their ability to quickly and efficiently metabolize labile, low molecular weight C, while fungi are thought to be k-strategists because of their roles in the degradation of recalcitrant components of soil organic matter, such as lignin and cellulose (*55–58*). However, studies monitoring the incorporation of ^{13}C into phospholipid fatty acids (PLFAs) in order to determine the roles of bacteria and fungi in soil priming have produced inconsistent results. Nottingham and colleagues found that when soil organic matter was primed with sucrose and maize leaf litter that most soil C was incorporated into the lipids of Gram negative bacteria (*59*). However, another study reported that fungi

preferentially incorporated soil C into their biomass when provided labeled cellulose (*60*). These results suggest that either (i) the assumptions about the roles of bacteria and fungi as r- and k-strategists respectively are incorrect; (ii) the mechanism for the shift from apparent to real PE is not as clear cut as the transition from the metabolic capabilities of one domain to another; or (iii) that a combination of both these factors is at play, giving rise to discrepancies between studies. While microbial community composition likely plays a role in priming, it is likely not as simple as bacteria degrade labile C and fungi degrade recalcitrant C. Instead, it is possible, and even likely, that organisms which degrade the labile C are also responsible for the remineralization of recalcitrant C.

Currently, there are three non-exclusive hypotheses for the mechanism of priming: co-metabolism, net-mutualism, and single population. The co-metabolism hypothesis suggests that labile C decomposers produce enzymes which in addition to acting on labile C components also degrade recalcitrant C. The resulting intermediate products are then available to a second community which utilizes these compounds, deriving the necessary energy to degrade the more recalcitrant C pool (*61*). Net mutualism is similar to the co-metabolism. However, in this mechanism the labile C degraders derive a benefit from the degradation of recalcitrant C by a second community due to the release of labile carbon and nutrients to both communities (*62*, *63*). The single population hypothesis posits that a single community produces enzymes to degrade both classes of C and that the degradation labile C provides energy for the subsequent decomposition of recalcitrant C (*64*, *65*). It is likely that all three hypotheses could induce priming and may occur under different circumstances or in different environments; however, further studies in which extracellular enzyme activities and community composition are assessed alongside the quantification of priming are needed to test these hypotheses. As of now, these proposed mechanisms provide a useful framework for thinking about the community interactions that may lead to priming.

Factors influencing PE

Although mechanisms for PE are largely speculative at this point, some factors have been identified as important in eliciting a PE: the concentration and chemical composition of the labile addition. A review by Blagodatskaya and Kuzyakov highlighted the importance of the concentration of added substrate to eliciting a priming effect. A comparison of 10 studies revealed that in order for positive priming to occur, the labile addition must be less than 15% of the microbial biomass C (*48*). Labile C added above this threshold resulted in a decrease in recalcitrant C biodegradation, which is thought to be due to selection of community members more adept at labile C use than recalcitrant. In addition to the amount of labile C added, the chemical composition of the labile C influences priming as soils provided with labile C of differing chemical compositions demonstrate preferential responses (*66*–*68*). However, applying the same labile treatment (catechol, in this example) to two different soil horizons resulted in positive priming in one and negative priming in the other (*67*). This differential response to the same labile C in different soils and preferential response to different sources of labile C in the same soil suggest that the ability of a labile compound to induce priming is, in part, dependent on the microbial community in the soil.

It has been proposed that inconsistencies between positive priming in one system and no priming in another is due to the underlying metabolic potential of the microbial community (*69*, *70*). This possibility seems likely in light of a recent study by Flynn et al. in which six distinct soil communities from different environments were incubated in the presence of 31 carbon sources falling into five broad structural categories: phenolic, carbohydrate, polymer, carboxylic acid, and amino acid (*71*). While amendment shifted the community composition (as assessed by 16S rRNA gene amplicons), it was still strongly affected by inoculum source. Additionally, communities amended with carbohydrates differed significantly compared to those amended with phenolic compounds, suggesting that chemical structure of amended carbon may play a role in selecting for specific community members. Furthermore, a recent study using ^{13}C-glucose and ^{18}O-water found that after repeated pulses of glucose weekly for six weeks, 163 of the 267 taxa present in a natural

community increased use of soil organic carbon. These taxa were not phylogenetically constrained, suggesting that the initial community demonstrates phenotypic plasticity to increase degradation of recalcitrant C (*72*). Taken together, these studies provide multiple lines of evidence that priming conditions are dependent on the underlying metabolic capabilities of the community. However, specific metabolic capabilities within the community still need to be linked to organic C processing in order to better understand the underlying mechanisms of priming.

Aquatic PE

While PE has been studied in soil systems for the past 100 years, it has only recently been applied as a framework for understanding interactive degradation effects between classes of organic matter (OM) with differing bioavailabilities. PE have been overlooked in aquatic systems due to the prevailing paradigm that OM degradation occurs following a multi-G model, in which classes of organic matter degrade according to their unique first-order degradation rate constant (*73*). However, recent evidence suggests that PE may be applicable in aquatic ecosystems.

The number of studies looking at priming in aquatic systems has dramatically increased in the past decade; however, a consensus has yet to be reached on whether priming occurs in aquatic systems and, if it does, what factors may govern it (*74*). A leading cause of the confounding results is the apparent transience of priming in aquatic ecosystems. Priming has been studied in aquatic ecosystems on vastly different time scales, ranging from incubation studies lasting one week with measurements taken every day to six month incubations with measurements taken at only at the onset and termination of the incubation (*75*, *76*). Generally speaking, those studies that measure priming on a daily basis report a positive PE; typically the priming effect appears within the first day of the incubation (*75*, *77*). Studies which measure aquatic priming on weekly or monthly scales often report no PE, likely because their sampling interval was too coarse to observe priming (*76*). However, the authors of these latter studies were using soil priming as a framework in which priming within the first week is considered apparent priming, which is turnover of

microbial biomass, and real priming does not occur for weeks or months following the start of the incubation (*51*). The distinction between real and apparent PE is easier to control for in aquatic systems in which the microbial community can be removed from the recalcitrant C via filtration and then incubated in the presence of labile and recalcitrant C alone. Thus, the framework of real and apparent priming is less applicable to aquatic systems. This contrast between the timing of priming in soils (months) versus aquatic (days) systems is probably due in large part to how dynamic and well-mixed aquatic systems are compared to soils which are largely static and receive pulses of nutrients (*78*). Given the fundamental difference between the timing of priming between these two systems, it is likely that other factors that drive priming in soils may be different in aquatic systems, but more studies on shorter timescales are needed to fully characterize these potential differences.

III. COASTAL SALT MARSHES OF THE SOUTHEASTERN UNITED STATES

The coastline of the Southeastern United States is characterized by a 4-6 mile band of salt marshes between the mainland and barrier islands that fringe the coastline (Figure 1.1). These marshes are important nurseries for juvenile species of fish that are significant global food commodities (*79*), and have some of the highest rates of net primary productivity (0.2-2.25 kg C m^{-2} yr^{-1}) (*80*). The high productivity of these ecosystems serves as an important sink of atmospheric CO_2. However, with very few metazoan grazers, these are principally detritus-based ecosystems (*81*). Additionally, the rivers flowing through these marshes are blackwater carrying high loads (400-3000 μM) of dissolved organic matter (DOM), up to 75% of which is t-DOM, enriched in aromatic moieties (*4*, *82*, *83*). The research detailed in this dissertation focuses on how microbial communities from these salt marshes degrade t-DOM. To this end, this section describes the geochemical characteristics and microbial ecology of these marshes, including a description of the Roseobacter clade, a group heterotrophic bacteria within the class α-proteobacteria often responsible for the degradation of recalcitrant C sources in these environments (*84–87*).

Biogeochemical characteristics

The rivers flowing through the salt marshes of the Southeastern United States are fed by blackwater rivers, which are characterized by long residence time in channel during which tannins leach into the water, staining it brown (*33*). The rivers flowing into these systems carry high loads of DOM, 75% of which is plant-derived or t-DOM (*83*). The dominance of t-DOM in these riverine systems shapes the chemical composition of the rivers, resulting in low pH and ionic strength (*33*). Spectroscopy and elemental composition analyses suggests that the DOM is largely composed of fulvic acids, which are the products of vascular plant degradation (*26*, *33*). As the DOM in these rivers flows downstream to the ocean, the O:C increases and the aliphatic residues which are considered to be the most bioavailable decrease, indicating that the DOM is becoming more recalcitrant with increased residence time (*26*). When the DOM reaches the ocean there is a shift from aromatic, terrestrial DOM to more aliphatic, marine DOM (*88*), suggesting that t-DOM is disappearing in the coastal margins.

These salt marshes of the Southeastern United States are dominated by monoculture stands of the cordgrass *Spartina alterniflora,* which has a net primary productivity of 1.35-3.7 kg dry mass m^{-2} yr^{-1}, and consequently represents an important source of labile C for heterotrophs in the marsh (*89*, *90*). Lignocellulose and lignin comprise approximately 70% and 10% of *S. alterniflora* biomass by weight respectively (*91*). Soluble degradation products of *S. alterniflora* decay constitute up to 44% of the C in the bulk DOC pool in these systems, roughly half of which is lignin (*92*). Usually in coastal wetlands, the sequestration of CO_2 into the biomass of primary producers outweighs the outgassing that results from the metabolic activities of the heterotrophs. Such systems are designated as autotrophic ecosystems (*93*). However, the wetlands along the coast of the Southeastern United States are net heterotrophic as a result of the microbial respiration exceeding the remarkably high rates of net primary productivity in these systems (*94*, *95*). The net heterotrophy of these systems suggests that the microbial community is actively decomposing the immense amount of plant-derived C being produced in and flowing through these systems. Yet, mechanisms for the degradation of t-DOM remain unclear.

Although *S. alterniflora* dominated marshes have high rates of net primary productivity, little of the detritus in these systems is derived from *S. alterniflora* biomass (*96*). This finding indicates (i) a high bioavailability for *S. alterniflora* biomass and (ii) that much of the detritus in these systems is riverine derived t-DOM. These salt marshes are dynamic ecosystems where marine and riverine systems mix, and the recalcitrant t-DOM being carried by the rivers combines with the labile sources of C derived from fresh *S. alterniflora* biomass and phytoplankton blooms. Thus, these ecosystems represent an ideal model system in which to study if PE is indeed a mechanism for the biodegradation of t-DOM.

Microbial ecology of salt marshes

In addition to their net heterotrophy despite high rates of primary productivity, the coastal salt marshes of the Southeastern United States are characterized by having few metazoan grazers (*97*). Without metazoan grazers the microbial community is responsible for the biodegradation of *S. alterniflora* biomass and other sources of detritus in these systems, making them excellent ecosystems to study the biochemistry and ecology of microbial decomposers (*81*). Historically fungi have been thought to be the predominant decomposers of recalcitrant, plant-derived C (*31*, *98–100*); however, studies in these systems suggest that bacteria may be even more important than fungi in the biodegradation of recalcitrant C (*101–103*). Fallon and Pfaender provided ^{14}C-labeled *S. alterniflora* to communities composed of bacteria, fungi, and bacteria and fungi and found that while fungi were the most efficient at incorporating the ^{14}C into biomass, the greatest remineralization of the *S. alterniflora* biomass occurred in the bacteria alone and mixed bacterial and fungal communities (*101*). While a large amount of research has been done to understand how fungi degrade lignin, much less is known about how bacteria perform this process.

Currently the ability to degrade lignin has been identified in three classes of Bacteria: α-Proteobacteria, γ-Proteobacteria, and Actinomycetes (*100*, *104*). These classes are numerically abundant and active in the coastal salt marshes of the Southeastern United States (*105*, *106*). Furthermore, multiple strains of Bacteria belonging to the classes α-

Proteobacteria and γ-Proteobacteria have been isolated from the high molecular weight fraction of paper mill effluent enriched with lignin. Several of these strains have been demonstrated to be ligninolytic (*107*, *108*). Microorganisms use multiple classes of enzymes to degrade lignin, including, but not limited to, laccases, lignin peroxidases, and dye-decolorizing peroxidases (*109*). Phylogenetic analyses have revealed that some Bacteria and Archaea possess homologs for these enzymes. Of the ligninolytic enzyme classes, laccases have the broadest phylogenetic distribution, being found in four phyla of Archaea and five phyla of Bacteria. Peroxidases appear limited to Actinomycetes and γ-Proteobacteria (*110*). The presence of genes encoding lignin-degrading enzymes indicates that this process may be more important in Bacteria and Archaea than previously thought, particularly in salt marshes where bacteria remineralize more *S. alterniflora* biomass than fungi.

Traditionally, Archaea have been overlooked when studying the degradation of plant-derived C, potentially due to their assumed roles as extremophiles. As Archaea continue to be found in non-extreme environments, their roles in fundamental biogeochemical cycling continue to expand (*111*). Members of the class Haloarchaea within the phylum Euryarcheota are able to catabolize aromatic monomers (*112*, *113*). Recent evidence suggests that Haloarchaea became adapted to oxygenated, saline environments by acquiring genetic information derived from bacterial genomes, largely involved in metabolic function (*114*). Furthermore, a recent study by Yu and colleagues suggests that the Bathy-8 subgroup of Bathyarcheota are capable of growing on lignin when it was applied exogenously to estuarine sediment (*115*). Furthermore, Bathyarcheota and Euryarcheota are among the most abundant phyla of Archaea present in estuarine environments (*116*). The ability of both these phyla to degrade plant-derived matter suggests that Archaea potentially contribute to the degradation of t-DOM in coastal margins.

The Roseobacter clade

Members of the Roseobacter clade are among the most numerically abundant and active members of the salt marsh microbial community (*84*, *117*, *118*). Roseobacters make up to 30% of the bacterial community in the salt marshes of the Southeastern United States, based on 16S rRNA gene analysis, and have been shown to actively use plant-derived C as growth sources via bromodeoxyuridine (BrdU) incorporation and metatranscriptomics (*106*, *119*, *120*). In addition to being dominant members of the salt marsh community, Roseobacters are ubiquitous in marine environments and are cultured representatives are typically characterized by a large genome size and metabolic versatility (*47*, *121*). Representatives of the Roseobacter clade are readily cultivable and exhibit a wide range of ecologically relevant physiologies positioning group members as mediators of key reactions in various biogeochemical cycles. For example, Roseobacters are adept at sulfur oxidation and transformations of the algal and plant osmolyte dimethylsulfoniopropionate (DMSP) (*122*, *123*). They also produce a wide variety of secondary metabolites, and are consequently found in close association with eukaryotic phytoplankton (*124*, *125*). Additionally, Roseobacters are prodigious surface colonizers and degraders of plant-derived C in marine environments, which is generally found in particulate form. The wide variety of ecologically relevant processes that Roseobacters participate in suggests that they are model marine heterotrophs, and as such they are used as model marine organisms for the degradation of t-DOM in this dissertation.

Degradation of plant-derived compounds is an important ecological process in the salt marshes of Southeastern United States, an ecosystem where Roseobacters are numerically dominant. Traditionally, fungi are thought to be the primary decomposers of plant-derived C; however, bacteria and fungi co-occur on decaying plant matter in salt marshes (*87*, *126*, *127*). An analysis of these communities revealed that while there was temporal variation in the community structure, the community composition was stable with four groups of fungi and seven groups of bacteria, one of which was the Roseobacters (*87*). A study by Buchan and colleagues found that 52% of *pcaH* (a diagnostic marker for aromatic ring cleavage) clones amplified from bacterial communities associated with decaying *Spartina*

alterniflora belonged to Roseobacters (*128*). This finding suggests that Roseobacters are the predominant bacterial degraders of plant-derived in these systems, and work detailed in this dissertation further bolsters this idea (Chapter 4).

Roseobacters are particularly adept at degrading aromatic compounds presumably via the deployment of the wealth of aromatic C catabolism pathways present in their genomes. Genes from the β-ketoadipate, gentisate, benzoate, phenylacetic acid, homoprotocatechuate, and homogentisate pathways have been found in the genomes of cultivated members of the Roseobacter clade. Many members possess multiple ring-cleaving pathways (*121*). Furthermore, Roseobacters are capable of simultaneously catabolizing aromatic C compounds, deriving a growth benefit growing on a mixture of aromatic compounds that proceed through different pathways (protocatechuate and benzoyl-CoA pathways) compared to either alone (*129*). This finding is contrary to the paradigm of substrate hierarchy reported in soil systems, where microorganisms will preferentially use aromatic substrates in a hierarchal manner (*130–133*). Furthermore, laccases, a broad class of extracellular enzymes with a wide range of aromatic substrates, have been well studied in fungi, specifically for their role in the degradation of lignin (*31*). Mounting evidence suggests that laccase-like genes are well distributed in many phyla of bacteria, and are particularly enriched in proteobacterial genomes (*134–137*). Recent metagenomic studies have found evidence for laccase-like genes in Roseobacter genomes (*137*, *138*). Roseobacters were selected as model marine heterotrophs for laboratory studies to gain a more mechanistic understanding of how the heterotrophic community of the Southeastern United States degrades t-DOM.

IV. OBJECTIVES

The work described in this dissertation aims to increase our understanding of microbial degradation of t-DOM. The first two research chapters focus on evaluating priming effects and their applicability to the remineralization of recalcitrant organic matter in estuarine environments using manipulative laboratory experiments with a natural community isolated from a coastal salt marsh (Chapter 2) and isolates from the Roseobacter clade

(Chapter 3). These studies provide insight into whether priming effects are relevant in estuarine environments and the factors that influence them. The remaining two research chapters aim to leverage ‘omics techniques to study the microbial communities of the coastal salt marshes lining the Southeastern United States. Chapter 4 seeks to understand how natural microbial communities interact with t-DOM in marshes through paired metagenomics and metatranscriptomics and will expand our knowledge of how microbial communities degrade t-DOM *in situ*. Chapter 5 examines how increased sample processing time influences the utility of metatranscriptomics.

V. REFERENCES

1. J. I. Hedges, R. G. Keil, R. Benner, in *Organic Geochemistry* (1997), vol. 27, pp. 195–212.
2. X. Cao *et al.*, Evidence for major input of riverine organic matter into the ocean. *Org. Geochem.* **116**, 62–76 (2018).
3. R. L. Vannote, G. W. Minshall, K. W. Cummins, J. R. Sedell, C. E. Cushing, The River Continuum Concept. *Can. J. Fish. Aquat. Sci.* **37**, 130–137 (1980).
4. A. Mannino, H. R. Harvey, Terrigenous dissolved organic matter along an estuarine gradient and its flux to the coastal ocean. *Org. Geochem.* **31**, 1611–1625 (2000).
5. C. L. Osburn *et al.*, Optical Proxies for Terrestrial Dissolved Organic Matter in Estuaries and Coastal Waters. *Front. Mar. Sci.* **2** (2016), doi:10.3389/fmars.2015.00127.
6. D. J. Burdige, Burial of terrestrial organic matter in marine sediments: A re-assessment. *Global Biogeochem. Cycles*. **19** (2005), doi:10.1029/2004GB002368.
7. T. G. Jones, C. D. Evans, D. L. Jones, P. W. Hill, C. Freeman, Transformations in DOC along a source to sea continuum; impacts of photo-degradation, biological processes and mixing. *Aquat. Sci.* **78** (2016), doi:10.1007/s00027-015-0461-0.
8. M. Seidel *et al.*, Molecular-level changes of dissolved organic matter along the Amazon River-to-ocean continuum. *Mar. Chem.* **177**, 218–231 (2015).
9. P. M. Medeiros *et al.*, Microbially-Mediated Transformations of Estuarine Dissolved Organic Matter. *Front. Mar. Sci.* **4** (2017), doi:10.3389/fmars.2017.00069.
10. F. G. Prahl, J. R. Ertel, M. A. Goni, M. A. Sparrow, B. Eversmeyer, Terrestrial organic carbon contributions to sediments on the Washington margin. *Geochim. Cosmochim. Acta* (1994), doi:10.1016/0016-7037(94)90177-5.
11. K. J. Meyers-Schulte, J. I. Hedges, Molecular evidence for a terrestrial component of organic matter dissolved in ocean water. *Nature* (1986), doi:10.1038/321061a0.
12. N. E. Blair, R. C. Aller, The Fate of Terrestrial Organic Carbon in the Marine Environment. *Ann. Rev. Mar. Sci.* (2012), doi:10.1146/annurev-marine-120709-

142717.

13. H. Osterholz, D. L. Kirchman, J. Niggemann, T. Dittmar, Environmental Drivers of Dissolved Organic Matter Molecular Composition in the Delaware Estuary. *Front. Earth Sci.* (2016), doi:10.3389/feart.2016.00095.
14. T. Riedel *et al.*, Molecular Signatures of Biogeochemical Transformations in Dissolved Organic Matter from Ten World Rivers. *Front. Earth Sci.* (2016), doi:10.3389/feart.2016.00085.
15. E. P. Odum, Input management of production systems. *Science (80-.).* (1989), doi:10.1126/science.243.4888.177.
16. J. J. Cole *et al.*, Plumbing the global carbon cycle: Integrating inland waters into the terrestrial carbon budget. *Ecosystems* (2007), doi:10.1007/s10021-006-9013-8.
17. P. Massicotte, E. Asmala, C. Stedmon, S. Markager, Global distribution of dissolved organic matter along the aquatic continuum: Across rivers, lakes and oceans. *Sci. Total Environ.* (2017), doi:10.1016/j.scitotenv.2017.07.076.
18. C. Lønborg, X. A. Álvarez–Salgado, R. T. Letscher, D. A. Hansell, Large Stimulation of Recalcitrant Dissolved Organic Carbon Degradation by Increasing Ocean Temperatures. *Front. Mar. Sci.* (2018), doi:10.3389/fmars.2017.00436.
19. B. P. Koch, M. Witt, R. Engbrodt, T. Dittmar, G. Kattner, Molecular formulae of marine and terrigenous dissolved organic matter detected by electrospray ionization Fourier transform ion cyclotron resonance mass spectrometry. *Geochim. Cosmochim. Acta* (2005), doi:10.1016/j.gca.2005.02.027.
20. A. T. Austin, C. L. Ballare, Dual role of lignin in plant litter decomposition in terrestrial ecosystems. *Proc. Natl. Acad. Sci. U. S. A.* (2010), doi:10.1073/pnas.0909396107.
21. A. Mostovaya, J. A. Hawkes, B. Koehler, T. Dittmar, L. J. Tranvik, Emergence of the Reactivity Continuum of Organic Matter from Kinetics of a Multitude of Individual Molecular Constituents. *Environ. Sci. Technol.* (2017), doi:10.1021/acs.est.7b02876.
22. A. Mentges, C. Feenders, M. Seibt, B. Blasius, T. Dittmar, Functional Molecular Diversity of Marine Dissolved Organic Matter Is Reduced during Degradation.

Front. Mar. Sci. (2017), doi:10.3389/fmars.2017.00194.

23. M. Gonsior *et al.*, Photochemically Induced Changes in Dissolved Organic Matter Identified by Ultrahigh Resolution Fourier Transform Ion Cyclotron Resonance Mass Spectrometry. *Environ. Sci. Technol.* (2009), doi:10.1021/es8022804.
24. A. Stubbins *et al.*, Illuminated darkness: Molecular signatures of Congo River dissolved organic matter and its photochemical alteration as revealed by ultrahigh precision mass spectrometry. *Limnol. Oceanogr.* (2010), doi:10.4319/lo.2010.55.4.1467.
25. M. Seidel *et al.*, Molecular-level changes of dissolved organic matter along the Amazon River-to-ocean continuum. *Mar. Chem.* **177** (2015), doi:10.1016/j.marchem.2015.06.019.
26. L. Sun, E. M. Perdue, J. L. Meyer, J. Weis, Use of elemental composition to predict bioavailability of dissolved organic matter in a Georgia river. *Limnol. Oceanogr.* **42**, 714–721 (1997).
27. C. Raghukumar, Marine fungal biotechnology: an ecological perspective. *Fungal Divers.* (2008).
28. M. Thevenot, M. F. Dignac, C. Rumpel, Fate of lignins in soils: A review. *Soil Biol. Biochem.* (2010), , doi:10.1016/j.soilbio.2010.03.017.
29. M. Dashtban, H. Schraft, T. A. Syed, W. Qin, Fungal biodegradation and enzymatic modification of lignin. *Int. J. Biochem. Mol. Biol.* (2010).
30. S. M. Hyde, P. M. Wood, A mechanism for production of hydroxyl radicals by the brown-rot fungus Coniophora puteana : Fe(III) reduction by cellobiose dehydrogenase and Fe(II) oxidation at a distance from the hyphae. *Microbiology* (1997), doi:10.1099/00221287-143-1-259.
31. G. Janusz *et al.*, Lignin degradation: Microorganisms, enzymes involved, genomes analysis and evolution. *FEMS Microbiol. Rev.* **41** (2017), pp. 941–962.
32. O. V. Morozova, G. P. Shumakovich, M. A. Gorbacheva, S. V. Shleev, A. I. Yaropolov, “Blue” laccases. *Biochem.* (2007), doi:10.1134/S0006297907100112.
33. K. C. Beck, J. H. Reuter, E. M. Perdue, Organic and inorganic geochemistry of some coastal plain rivers of the southeastern United States. *Geochim. Cosmochim. Acta*.

38, 341–364 (1974).

34. D. O. Hessen, The relation between bacterial carbon and dissolved humic compounds in oligotrophic lakes. *FEMS Microbiol. Lett.* (1985), doi:10.1016/0378-1097(85)90406-9.
35. R. Benner, S. Opsahl, G. Chin-Leo, J. E. Richey, B. R. Forsberg, Bacterial carbon metabolism in the Amazon River system. *Limnol. Oceanogr.* (1995), doi:10.4319/lo.1995.40.7.1262.
36. J. L. Meyer, R. T. Edwards, R. Risley, Bacterial growth on dissolved organic carbon from a blackwater river. *Microb. Ecol.* (1987), doi:10.1007/BF02014960.
37. M. A. Moran, R. E. Hodson, Support of bacterioplankton production by dissolved humic substances from three marine environments. *Mar. Ecol. Prog. Ser.* (1994), doi:10.3354/meps110241.
38. M. A. Moran, R. E. Hodson, Bacterial production on humic and nonhumic components of dissolved organic carbon. *Limnol. Oceanogr.* (1990), doi:10.4319/lo.1990.35.8.1744.
39. E. S. Kritzberg, J. J. Cole, M. L. Pace, W. Granéli, D. L. Bade, Autochthonous versus allochthonous carbon sources of bacteria: Results from whole-lake13C addition experiments. *Limnol. Oceanogr.* (2004), doi:10.4319/lo.2004.49.2.0588.
40. F. Guillemette, S. L. McCallister, P. A. del Giorgio, Selective consumption and metabolic allocation of terrestrial and algal carbon determine allochthony in lakes. *ISME J.* (2015), doi:10.1038/ismej.2015.215.
41. F. Guillemette, S. L. McCallister, P. A. Del Giorgio, Differentiating the degradation dynamics of algal and terrestrial carbon within complex natural dissolved organic carbon in temperate lakes. *J. Geophys. Res. Biogeosciences* (2013), doi:10.1002/jgrg.20077.
42. A. M. Anesio *et al.*, Effect of Humic Substance Photodegradation on Bacterial Growth and Respiration in Lake Water Effect of Humic Substance Photodegradation on Bacterial Growth and Respiration in Lake Water. *Appl. Environ. Microbiol.* (2005), doi:10.1128/AEM.71.10.6267.
43. C. S. Fortunato, B. C. Crump, Microbial gene abundance and expression patterns

across a river to ocean salinity gradient. *PLoS One* (2015), doi:10.1371/journal.pone.0140578.

44. B. J. Campbell, D. L. Kirchman, Bacterial diversity, community structure and potential growth rates along an estuarine salinity gradient. *ISME J.* (2013), doi:10.1038/ismej.2012.93.
45. D. Rocker *et al.*, Differential decomposition of humic acids by marine and estuarine bacterial communities at varying salinities. *Biogeochemistry* (2012), doi:10.1007/s10533-011-9653-4.
46. R. E. Sipler *et al.*, Microbial Community Response to Terrestrially Derived Dissolved Organic Matter in the Coastal Arctic. *Front. Microbiol.* **8**, 1018 (2017).
47. A. Buchan, J. M. González, M. A. Moran, Overview of the marine Roseobacter lineage. *Appl. Environ. Microbiol.* **71** (2005), pp. 5665–5677.
48. E. Blagodatskaya, Y. Kuzyakov, Mechanisms of real and apparent priming effects and their dependence on soil microbial biomass and community structure: Critical review. *Biol. Fertil. Soils*. **45** (2008), pp. 115–131.
49. E. Blagodatskaya *et al.*, Microbial interactions affect sources of priming induced by cellulose. *Soil Biol. Biochem.* **74**, 39–49 (2014).
50. Y. Kuzyakov, Priming effects: Interactions between living and dead organic matter. *Soil Biol. Biochem.* **42**, 1363–1371 (2010).
51. S. Blagodatsky, E. Blagodatskaya, T. Yuyukina, Y. Kuzyakov, Model of apparent and real priming effects: Linking microbial activity with soil organic matter decomposition. *Soil Biol. Biochem.* **42**, 1275–1283 (2010).
52. Y. Kuzyakov, J. K. Friedel, K. Stahr, Review of mechanisms and quantification of priming effects. *Soil Biol. Biochem.* **32** (2000), pp. 1485–1498.
53. F. A. Dijkstra, W. Cheng, Interactions between soil and tree roots accelerate long-term soil carbon decomposition. *Ecol. Lett.* (2007), doi:10.1111/j.1461-0248.2007.01095.x.
54. S. Fontaine, A. Mariotti, L. Abbadie, The priming effect of organic matter: A question of microbial competition? *Soil Biol. Biochem.* (2003), doi:10.1016/S0038-0717(03)00123-8.

55. M. J. Swift, O. W. Heal, J. M. Anderson, Decomposition in terrestrial ecosystems. *Rev. Lit. Arts Am.* (1979), , doi:10.1007/s00114-006-0159-1.

56. W. De Boer, L. B. Folman, R. C. Summerbell, L. Boddy, Living in a fungal world: Impact of fungi on soil bacterial niche development. *FEMS Microbiol. Rev.* (2005), , doi:10.1016/j.femsre.2004.11.005.

57. T. M. Henriksen, T. A. Breland, Nitrogen availability effects on carbon mineralization, fungal and bacterial growth, and enzyme activities during decomposition of wheat straw in soil. *Soil Biol. Biochem.* (1999), doi:10.1016/S0038-0717(99)00030-9.

58. C. Poll, S. Marhan, J. Ingwersen, E. Kandeler, Dynamics of litter carbon turnover and microbial abundance in a rye detritusphere. *Soil Biol. Biochem.* (2008), doi:10.1016/j.soilbio.2007.04.002.

59. A. T. Nottingham, H. Griffiths, P. M. Chamberlain, A. W. Stott, E. V. J. Tanner, Soil priming by sugar and leaf-litter substrates: A link to microbial groups. *Appl. Soil Ecol.* (2009), doi:10.1016/j.apsoil.2009.03.003.

60. S. Fontaine *et al.*, Fungi mediate long term sequestration of carbon and nitrogen in soil through their priming effect. *Soil Biol. Biochem.* (2011), doi:10.1016/j.soilbio.2010.09.017.

61. R. S. Horvath, Microbial co-metabolism and the degradation of organic compounds in nature. *Bacteriol. Rev.* **36**, 146–155 (1972).

62. Y. Kuzyakov, Review: Factors affecting rhizosphere priming effects. *J. Plant Nutr. Soil Sci. Fur Pflanzenernahrung Und Bodenkd.* (2002), doi:10.1002/1522-2624(200208)165:4<382::AID-JPLN382>3.0.CO;2-#.

63. S. Fontaine, S. Barot, Size and functional diversity of microbe populations control plant persistence and long-term soil carbon accumulation. *Ecol. Lett.* (2005), doi:10.1111/j.1461-0248.2005.00813.x.

64. C. Neill, J. Gignoux, Soil organic matter decomposition driven by microbial growth: A simple model for a complex network of interactions. *Soil Biol. Biochem.* (2006), doi:10.1016/j.soilbio.2005.07.007.

65. X. Raynaud, J. C. Lata, P. W. Leadley, Soil microbial loop and nutrient uptake by

plants: A test using a coupled C:N model of plant-microbial interactions. *Plant Soil* (2006), doi:10.1007/s11104-006-9003-9.

66. R. Chen *et al.*, Soil C and N availability determine the priming effect: Microbial N mining and stoichiometric decomposition theories. *Glob. Chang. Biol.* (2014), doi:10.1111/gcb.12475.
67. U. Hamer, B. Marschner, Priming effects in different soil types induced by fructose, alanine, oxalic acid and catechol additions. *Soil Biol. Biochem.* (2005), doi:10.1016/j.soilbio.2004.07.037.
68. M. Shahbaz *et al.*, Microbial decomposition of soil organic matter is mediated by quality and quantity of crop residues: mechanisms and thresholds. *Biol. Fertil. Soils* (2017), doi:10.1007/s00374-016-1174-9.
69. C. Mondini, M. L. Cayuela, M. A. Sanchez-Monedero, A. Roig, P. C. Brookes, Soil microbial biomass activation by trace amounts of readily available substrate. *Biol. Fertil. Soils* (2006), doi:10.1007/s00374-005-0049-2.
70. B. Chaves *et al.*, Influence of DCD and DMPP on soil N dynamics after incorporation of vegetable crop residues. *Biol. Fertil. Soils* (2006), doi:10.1007/s00374-005-0061-6.
71. T. M. Flynn *et al.*, Parallelized, Aerobic, single carbon-source enrichments from different natural environments contain divergent microbial communities. *Front. Microbiol.* (2017), doi:10.3389/fmicb.2017.02321.
72. E. M. Morrissey *et al.*, Bacterial carbon use plasticity, phylogenetic diversity and the priming of soil organic matter. *ISME J.* (2017), doi:10.1038/ismej.2017.43.
73. J. T. Westrich, R. A. Berner, The role of sedimentary organic matter in bacterial sulfate reduction: The G model tested. *Limnol. Oceanogr.* (1984), doi:10.4319/lo.1984.29.2.0236.
74. M. M. Bengtsson, K. Attermeyer, N. Catalán, Interactive effects on organic matter processing from soils to the ocean: are priming effects relevant in aquatic ecosystems? *Hydrobiologia* (2018), doi:10.1007/s10750-018-3672-2.
75. T. S. Bianchi *et al.*, Positive priming of terrestrially derived dissolved organic matter in a freshwater microcosm system. *Geophys. Res. Lett.* (2015),

doi:10.1002/2015GL064765.

76. N. Catalán, A. M. Kellerman, H. Peter, F. Carmona, L. J. Tranvik, Absence of a priming effect on dissolved organic carbon degradation in lake water. *Limnol. Oceanogr.* **60**, 159–168 (2015).
77. A. D. Steen, L. N. Quigley, A. Buchan, Evidence for the Priming Effect in a Planktonic Estuarine Microbial Community Andrew. *Front. Mar. Sci.* (2016), doi:10.3389/fmars.2016.00006.
78. J. G. Leahy, R. R. Colwell, Microbial degradation of hydrocarbons in the environment. *Microbiol. Rev.* (1990).
79. R. G. Wiegert, L. R. Pomeroy, W. J. Wiebe, in *The Ecology of a Salt Marsh* (1981), pp. 3–20.
80. R. G. Wiegart, B. J. Freeman, Tidal marshes of the southeastern Atlantic coast: a community profile. *U.S. Fish Wildl. Serv.* **85**, 1–80 (1990).
81. L. R. Pomeroy *et al.*, in *Estuarine Processes* (1977; http://www.sciencedirect.com/science/article/pii/B9780127518022500278), pp. 270–279.
82. R. G. Wiegert *et al.*, The Georgia Rivers Land Margin Ecosystem Research Program. *Limnologica*. **29**, 286–292 (1999).
83. J. J. Alberts, M. Takács, in *Organic Geochemistry* (1999), vol. 30, pp. 385–395.
84. J. M. González, W. B. Whitman, R. E. Hodson, M. A. Moran, Identifying numerically abundant culturable bacteria from complex communities: An example from a lignin enrichment culture. *Appl. Environ. Microbiol.* **62**, 4433–4440 (1996).
85. A. Buchan, L. S. Collier, E. L. Neidle, M. A. Moran, Key aromatic-ring-cleaving enzyme, protocatechuate 3,4-dioxygenase, in the ecologically important marine Roseobacter lineage. *Appl. Environ. Microbiol.* **66**, 4662–4672 (2000).
86. A. Buchan, E. L. Neidle, M. A. Moran, Diversity of the Ring-Cleaving Dioxygenase Gene pcaH in a Salt Marsh Bacterial Community. *Appl. Environ. Microbiol.* (2001), doi:10.1128/AEM.67.12.5801-5809.2001.
87. A. Buchan *et al.*, Dynamics of Bacterial and Fungal Communities on Decaying Salt Marsh Grass. *Appl Env. Microbiol*. **69**, 6676–6687 (2003).

88. R. L. Sleighter, P. G. Hatcher, Molecular characterization of dissolved organic matter (DOM) along a river to ocean transect of the lower Chesapeake Bay by ultrahigh resolution electrospray ionization Fourier transform ion cyclotron resonance mass spectrometry. *Mar. Chem.* **110**, 140–152 (2008).

89. J. P. Schubauer, C. S. Hopkinson, Above- and belowground emergent macrophyte production and turnover in a coastal marsh ecosystem, Georgia. *Limnol. Oceanogr.* **29**, 1052–1065 (1984).

90. I. Valiela, J. M. Teal, W. G. Deuser, The nature of growth forms in the salt marsh grass Spartina alterniflora. *Am. Nat.* **112**, 461–470 (1978).

91. R. E. Hodson, R. R. Christian, A. E. Maccubbin, Lignocellulose and lignin in the salt marsh grass Spartina alterniflora: initial concentrations and short-term, post-depositional changes in detrital matter. *Mar. Biol.* **81**, 1–7 (1984).

92. M. Moran, R. Hodson, Contributions of degrading Spartina alterniflora lignocellulose to the dissolved organic carbon pool of a salt marsh. *Mar. Ecol. Prog. Ser. Oldend.* **62**, 161–168 (1990).

93. W. J. Mitsch *et al.*, Wetlands, carbon, and climate change. *Landsc. Ecol.* **28**, 583–597 (2013).

94. G. A. Hyndes *et al.*, Mechanisms and ecological role of carbon transfer within coastal seascapes. *Biol. Rev.* **89**, 232–254 (2014).

95. W.-J. Cai, Z. A. Wang, Y. Wang, The role of marsh-dominated heterotrophic continental margins in transport of CO_2 between the atmosphere, the land-sea interface and the ocean. *Geophys. Res. Lett.* **30** (2003), doi:10.1029/2003GL017633.

96. E. B. Haines, The origins of detritus in Georgia salt marsh estuaries. *Oikos*. **29**, 254–260 (1977).

97. J. M. Teal, Energy Flow in the Salt Marsh Ecosystem of Georgia. *Ecology*. **43**, 614–624 (1962).

98. A. Leonowicz *et al.*, Biodegradation of lignin by white rot fungi. *Fungal Genet. Biol.* **27** (1999), pp. 175–185.

99. J. I. Hedges, R. A. Blanchette, K. Weliky, A. H. Devol, Effects of fungal degradation on the CuO oxidation products of lignin: A controlled laboratory study. *Geochim.*

Cosmochim. Acta. **52**, 2717–2726 (1988).

100. T. D. H. Bugg, M. Ahmad, E. M. Hardiman, R. Rahmanpour, Pathways for degradation of lignin in bacteria and fungi. *Nat. Prod. Rep.* **28**, 1883 (2011).
101. R. D. Fallon, F. K. Pfaender, Carbon metabolism in model microbial systems from a temperate salt marsh. *Appl. Environ. Microbiol.* **31**, 959–968 (1976).
102. R. Benner, M. A. Moran, R. E. Hodson, Biogeochemical cycling of lignocellulosic carbon in marine and freshwater ecosystems: Relative contributions of procaryotes and eucaryotes. *Limnol. Oceanogr.* **31**, 89–100 (1986).
103. R. Benner, S. Y. Newell, A. E. Maccubbin, R. E. Hodson, Relative contributions of bacteria and fungi to rates of degradation of lignocellulosic detritus in salt-marsh sediments. *Appl. Environ. Microbiol.* **48**, 36–40 (1984).
104. X. F. Huang *et al.*, Isolation and characterization of lignin-degrading bacteria from rainforest soils. *Biotechnol. Bioeng.* (2013), doi:10.1002/bit.24833.
105. X. Mou, S. Sun, R. A. Edwards, R. E. Hodson, M. A. Moran, Bacterial carbon processing by generalist species in the coastal ocean. *Nature*. **451**, 708–711 (2008).
106. X. Mou, R. E. Hodson, M. A. Moran, Bacterioplankton assemblages transforming dissolved organic compounds in coastal seawater. *Environ. Microbiol.* **9**, 2025–2037 (2007).
107. J. M. Gonzalez, F. Mayer, M. a Moran, R. E. Hodson, W. B. Whitman, Sagittula stellata gen. nov., sp. nov., a lignin-transforming bacterium from a coastal environment. *Int. J. Syst. Bacteriol.* **47**, 773–780 (1997).
108. J. M. GONZaLEZ, F. MAYER, M. A. MORAN, R. E. HODSON, W. B. WHITMAN, Microbulbifer hydrolyticus gen. nov., sp. nov., and Marinobacterium georgiense gen. nov., sp. nov., Two Marine Bacteria from a Lignin-Rich Pulp Mill Waste Enrichment Community. *Int. J. Syst. Bacteriol.* (1997), doi:10.1099/00207713-47-2-369.
109. K. E. Hammel, D. Cullen, Role of fungal peroxidases in biological ligninolysis. *Curr. Opin. Plant Biol.* (2008), , doi:10.1016/j.pbi.2008.02.003.
110. J. H. Tian, A. M. Pourcher, T. Bouchez, E. Gelhaye, P. Peu, Occurrence of lignin degradation genotypes and phenotypes among prokaryotes. *Appl. Microbiol.*

Biotechnol. (2014), , doi:10.1007/s00253-014-6142-4.

111. A. Spang, E. F. Caceres, T. J. G. Ettema, Genomic exploration of the diversity, ecology, and evolution of the archaeal domain of life. *Science (80-.).* (2017), , doi:10.1126/science.aaf3883.
112. D. Emerson, S. Chauhan, P. Oriel, J. A. Breznak, Haloferax sp. D1227, a halophilic Archaeon capable of growth on aromatic compounds. *Arch. Microbiol.* (1994), doi:10.1007/BF00307764.
113. S. F. Erdoğmuş, B. Mutlu, S. E. Korcan, K. Güven, M. Konuk, Aromatic hydrocarbon degradation by halophilic archaea isolated from ÇamaltI Saltern, Turkey. *Water. Air. Soil Pollut.* (2013), doi:10.1007/s11270-013-1449-9.
114. R. Méheust *et al.*, Hundreds of novel composite genes and chimeric genes with bacterial origins contributed to haloarchaeal evolution, 1–12 (2018).
115. T. Yu *et al.*, Growth of sedimentary Bathyarchaeota on lignin as an energy source. *Proc. Natl. Acad. Sci. U. S. A.*, 201718854 (2018).
116. X. Liu, J. Pan, Y. Liu, M. Li, J. D. Gu, Diversity and distribution of Archaea in global estuarine ecosystems. *Sci. Total Environ.* (2018), doi:10.1016/j.scitotenv.2018.05.016.
117. M. A. Moran *et al.*, Ecological genomics of marine roseobacters. *Appl. Environ. Microbiol.* **73**, 4559–4569 (2007).
118. I. Bakenhus *et al.*, Composition of total and cell-proliferating bacterioplankton community in early summer in the North Sea - roseobacters are the most active component. *Front. Microbiol.* **8** (2017), doi:10.3389/fmicb.2017.01771.
119. J. M. Gonzalez, M. A. Moran, Numerical dominance of a group of marine bacteria in the alpha-subclass of the clas Proteobacteria in coastal seawater. *Appl. Environ. Microbiol.* **63**, 4237–4242 (1997).
120. R. S. Poretsky, S. Sun, X. Mou, M. A. Moran, Transporter genes expressed by coastal bacterioplankton in response to dissolved organic carbon. *Environ. Microbiol.* **12**, 616–627 (2010).
121. R. J. Newton *et al.*, Genome characteristics of a generalist marine bacterial lineage. *ISME J.* **4**, 784–798 (2010).

122. J. M. González, R. P. Kiene, M. A. Moran, Transformation of sulfur compounds by an abundant lineage of marine bacteria in the α-subclass of the class Proteobacteria. *Appl. Environ. Microbiol.* **65**, 3810–3819 (1999).
123. S. Lenk *et al.*, Roseobacter clade bacteria are abundant in coastal sediments and encode a novel combination of sulfur oxidation genes. *ISME J.* **6**, 2178–2187 (2012).
124. I. Wagner-Döbler *et al.*, The complete genome sequence of the algal symbiont Dinoroseobacter shibae: a hitchhiker's guide to life in the sea. *ISME J.* **4**, 61–77 (2010).
125. A. Buchan, G. R. LeCleir, C. A. Gulvik, J. M. González, Master recyclers: features and functions of bacteria associated with phytoplankton blooms. *Nat. Rev. Microbiol.* **12** (2014), pp. 686–698.
126. R. E. Hicks, S. Y. Newell, Direct-count Estimates of Fungal and Bacterial Biovolume in Dead Leaves of Smooth Cordgrass (Spartina alterniflora Loisel). *Estuaries*. **5**, 246–260 (1982).
127. S. Y. Newell, R. D. Fallon, J. D. Miller, Decomposition and microbial dynamics for standing, naturally positioned leaves of the salt-marsh grass Spartina alterniflora. *Mar. Biol.* **101**, 471–481 (1989).
128. A. Buchan, E. L. Neidle, M. A. Moran, Diversity of the Ring-Cleaving Dioxygenase Gene pcaH in a Salt Marsh Bacterial Community. *Appl. Environ. Microbiol.* **67**, 5801–5809 (2001).
129. C. A. Gulvik, A. Buchan, Simultaneous Catabolism of Plant-Derived Aromatic Compounds Results in Enhanced Growth for Members of the Roseobacter Lineage. *Appl. Environ. Microbiol.* **79**, 3716–3723 (2013).
130. D. Pérez-Pantoj *et al.*, Hierarchy of carbon source utilization in soil bacteria: Hegemonic preference for benzoate in complex aromatic compound mixtures degraded by Cupriavidus pinatubonensis strain JMP134. *Appl. Environ. Microbiol.* **81**, 3914–3924 (2015).
131. R. Mazzoli *et al.*, Degradation of aromatic compounds by Acinetobacter radioresistens S13: Growth characteristics on single substrates and mixtures. *Arch.*

Microbiol. **188**, 55–68 (2007).

132. F. Ampe, D. Léonard, N. D. Lindley, Growth performance and pathway flux determine substrate preference of Alcaligenes eutrophus during growth on acetate plus aromatic compound mixtures. *Appl. Microbiol. Biotechnol.* **46**, 562–569 (1996).
133. R. Brückner, F. Titgemeyer, Carbon catabolite repression in bacteria: Choice of the carbon source and autoregulatory limitation of sugar utilization. *FEMS Microbiol. Lett.* **209** (2002), pp. 141–148.
134. L. Ausec, M. Zakrzewski, A. Goesmann, A. Schlüter, I. Mandic-Mulec, Bioinformatic analysis reveals high diversity of bacterial genes for laccase-like enzymes. *PLoS One*. **6** (2011), doi:10.1371/journal.pone.0025724.
135. R. Singh *et al.*, Enhanced delignification of steam-pretreated poplar by a bacterial laccase. *Sci. Rep.* **7** (2017), doi:10.1038/srep42121.
136. H. Kellner, P. Luis, B. Zimdars, B. Kiesel, F. Buscot, Diversity of bacterial laccase-like multicopper oxidase genes in forest and grassland Cambisol soil samples. *Soil Biol. Biochem.* **40**, 638–648 (2008).
137. L. Luo, R. N. Wu, H. Meng, X. Y. Li, J. D. Gu, Seasonal and spatial variations in diversity and abundance of bacterial laccase-like genes in sediments of a subtropical mangrove ecosystem. *Int. Biodeterior. Biodegrad.* **114**, 260–267 (2016).
138. Z. Fang *et al.*, A bacterial laccase from marine microbial metagenome exhibiting chloride tolerance and dye decolorization ability. *Appl. Microbiol. Biotechnol.* **89**, 1103–1110 (2011).

VI. APPENDIX: FIGURES

Figure 1.1. Aerial photograph of the coastal marshes fringing the coastline of Georgia, USA.

Photography credit to the Georgia Coast Atlas project at the Emory Center for Digital Scholarship.

CHAPTER TWO - EVIDENCE FOR THE PRIMING EFFECT IN A PLANKTONIC ESTUARINE MICROBIAL COMMUNITY

A VERSION OF THIS CHAPTER HAS BEEN PUBLISHED:

Andrew D. Steen, Lauren N. M. Quigley, and Alison Buchan. "Evidence for the Priming Effect in a Planktonic Estuarine Microbial Community." *Front. Mar. Sci.* 3:6 (2016).

Three individuals significantly contributed to this chapter: Lauren N. M. Quigley, Andrew D. Steen, and Alison Buchan. Conceived the experiment: ADS, AB. Performed the experiment: LNMQ, ADS. Analyzed the data: LNMQ, ADS. Wrote the paper: LNMQ, ADS, AB.

I. ABSTRACT

The 'priming effect', in which addition of labile carbon and/or nutrients changes remineralization rate of recalcitrant organic matter, has been intensively studied in soils, but is less well-documented in aquatic systems. We investigated the extent to which additions of nutrients or labile organic carbon could influence remineralization rates of ^{14}C-labeled, microbially-degraded, phytoplankton-derived organic matter in microcosms inoculated with microbial communities drawn from Grove's Creek Estuary in coastal Georgia, USA. We found that amendment with labile protein plus phosphorus increased remineralization rates of degraded, phytoplankton-derived OM by up to 100%, whereas acetate slightly decreased remineralization rates relative to an unamended control. Addition of ammonium and phosphate induced a smaller effect, whereas addition of ammonium alone had no effect. Counterintuitively, alkaline phosphatase activities increased in response to the addition of protein under P-replete conditions, indicating that production of enzymes unrelated to the labile priming compound may be a mechanism for the priming effect. The observed priming effect was transient: after 36 days of incubation roughly the same quantity of organic carbon had been mineralized in all treatments including no-addition controls. This timescale is on the order of the typical hydrologic residences times of well-flushed estuaries suggesting that priming in estuaries has the potential to influence whether OC is remineralized *in situ* or exported to the coastal ocean.

II. INTRODUCTION

The 'priming effect' refers to changes in the remineralization rate of less bioavailable organic matter (OM) in response to the addition of more bioavailable substances (1, 2). Although this effect has been the subject of intensive study in soils, it has only recently begun to attract substantial attention in aquatic systems (3–5). Among aquatic systems, the priming effect may be particularly relevant in estuaries, where labile organic matter (OM, for instance autochthonous production) mix with more recalcitrant OM, such as aged terrestrial OM and recalcitrant marine OM (3).

Despite the voluminous evidence for the priming effect in soils (6), the evidence for priming in aquatic systems is more ambiguous. Several studies using unlabeled labile organic matter to aquatic ecosystems showed by mass balance that additions of labile OM must have stimulated oxidation of more recalcitrant OM (7–9); other investigators in freshwater environments have not found evidence for the priming effect (10, 11), while Bianchi et al. (2015) observed priming of a freshwater bacterial isolate of *Acinetobacter* induced by a disaccharide or algal exudate. With the exception of Farjalla et al. (2009), which concerns a tropical lagoon, these studies were not performed in estuaries. Perhaps more importantly, the priming effect refers to changes in remineralization of recalcitrant OM in response to the addition of more labile OM and/or nutrients. It can be challenging to distinguish remineralization of labile versus recalcitrant OM using a mass-balance approach, in which only total fluxes of are measured, because these approaches do not distinguish between oxidation of pre-existing, recalcitrant OM and added labile OM.

To assess the extent to which additions of labile OM and/or nutrients may influence the remineralization rates of recalcitrant OM in coastal estuaries, we performed microcosm experiments and monitored the remineralization by a surface water microbial community collected from a temperate coastal estuary (Grove's Creek, Georgia, USA). Phytoplankton were labeled with ^{14}C so fluxes of $^{14}CO_2$ derived from phytoplankton-derived OM could unambiguously be distinguished from unlabeled CO_2 derived from labile carbon. Periodic

measurements of cell abundance, extracellular enzyme activities, and dissolved organic matter (DOM) fluorescence provided insight into the mechanisms of interactions between labile OM, nutrients, and phytoplankton-derived OM. These microcosms provided a tractable experimental system in which to assess the influence of simple (acetate) vs complex (protein) labile OM as well as nutrient addition (N or N+P) on degraded OM in estuaries.

III. MATERIALS AND METHODS

Generation of ^{14}C-labeled organic matter

The marine phytoplankter *Synechococcus* sp. strain CB0101 was grown on SN15 medium (750 mL filtered seawater, 250 mL distilled water, 2.5 mL 3.53 M $NaNO_3$, 2.6 mL 352 mM K_2HPO_4, 5.6 mL 342 mM Na_2EDTA, 2.6 mL 37.7 mM Na_2CO_3, 1 mL 737 μM cobalamin, 1 mL cyano trace metal solution [400 mL distilled water, 100 mL 297 mM citric acid • H_2O, 100 mL 229 mM ferric ammonium citrate, 100 mL 27 mM $MnCl_2$ • $4H_20$, 100 mL 17.8 mM Na_2MoO_4 •$2H_2O$, 100 mL 859 μM $Co(NO_3)_2$ • $6H_20$, 100 mL 7.7 mM $ZnSO_4$ • $7H_2O$]) in a sealed, 4-liter flask in the presence of 0.5 mCi $NaH^{14}CO_3^-$ (MP Biomedicals, Santa Ana, CA) under artificial illumination on a 12-hr/12-hr cycle at 28°C. Stationary phase cultures were collected on 0.22 μM Supor filters (Pall Corporation, Port Washington, NY) and resuspended in artificial seawater (ASW) (Sigma Sea Salts, 20 g/L [Sigma-Aldrich, St. Louis, MO]), pH 8.1. A microbial community inoculum (collected at Bogue Sound, NC, from the dock of the Institute of Marine Sciences, University of North Carolina-Chapel Hill) was added to the phytoplankton biomass at 1% v/v and incubated in the dark at room temperature for 45 days. During the course of the incubation, the quantity of $O^{14}C$ was periodically measured using a Perkin-Elmer TriCarb 2910-TR liquid scintillation analyzer (Perkin-Elmer, Waltham, MA). The concentration of remaining OC was calculated by assuming the specific activity of degraded, phytoplankton-derived OC was equal to the specific activity of $DI^{14}C$ in the growth medium.

Phytoplankton-derived OC decay was modeled according to first-order kinetics:

$$OC_t = OC_0 e^{-kt} \quad (1)$$

where OC_t is the concentration of organic carbon at time t, OC_0 is the initial concentration of organic carbon, and k is the decay rate constant. k was determined from a nonlinear least squares regression of the OC concentration data to equation 1, and half-life was calculated as $t_{1/2} = ln(2)/k$. At the end of this initial degradation phase, ^{14}C-POM was collected by filtration (0.22 m), resuspended in ASW (salinity = 20) and heat killed by boiling for 5 min. The POM was allowed to return to room temperature and added to the microcosms as described below.

Microcosm incubations

Microcosms containing 1 mM PO^{14}C were established using combinations of labile carbon, in the form of sodium acetate or protein as bovine serum albumin [BSA]), phosphorus as phosphate, and/or nitrogen as ammonium. This concentration was selected as it is consistent with OC concentrations in Georgia coastal estuarine systems from which the microbial community inoculum was derived (400-3000 μM-C) (12). BSA was selected as a representative protein source due to its well-defined chemical character and because it has frequently been used as a model protein in aquatic biogeochemical research. The labile carbon, N, and P were added at final concentrations of 500 μM-C, 75 μM-N, and 4.7 μM-P, respectively. BSA contains both C and N, at a ratio of 6.6 C:N. Thus, the concentration of inorganic N added to select microcosms was chosen to match this ratio. The P concentration was selected based on the Redfield ratio for N:P of 16. The treatments were as follows: 1) sodium acetate (250 μM acetate or 500 μM-C); 2) protein plus P (500 μM-C as BSA, 75 μM-N as BSA, 4.7 μM K_2HPO_4); 3) N (75 μM NH_4Cl); 4) N plus P (75 μM NH_4Cl, 4.7 μM K_2HPO_4); and 5) control treatment with no C, N or P addition.

Microcosms were constructed as follows: the natural microbial community was obtained by pre-filtering a sample of estuarine water (from Skidaway Island, Georgia) using a Whatman GF/A filter (Whatman, GE Healthcare Biosciences Corporation, Piscataway, NJ; nominal pore size 1.6 μm) to reduce grazer abundance. Prefiltered estuarine water was then filtered onto a 0.22 μm filter (Supor-200 Pall Corp, Ann Arbor, MI). Cells captured on the second filter were resuspended into artificial seawater (Sigma Sea Salts, 15.0 g/L). The cell

suspension was mixed and then 3.9 mL was dispensed into "master mixes" for each treatment with 383 mL artificial seawater (15.0 g/L, adjusted to pH 8.1) for a targeted cell density of 10^6 cells ml^{-1}. C, N and P were added to the master mixes as appropriate for each treatment, and $PO^{14}C$ (0.3779 Ci/ 1 mg $PO^{14}C$) was added to each master mix for a final concentration of 1 mM OC. Sixty-five mL of each master mix was dispensed after gentle mixing into five replicate, 125 mL serum vials and capped with gastight butyl stoppers (National Scientific Supply, Rockwood, TN). The microcosms were then incubated in an incubator at 25 °C in the dark.

^{14}C measurements

Throughout the course of the first 36 days of incubation, samples were collected to monitor the concentrations of total ^{14}C labeled organic carbon ($O^{14}C$), particulate organic carbon ($PO^{14}C$) and dissolved inorganic carbon ($DI^{14}C$). Total $O^{14}C$ was measured on days 0, 1, 2, 3, 6, 8, 10, 14, 17, 20, 22, 27, 30 and 36; $PO^{14}C$ was measured on days 0, 1, 2, 8, 14, 22, 30 and 36; and $DI^{14}C$ was measured on days 1, 2, 3, 6, 8, 10, 14, 17, 20, 22, 27, 30 and 36. In all cases, 0.5 ml samples were collected from serum vials using a 22.5-guage needle and a 1 ml syringe. To quantify total $O^{14}C$, the sample was added to a 20 ml scintillation vial preloaded with 50 μL of 10% H_2SO^4, to drive off $^{14}CO_2$. Samples were allowed to degas for 15 min in a fume hood. Finally, 5 ml of Ecoscint scintillation cocktail (National Diagnostics, Mississauga, OH) was added to each serum vial. To quantify $PO^{14}C$, the samples were filtered through a 0.22 μm filter polycarbonate filter (Millipore, Billerica, MA). The filters were added to scintillation vials containing 5 mL of scintillation fluid. To quantify $DI^{14}C$, samples were initially stored with 50 μL of 1 M NaOH. Just prior to measurement with a Perkin-Elmer TriCarb 2910-TR scintillation counter, samples were acidified by the addition of 0.5 mL of 0.2 M HCl. CO_2 was trapped by bubbling a stream of air through the sample into a 20 mL scintillation vial with a Teflon-septum cap containing 10 mL modified Woeller's solution (50% scintillation fluid/50% β-phenylethylamine) for 20 minutes (13). Tests with $NaH^{14}CO_3$ standards indicated $^{14}CO_2$ trapping efficiency was at least 95%. For all scintillation measurements, vials were

vortexed, allowed to 'rest' for 24-72 h, and vortexed again prior to measurement in order to minimize particle-induced quenching.

Modeling ^{14}C data

Total $O^{14}C$ and $PO^{14}C$ data were modeled assuming a reactive fraction, which decayed according to first-order kinetics, plus an unreactive fraction, in accordance with Equation 1:

$$OC_t = (OC_0 - R)e^{-kt} + R \quad (2)$$

where OC_t is the concentration of total OC or POC at time t, OC_0 is the initial total OC or POC concentration, R is the concentration of recalcitrant OC or POC (modeled here as totally unreactive, in contrast with the way the term is used elsewhere in this paper), k is the first-order degradation rate constant, and t is the incubation time. These models were fit to the data using nonlinear least squares regressions, with k and R as fitted parameters and OC_0 as a constant determined from measurements of the source phytoplankton (960 μM-C for total OC, 926 μM-C for POC). CO_2 production was modeled similarly (Equation 3), assuming that the only source of $^{14}CO_2$ was the remineralization of degraded, phytoplankton-derived $O^{14}C$.

$$CO_{2,t} = A(1 - e^{-kt}) \quad (3)$$

Ninety five percent confidence intervals were calculated using a Monte Carlo algorithm as implemented in the propagate R package. For the CO_2 data, priming at time t was defined as

$$p_t = \frac{\Sigma CO_{2treatment,t}}{\Sigma CO_{2control,t}} - 1 \quad (4)$$

Because observed $^{14}CO_2$ concentrations were non-normally distributed and temporally autocorrelated, a custom permutation test was used to test the null hypothesis that the kinetics of CO_2 production in each treatment were different from that in the control. In this approach, which was an implementation of the generic permutation test described by Good (14), treatment and control labels at each timepoint were randomly shuffled, the resulting data for each reshuffled treatment were fit to Equation 3. Priming for each permuted synthetic dataset was calculated as in Equation 4 from the fits to Equation 3. Ninety-five

percent confidence intervals for the size of the null effect on each day, including days on which $^{14}CO_2$ was not measured, were calculated as the band containing 95% of priming observations out of an ensemble of 1000 randomly permuted data sets. This procedure was chosen to be insensitive to non-normality and autocorrelation, and to allow determination of whether priming occurred between measurement timepoints.

Potential extracellular enzyme activities

Activities of three different extracellular enzymes were assayed during the course of the incubations on days 0 (3 hours after the start of incubations), 7, 16, 21, 29 and 35. β-glucosidase was assessed using 4-methylumbelliferyl- β -D-glucopyranoside (MUB- β -glu; Sigma-Aldrich, St. Louis, MO) at a final concentration of 200 μ M. Leucyl aminopeptidase was assessed using L-leucine-7-amido-4-methylcoumarin (Leu-AMC; Chem-Impex International Inc., Wood Dale, IL) at a final concentration 400 μM. Alkaline phosphatase was assessed using 4-methylumbelliferyl phosphate (MUB-PO_4; Chem-Impex International Inc, Wood Dale, IL) at a final concentration 50 μM. At each measurement timepoint, 0.5 ml of each sample was added to 0.5 ml artificial seawater buffer and a small volume of substrate (MUB- β-glu: 20 μL, Leu-AMC: 20 μL, MUB-PO_4: 50 μL). Cuvettes were capped and shaken and incubated at 22 °C. Fluorescence was periodically measured using a QuantiFluor ST single-cuvette fluorimeter over the course of approximately 2 hours as described in Steen and Arnosti (15). Fluorescence values were calibrated with 4-methylumbelliferone and 7-amido-4-methylcoumarin as appropriate.

Cell counts

Cell densities were assessed on days 1, 3, 6, 10, 14, 17, 20, 22, 27, 30, 36 and 57 days by microscopic direct counting following Ortmann and Suttle (16). 0.5 mL of sample were taken from replicate A of each treatment and stored in cryovials. 10 μL of 25% filter-sterilized glutaraldehyde was added to the samples. Samples were stored at -80 °C. 100 μL of sample was added to 900 μL of water. 50 μL of SYBR gold (25X) was added to each sample. Samples were incubated in the dark for 15 min. Stained samples were vacuum filtered through a 0.22 μm filter. The filter was removed and placed on a glass slide. 20 μL

of anti-fade solution (480 µL 50% glycerol / 50% PBS; 20 µL p-phenylenediamine) was added on top of the filter on the slide before placing a cover slip on the slide. Bacteria were manually enumerated using a Leica CTR6000 microscope (Leica Microsystems, Buffalo Grove, IL).

Fluorescence spectroscopy of dissolved organic matter

Based on preliminary evidence that conditions in the treatments had begun to converge by 36 days, after 57 days we assessed the character of remaining DOM in selected samples using excitation-emission matrix (EEM) fluorescence spectroscopy. Due to the radioactive nature of the samples, fluorescence spectra were measured in sealed 1 cm × 1 cm methacrylate cuvettes (Fisher Scientific, Waltham, MA), which are advertised as transparent above 285 nm. In order to control for potential variability in optical properties among cuvettes, a Milli-Q water blank was measured in each cuvette prior to adding sample. For each measurement, a blank UV-vis absorbance scan was collected using Milli-Q water water on a Thermo Scientific Evolution 200 series spectrophotometer, and a blank fluorescence scan was collected on a Horiba Jobin Yvon Fluoromax 4 fluorescence spectrometer (Horiba Scientific, Kyoto, Japan). The excitation scan was from 240-450 nm in 5 nm increments, and the emission scan was from 250-550 nm in 2.5 nm increments. Finally, the Milli-Q water was removed from the cuvette, sample water was added and diluted 50% with Milli-Q water, and a sample fluorescence scan was collected using the same instrument settings. Sample 5B, which had an unacceptable blank, was discarded.

UV scans indicated that the methacrylate cuvettes began to absorb light below about 290 nm, so all excitation and emission wavelengths shorter than 295 nm were discarded. Sample fluorescence spectra were then corrected for inner-filtering effects, blank-subtracted, normalized to the appropriate day's Raman spectrum, and masked for Raman and Rayleigh scattering.

BSA was the only fluorescent priming compound. For that reason, an initial fluorescence sample was taken from the control treatment prior to the addition of any priming

compounds, and a separate initial sample was taken from the +BSA+P treatment to assess the fluorescence characteristics of the added BSA. Duplicate final samples were taken after 57 days incubation from each treatment.

EEMs data analysis techniques can be highly sensitive to the specific conditions under which fluorescence EEMs were measured. Since our EEMs were collected using a nonstandard cuvette type at a restricted set of wavelengths, we present the data qualitatively.

Data analysis

Data were analyzed using the R statistical platform (17) and visualized using the ggplot2 package (18). All raw data and data-processing scripts are available at http://github.com/adsteen/priming2015.

IV. RESULTS

Character of ^{14}C-labeled phytoplankton-derived OM

To generate less-reactive organic matter for microcosm studies, a culture of the marine phytoplankton species *Synecococcus* sp. CB101 was first grown in the presence of ^{14}C-labeled bicarbonate. The labeled biomass was then subject to degradation by an estuarine microbial community for 45 days. At the end of the incubation period, 45 ± 4 % of the initial phytoplankton remained O^{14}C (Figure 2.1) consistent with a half-life for phytoplankton OC of 36 ± 2 days based on a first-order decay kinetics

Decay of total and particulate OC

Total ^{14}OC (i.e., D^{14}OC+P^{14}OC) and P^{14}OC decayed according to similar kinetics (Figure 2.2). POC in the +BSA+P treatment decayed with a faster rate constant (0.62 ± 0.46 day^{-1}) than any other treatment (in the range of 0.06-0.19 day^{-1}, with error of 0.06-0.08 day^{-1}). Substantial noise in the data obscured any other differences that might have existed in decay rate constant or concentrations of degraded, phytoplankton-derived OM.

CO_2 production and priming

$^{14}CO_2$ production was faster in the +BSA+P treatment than in the control, indicating a positive priming effect which was distinguishable from zero ($p < 0.05$) from day 1 through day 21 (Figure 2.3; Table 2.1). The +N+P treatment also increased the rate of $^{14}CO_2$ production relative to control (Table 2.2). The rate constant for $^{14}CO_2$ production was also larger in the +N+P treatment than the control ($p < 0.05$), but the extent of priming in this treatment was never distinguishable from zero for an alpha of 0.05. $^{14}CO_2$ production in the +acetate treatment was slightly slower than in the control, consistent with a negative or anti-priming effect; this effect was significant between day 14 and day 24, and the $^{14}CO_2$ production in the +N treatment was indistinguishable from the control. While the magnitude of anti-priming in the +acetate treatment was nearly constant throughout the incubation, positive priming in the +BSA+P treatment (and the +N+P treatments, if the observed priming in that treatment was not due to experimental error) was maximal at the first timepoint after labile organic matter was added and decreased steadily thereafter. After 30-36 days of incubation, the total amount of $^{14}CO_2$ remineralized was indistinguishable among all treatments. After 36 days of incubation our quantification indicated that more TOC was removed from the system (320-370 μM) than CO_2 produced (165-186 μM). The average deficit of 147 ± 30 μM likely represents biofilms attached to the incubation vessel walls, which would have been missed by our sampling method.

Cell abundance and extracellular enzymes

Cell abundances in the incubations increased from approx. 1.0×10^6 cells ml^{-1} in each treatment after 1 day of incubation to 1.4-2.5 $\times$ 10^6 cells ml^{-1} after 57 days of incubation, with relatively little difference among treatments (Figure 2.4). However, substantial differences among treatments occurred during the course of the incubation. In the +BSA+P treatment, cell densities quickly increased to a maximum of 1.2×10^7 cells ml^{-1} after 3 days and then decreased steadily through the end of the incubation. Other treatments were characterized by an initial peak at 6 days incubation. Cell abundance in the +N treatment remained roughly constant after 6 days, whereas the control, +acetate, and +N+P

treatments, followed by a minimum in cell abundance at approximately 17 days, and, in the case of the +acetate treatment, a second, larger peak in cell abundance at 27 days.

Potential activities of extracellular enzymes also varied as a function of both time and treatment (Figure 2.5). β -glucosidase activities were generally indistinguishable from zero throughout the incubation for all treatments. Leucyl aminopeptidase activities were far greater in the +BSA+P treatment than in any other treatment, although activities were significantly greater than zero in each treatment. The timecourse of leucyl aminopeptidase activities followed cell counts closely. Alkaline phosphatase activities were also greater in the +BSA+P treatment than in any other treatment, but the timecourse of activities followed a different path than the timecourse of cell counts: the maximum value was at 17 days rather than 6 days, and the peak in activities was less dramatic than either the peak in leucyl aminopeptidase activities or cell counts. While most measures of biological activity ceased at day 35 due to limited sample volume, a final measurement of cell density was made at day 57 and found to range from 1.4×10^6 cells ml^{-1} (+acetate treatment) to 2.5×10^6 cells ml^{-1} (+BSA+P, +N, +N+P treatments).

Chemical transformations of DOM

At the conclusion of the incubation period (day 57), the remaining sample volume was sacrificed for excitation-emission matrix (EEM) fluorescence spectroscopic analysis and compared with samples preserved from the first day of the incubation. The intensity of the FDOM signal increased in all samples over the course of the incubation (Figure 2.6). The nature of the signal, as revealed by EEM, however, did not vary much by treatment, with the exception of the +BSA+P treatment. In this treatment, the protein peak from the added BSA (visible at the bottom of the panel for the initial +BSA+P treatment in Figure 2.6) dominated the degraded, phytoplankton-derived OM signal. By the end of the incubation, however, there was no distinct protein signal, and the overall form of the EEM in the +BSA+P treatment was considerably more intense but similarly shaped to the signals from the other treatments.

V. DISCUSSION

Reactivity of source $O^{14}C$

For this study, we selected a representative strain of phytoplankton, *Synechococcus* sp. CB0101, which was originally isolated from the Chesapeake Bay (19). *Synechococcus* can account for a substantial fraction of total phototrophic cells, chlorophyll *a*, and primary production in estuaries (20–22). During preparation, the phytoplankton-derived organic matter used in this experiment decayed with a half-life of 36 $\pm$ 2 days, consistent with semi-labile estuarine DOC (23). Although the phytoplankton-OM decay data here were too sparse to accurately model with a multi-G model (Figure 2.1) the success of more complex diagenetic models indicates that organic matter becomes less reactive as it is oxidized by microorganisms (24). It is therefore likely that the remaining organic matter at the end of the pre-degradation phase was less reactive than the half-life of 36 days would suggest.

Priming as a transient effect

Recalcitrant OM was remineralized up to 100% faster in the +BSA+P treatment than in the control, but this effect was transient (Figure 2.3). After about 30 days, roughly the same amount of recalcitrant OM had been remineralized in each experiment. Cell densities (Figure 2.4) and enzyme activities (Figure 2.5) also converged towards the end of the experiment. Fluorescence spectroscopy indicated that, after 57 days of incubation, the composition of fluorescent DOM was indistinguishable among all treatments except for +BSA+P. In that treatment a large protein-like peak persisted at the end of the incubation (Figure 2.6). Other than the large protein-like peak, post-incubation fluorescence spectra of the +BSA+P treatment were qualitatively similar to post-incubation spectra for the other treatments (Figure 2.6).

Interestingly, Catalan et al (2015) recently found no evidence of priming in Swedish lakes. That study contained a very large number of experimental treatments, but only a single timepoint, after 35 days of incubation, whereas in the experiment reported here, priming effects were no longer observable after 21 - 24 days. The priming effect arises from

interactions between disparate microorganisms and pools of organic carbon and nutrients (25). Given the complexities of these interactions, it is likely that the magnitude, direction and timing of priming varies substantially among aquatic environments.

Priming vs. stoichiometric control on CO_2 production

The results provide evidence of faster OM mineralization in the presence of added protein plus phosphate (+BSA+P treatment) and possibly added inorganic N and phosphate (+N+P), but not inorganic N alone (+N). These data suggest that heterotrophic metabolism of recalcitrant OM was limited in part by phosphorus. It is important to note that the factors limiting the remineralization of recalcitrant OM may differ from the factors limiting overall bacterial production. Because this experiment involves comparing treatments that received additional nutrient inputs to a control in which no nutrients were added, it is important to distinguish potential stoichiometric effects of nutrient addition from a priming effect. The addition of N and P in the +BSA+P, +N+P, and +N treatments could be expected to spur remineralization of excess $^{14}CO_2$ relative the control, purely to maintain stoichiometric balance. However, two lines of evidence indicate that some fraction of the excess $^{14}CO_2$ observed in the +BSA+P treatment was due to priming by BSA. First, the magnitude of the effect in the +BSA+P treatment was roughly twice as large as in the +N+P treatment, despite the identical N:P stoichiometry in the two treatments. Second, the fact that the effects observed here were transient is difficult to reconcile with stoichiometric effects: we are not aware of a mechanism by which stoichiometric effects could cause the $^{14}CO_2$ production in the control to catch up" to that in the experimental treatments as we observed here, without additional input of nutrients, where was priming effects are well-known to be time dependent (25).

Potential mechanism of priming

Cell abundances, leucyl aminopeptidase activity and phosphatase activity all increased substantially and rapidly in the +BSA+P treatment (Figures 2.4 and 2.5). This is consistent with a scenario in which cells grew rapidly using BSA as a substrate, producing excess leucyl aminopeptidase, which released bioavailable compounds (e.g., amino acids) from

the protein-like organic matter that comprises the major fraction of organic N in degraded organic matter (26, 27). Kuzyakov et al. (2) cite changes in microbial biomass as a primary mechanism of priming in soils. Surprisingly, alkaline phosphatase activity also increased in the +BSA+P treatment, despite the substantial addition of P in that treatment. Some marine bacteria produce alkaline phosphatase constitutively (28), which may account for the observed increase in alkaline phosphatase activity in the +BSA+P treatment here. Alternatively, since the peak in phosphatase activity occurred at 17 days while cell abundance was declining, it is possible that the extracellular phosphatase enzymes may have been released from cytoplasm as cells lysed following the peak in cell abundance at day 3. Alkaline phosphatase can cleave phosphate from phosphoproteins (29), so the extra peptidases present in the +BSA+P treatment may have liberated phosphoproteins which induced the expression of alkaline phosphatase-like enzymes. In any case, the observed increase in the activity of phosphatase provides mechanistic support for the hypothesis that addition of one compound can spur hydrolysis of chemically unrelated compounds, thereby making them bioavailable. Many aquatic extracellular peptidases (protein-degrading enzymes) are relatively promiscuous (30) which suggests that peptidases produced in order to degrade BSA likely hydrolyzed some fraction of the recalcitrant $O^{14}C$ as well.

The microcosms used in this study contained planktonic cells, suspended particles and flocs, and probably biofilms attached to incubation vessel walls. The physiological state of bacteria growing attached to surfaces is dramatically different than when they are unattached (31), and is, therefore, and important consideration for microbial transformation studies. It is possible that the mechanisms and extent of priming different among these microenvironments as suggested by Catalan et al. (11).

Relevance to carbon processing in estuaries

Priming in this study was substantial but transient. The relevant priming timescale observed here of days-to-tens-of-days, coincides with typical hydrologic residence times of passive-margin estuaries (32). Priming in estuaries may therefore influence whether OC is remineralized *in situ* or exported to the coastal ocean.

Is the priming effect that we observed in microcosm incubations with defined substrate additions relevant to natural systems? In estuaries, degraded OM (e.g. terrestrial OM or dissolved remnants of coastal phytoplankton blooms) can come into contact with fresh DOC produced *in situ* (23). Marsh grasses exude substantial amounts of labile compounds, including acetate (33, 34), and phytoplankton growing in estuaries likely also serve as a source of labile OM (35). Here, we have shown that estuarine microbial communities are capable of being 'primed' (or 'anti-primed') by the addition of labile OM and nutrients to mineralize recalcitrant OM more quickly. Therefore, we hypothesize that inputs of labile OM and nutrients to estuaries may influence fluxes of organic carbon between estuaries and the coastal ocean. Given the numerous environmental variables that cannot by accounted for in lab-scale experiments, this hypothesis should be tested with field-scale experiments.

VI. ACKNOWLEDGMENTS

We thank Aron Stubbins (Skidaway Institute of Oceanography) and Mike Piehler (University of North Carolina Institute of Marine Sciences) for help collecting microbial inocula. Steven Wilhelm (UT-Microbiology) shared lab space for experiments, Annette Engel shared the fluorimeter used to collect DOM fluorescence spectra, and Kathleen Brannen-Donnelly gave valuable help with data processing.

VII. REFERENCES

1. D. S. Jenkinson, R. H. Fox, J. H. Rayner, Interactions between fertilizer nitrogen and soil nitrogen—the so‐called "priming" effect. *J. Soil Sci.* **36**, 425–444 (1985).
2. Y. Kuzyakov, J. K. Friedel, K. Stahr, Review of mechanisms and quantification of priming effects. *Soil Biol. Biochem.* **32** (2000), pp. 1485–1498.
3. B. Guenet, M. Danger, L. Abbadie, G. Lacroix, Priming effect: Bridging the gap between terrestrial and aquatic ecology. *Ecology*. **91**, 2850–2861 (2010).
4. T. S. Bianchi, The role of terrestrially derived organic carbon in the coastal ocean: a changing paradigm and the priming effect. *Proc. Natl. Acad. Sci. U. S. A.* **108**, 19473–81 (2011).
5. T. S. Bianchi *et al.*, Positive priming of terrestrially derived dissolved organic matter in a freshwater microcosm system. *Geophys. Res. Lett.* **42**, 5460–5467 (2015).
6. Y. Kuzyakov, Priming effects: Interactions between living and dead organic matter. *Soil Biol. Biochem.* **42**, 1363–1371 (2010).
7. H. de Haan, Effect of benzoate on microbial decomposition of fulvic acids in Tjeukemeer (the Netherlands). *Limnol. Oceanogr.* **22**, 38–44 (1977).
8. R. Shimp, F. K. Pfaender, Influence of naturally occurring humic acids on biodegradation of monosubstituted phenols by aquatic bacteria. *Appl. Environ. Microbiol.* **49** (1985), pp. 402–407.
9. V. F. Farjalla *et al.*, Synergy of fresh and accumulated organic matter to bacterial growth. *Microb. Ecol.* **57**, 657–666 (2009).
10. M. M. Bengtsson *et al.*, No evidence of aquatic priming effects in hyporheic zone microcosms. *Sci. Rep.* **4**, 13–47 (2014).
11. N. Catalán, A. M. Kellerman, H. Peter, F. Carmona, L. J. Tranvik, Absence of a priming effect on dissolved organic carbon degradation in lake water. *Limnol. Oceanogr.* **60**, 159–168 (2015).
12. J. J. Alberts, M. Takács, in *Organic Geochemistry* (1999), vol. 30, pp. 385–395.
13. A. D. Steen, K. Ziervogel, S. Ghobrial, C. Arnosti, Functional variation among polysaccharide-hydrolyzing microbial communities in the Gulf of Mexico. *Mar.*

Chem. **138–139**, 13–20 (2012).

14. P. Good, *Permutation Tests: A Practical Guide to Resampling Methods for Testing Hypotheses* (1994; http://www.amazon.ca/exec/obidos/redirect?tag=citeulike09-20&path=ASIN/038798898X).
15. A. D. Steen, C. Arnosti, Extracellular peptidase and carbohydrate hydrolase activities in an Arctic fjord (Smeerenburgfjord, Svalbard. *Aquat. Microb. Ecol.* **69**, 93–99 (2013).
16. A. C. Ortmann, C. A. Suttle, in *Bacteriophages - Methods and Protocols, Volume 1: Isolation, Characterization, and Interactions* (2009; http://www.springerlink.com/index/10.1007/978-1-60327-164-6), vol. 501, pp. 87–95.
17. R Core team, R Core Team. *R A Lang. Environ. Stat. Comput. R Found. Stat. Comput. , Vienna, Austria. ISBN 3-900051-07-0, URL http//www.R-project.org/*. **55** (2015), pp. 275–286.
18. H. Wickham, ggplot 2 Version 1. *Media*. **35**, 211 (2009).
19. D. Marsan, K. E. Wommack, J. Ravel, F. Chen, Draft Genome Sequence of Synechococcus sp. Strain CB0101, Isolated From the Chesapeake Bay Estuary. *Genome Announc.* **2**, e01111-13 (2014).
20. X. R. Ning, J. E. Cloern, B. E. Cole, Spatial and temporal variability of picocyanobacteria Synechococcus sp in San Francisco Bay. *Limnol. Oceanogr.* **45**, 695–702 (2000).
21. L. A. Pan, J. Zhang, L. H. Zhang, Picophytoplankton, nanophytoplankton, heterotrohpic bacteria and viruses in the Changjiang Estuary and adjacent coastal waters. *J. Plankton Res.* **29**, 187–197 (2007).
22. K. Wang, K. E. Wommack, F. Chen, Abundance and distribution of Synechococcus spp. and cyanophages in the Chesapeake Bay. *Appl. Environ. Microbiol.* **77**, 7459–7468 (2011).
23. P. a. Raymond, J. E. Bauer, DOC cycling in a temperate estuary: A mass balance approach using natural 14C and 13C isotopes. *Limnol. Oceanogr.* **46**, 655–667 (2001).

24. H. Røy *et al.*, Aerobic microbial respiration in 86-million-year-old deep-sea red clay. *Science (80-.).* **336**, 922–925 (2012).
25. E. Blagodatskaya, Y. Kuzyakov, Mechanisms of real and apparent priming effects and their dependence on soil microbial biomass and community structure: Critical review. *Biol. Fertil. Soils*. **45** (2008), pp. 115–131.
26. B. L. Nunn *et al.*, The path to preservation: Using proteomics to decipher the fate of diatom proteins during microbial degradation. *Limnol. Oceanogr.* **55**, 1790–1804 (2010).
27. M. D. Mccarthy, T. Pratum, J. I. Hedges, R. Benner, Chemical composition of dissolved organic nitrogen in the ocean. *Nature*. **390**, 150–154 (1997).
28. H. Moustafa Hassan, D. Pratt, Biochemical and physiological properties of alkaline phosphatases in five isolates of marine bacteria. *J. Bacteriol.* **129**, 1607–1612 (1977).
29. R. L. Mellgren, G. R. Slaughter, J. A. Thomas, Dephosphorylation of phosphoproteins by Escherichia coli alkaline phosphatase. *J. Biol. Chem.* **252**, 6082–6089 (1977).
30. A. D. Steen, J. P. Vazin, S. M. Hagen, K. H. Mulligan, S. W. Wilhelm, Substrate specificity of aquatic extracellular peptidases assessed by competitive inhibition assays using synthetic substrates. *Aquat. Microb. Ecol.* **75**, 271–281 (2015).
31. J. W. Costerton, Z. Lewandowski, D. E. Caldwell, D. R. Korber, H. M. Lappin-Scott, Microbial Biofilms. *Annu. Rev. Microbiol.* **49**, 711–745 (1995).
32. M. Alber, J. E. Sheldon, Use of a date-specific method to examine variability in the flushing times of Georgia estuaries. *Estuar. Coast. Shelf Sci.* **49**, 469–482 (1999).
33. M. E. Hines, Acetate concentrations and oxidation in salt‐marsh sediments. *Limnol. Oceanogr.* **39** (1994), pp. 140–148.
34. D. L. Jones, Organic acids in the rhizosphere - A critical review. *Plant Soil*. **205** (1998), pp. 25–44.
35. C. A. Carlson, D. A. Hansell, in *Biogeochemistry of Marine Dissolved Organic Matter: Second Edition* (2014), pp. 65–126.

VIII. APPENDIX: TABLES

Table 2.1. Modeled rate constants (K) and modeled recalcitrant organic carbon concentrations (R) for total O14C and PO14C in each incubation.

Test	Treatment	k, day^{-1}	R, μM-C
Total	+acetate	0.32 ± 0.14	630 ± 29
Total	+BSA+P	0.33 ± 0.11	590 ± 25
Total	+N	0.24 ± 0.076	640 ± 24
Total	+N+P	0.44 ± 0.2	680 ± 22
Total	Control	0.3 ± 0.12	630 ± 24
POC	+acetate	0.058 ± 0.069	630 ± 140
POC	+BSA+P	0.62 ± 0.46	710 ± 21
POC	+N	0.13 ± 0.063	620 ± 41
POC	+N+P	0.15 ± 0.077	740 ± 23
POC	Control	0.19 ± 0.062	670 ± 19

Table 2.2. Modeled asymptotes (A) and rate constants (k) for $^{14}CO_2$ production in each incubation.

Treatment	A, μM-C	k, day^{-1}
+acetate	165 ± 10.6	0.969 ± 0.016
+BSA+P	185 ± 7.9	0.2023 ± 0.0287
+N	186 ± 12.3	0.1001 ± 0.017
+N+P	173 ± 8.4	0.1741 ± 0.026
Control	185 ± 10.0	0.1001 ± 0.017

IX. APPENDIX: FIGURES

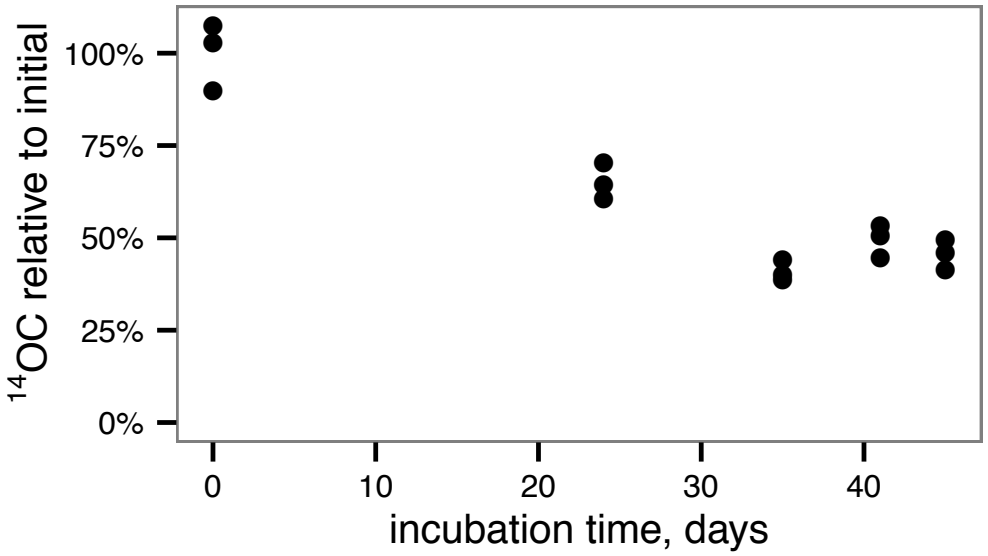

Figure 2.1. Degradation of ^{14}C-labeled, phytoplankton-derived OM by an estuarine microbial community yields relatively recalcitrant, ^{14}C-labeled OM for use in microcosm experiments.

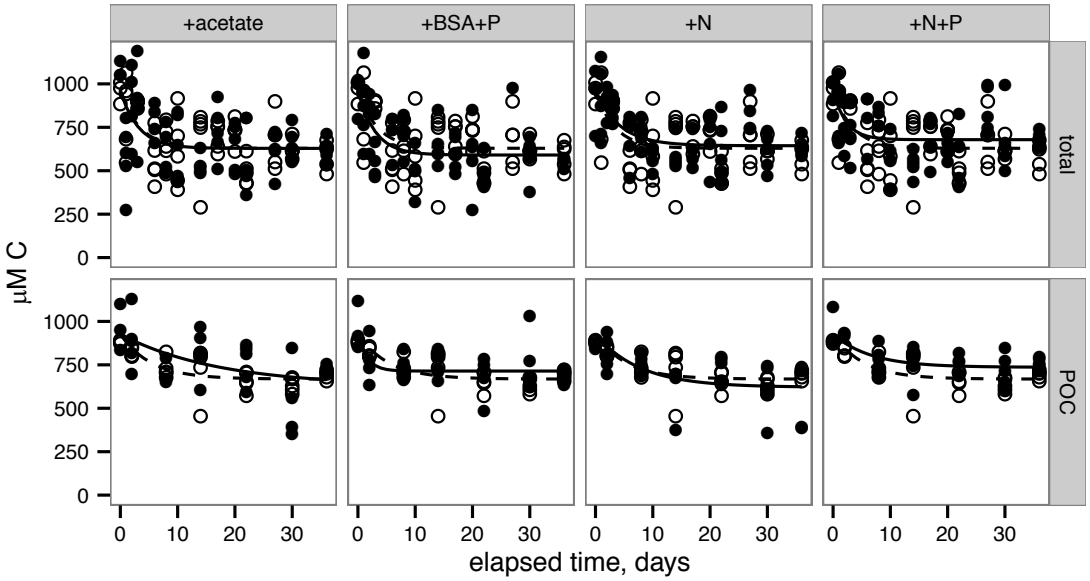

Figure 2.2. Remineralization of total OC and particulate OC.

Lines indicate nonlinear least squares regressions to Equation 2 (provided in methods). Filled circles and solid lines indicate data for each treatment, as indicated across the top panels. Open circles and dashed lines indicate control data.

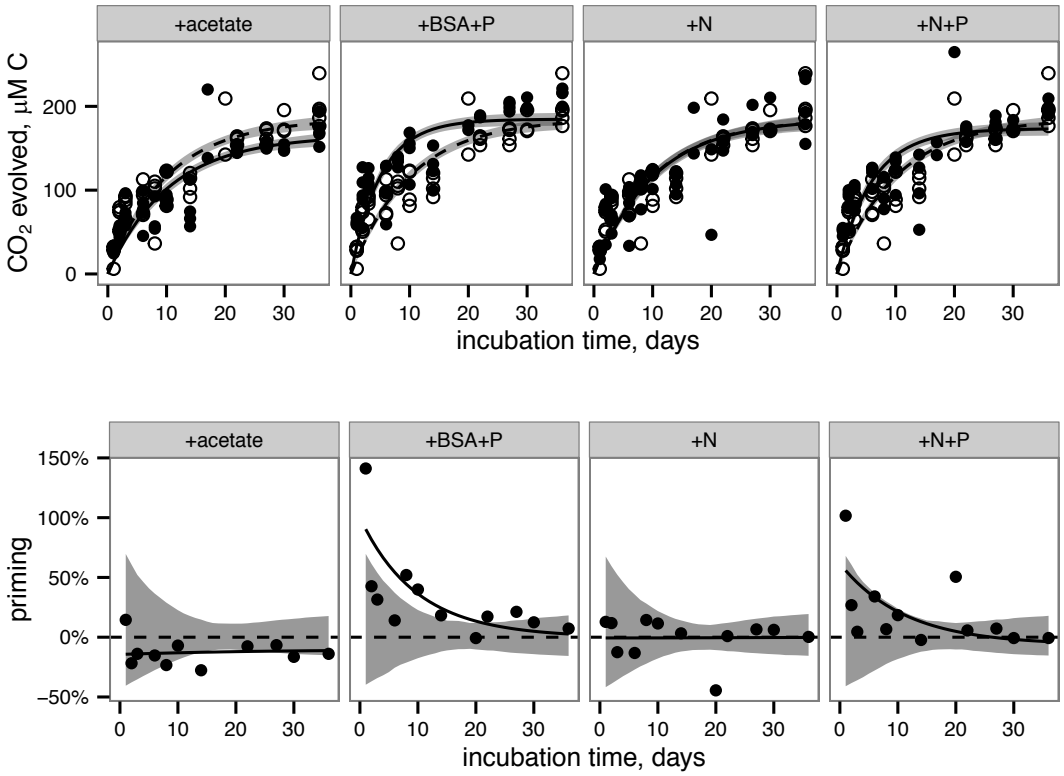

Figure 2.3. CO_2 production and priming in each treatment.

Top row: filled circles and solid lines indicate data from treatments. Open circles and dashed lines indicate data from the control (i.e. no added compounds) and are repeated in each panel for reference. Lines indicate best fits to Equation 3 (provided in methods). Shaded bands indicate standard error of the model fits estimated by a Monte Carlo technique. Bottom row: priming, calculated according to Equation 4 (provided in the methods). Circles indicate priming calculated from the average CO_2 concentrations at each timepoint. Solid lines represent priming calculated from the fit lines shown in the top panel for each corresponding treatment. Shaded bands indicate the region that is indistinguishable from zero priming.

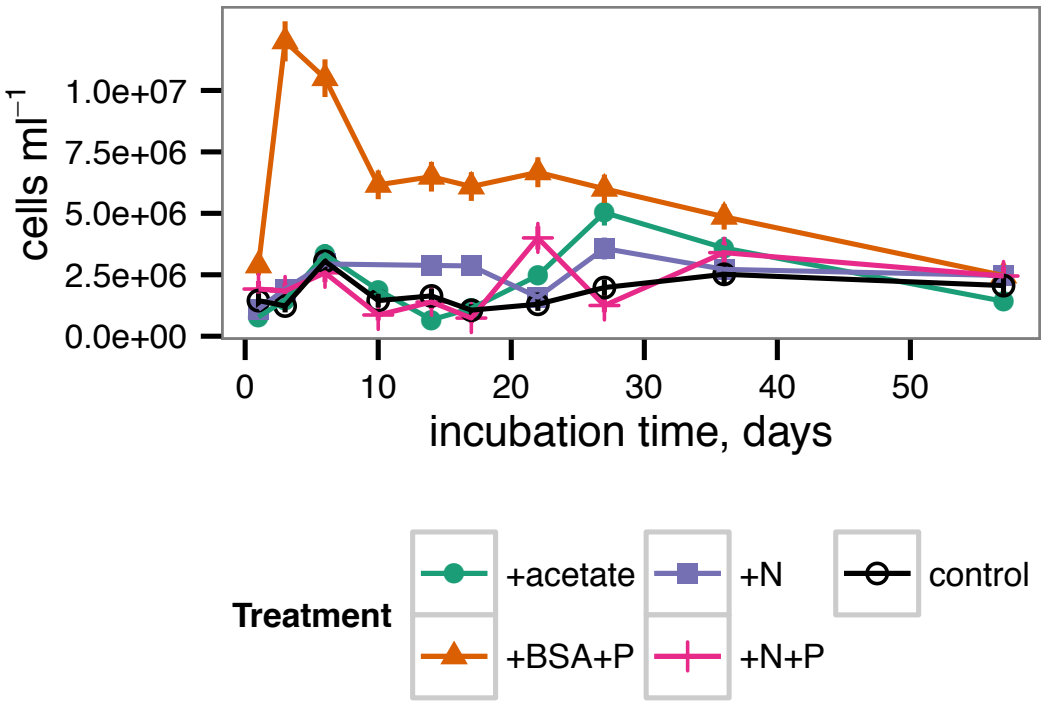

Figure 2.4. Cell abundance during the incubation.

Error bars represent the stand error of cell counts.

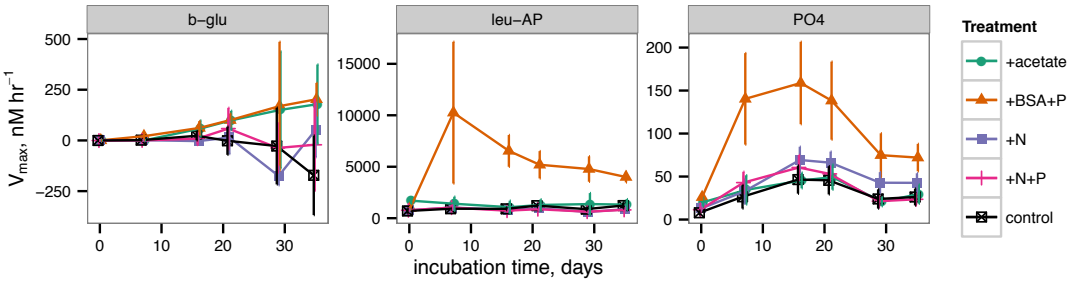

Figure 2.5. Potential extracellular enzyme activities during the incubation.

b-glu represents β–glucosidase, leu-AP represents leucyl aminopeptidase, and PO_4 represents alkaline phosphatase.

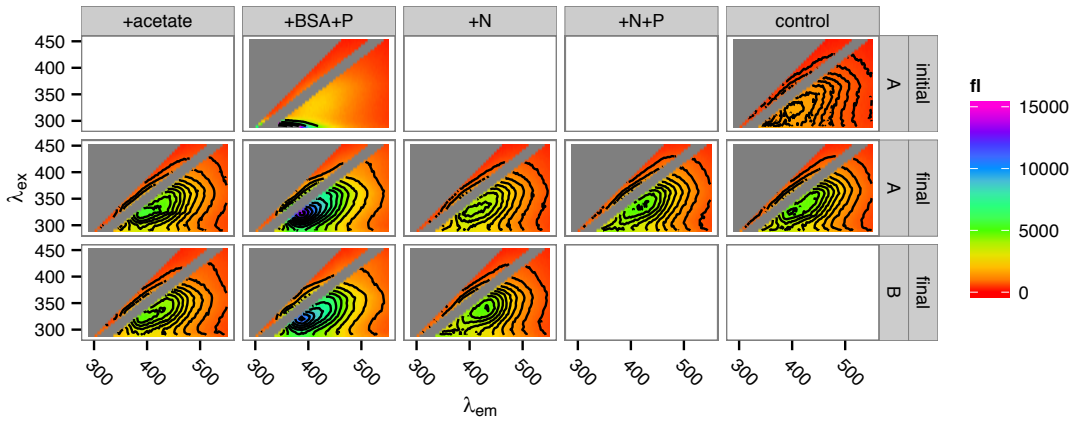

Figure 2.6. Fluorescence spectra of incubation DOM at the start and at the end of the incubations.

Top row: spectra of the +BSA+P treatment and the control treatment at time zero ('initial'). In sufficient sample remained for duplicate measurement of the +N+P and control samples after 57 days. 'A' and 'B' in the right-side panel label refer to incubation replicates.

CHAPTER THREE – LABILE ORGANIC MATTER TYPE AND CONCENTRATION DIFFERENTIALLY STIMULATE MARINE BACTERIAL GROWTH AND RESPIRATION IN THE PRESENCE OF TERRESTRIALLY-DERIVED, DISSOLVED ORGANIC MATTER

A VERSION OF THIS CHAPTER HAS BEEN SUBMITTED FOR PUBLICATION:

Lauren N. M. Quigley, Abigail A. Edwards, Andrew D. Steen and Alison Buchan. "Labile organic matter type and concentration differentially stimulate marine bacterial growth and respiration in the presence of terrestrially-derived, dissolved organic matter." *FEMS Microbiol Ecol*.

Four individuals significantly contributed to this chapter: Lauren N. M. Quigley, Abigail A. Edwards, Andrew D. Steen, and Alison Buchan. Conceived the experiment: LNMQ, ADS, AB. Performed the experiment: LNMQ, AAE. Analyzed the data: LNMQ. Wrote the paper: LNMQ, ADS, AB.

I. ABSTRACT

The presence of a labile carbon source can strongly influence the rate at which more recalcitrant organic carbon is metabolized by microorganisms. This phenomenon has been referred to as the priming effect, and can be broadly understood as the interactive effect of distinct pools of organic matter on microbial metabolism. These effects can be either positive (synergistic) or negative (antagonistic), both of which have recently been demonstrated in aquatic environments. The relevance of interactive effects within marine systems is under debate and fueled by a general lack of mechanistic understanding. As a first step toward uncovering processes that mediate interactive effects, marine bacteria were provided with terrestrially-derived natural organic matter (NOM) and different concentrations and forms of labile organic matter (LOM). The microbial response to these mixed substrate additions was assessed using viable cell densities and respiration. Two marine bacteria, *Sagittula stellata* E-37 and *Citreicella* sp. SE45, and a constructed community of six bacterial species belonging to the Roseobacter lineage were used as inocula in these experiments. Each inoculum was grown with 1, 4, 40, and 400 μM-C as acetate, casamino acids, tryptone or coumarate in the presence of 2 mM-C NOM. Both synergistic and antagonistic growth responses were evident for all strains and the constructed community. However, the specific substrate conditions promoting a response, and the direction, varied amongst strains. These results highlight the species-specificity of mixed substrate conditions.

II. INTRODUCTION

2.5 Tg-C of terrestrially-derived dissolved organic matter (t-DOM) flows through riverine systems annually, where the microbial community preferentially utilizes the more labile components (*1*, *2*). This process leads to the development of an increasingly recalcitrant organic carbon pool, enriched in aromatic moieties, as headwaters move towards coastal margins (*3*, *4*). Most chemical tracers diagnostic of t-DOM (*e.g.,* lignin-derived phenols) are removed before reaching the open oceans (*1*, *5*), suggesting that this material is transformed at land-sea margins. Microbial degradation clearly contributes to the disappearance of t-DOM in these dynamic aquatic systems (*6*).

It has been recently postulated that biological interactions among different pools of organic compounds drive OM transformations in aquatic environments (*7*, *8*). This hypothesis has been framed within the concept of the priming effect (PE). Under the broadest definition of the term, PE occurs when the addition of a labile carbon substrate and/or nutrients alters the rate at which microorganisms degrade recalcitrant organic carbon (*9*). These interactive effects are non-additive and can be either positive (synergistic) or negative (antagonistic). The microbial response may rely critically on the concentration and molecular composition of organic compounds, experimental timescale, nutrient status and microbial community composition (*10–12*). While PE has long been recognized as an important factor in soil organic matter turnover, this framework has only recently been applied to aquatic systems, in which its present role is enigmatic (*8*, *13*, *14*). Bengtsson et al. propose that the variable PE responses reported in the aquatic sciences literature suggests OM interactive effects are likely context dependent. As such, an improved mechanistic understanding of the microbial response to mixed OM pools is needed to enable predictive modeling of OM fate in various environments (*15*).

The salt marshes fringing the coast of the Southeastern United States and the microbial communities residing within these systems provide a relevant system in which to study factors relevant to OM interactions and microbial processing. The rivers flowing through

these marshes carry 400 to 2300 μM-C dissolved organic carbon (DOC), approximately 75% of which is terrestrially-derived (*16*). Additionally, these salt marshes are among the most productive ecosystems on Earth, with net primary production rates ranging from 0.2 to 2.25 kg C m^{-2} yr^{-1} (*17*, *18*). Within these systems, autochthonous labile inputs from salt marsh vegetation and phytoplankton mix with the recalcitrant t-DOM imported by riverine systems at the land-sea interface, setting the stage for OM interactions that may stimulate resident coastal microbial communities to degrade recalcitrant t-DOM. Potential for positive, albeit transient, priming of southeastern coastal microbial communities has been recently demonstrated (*11*). However, the specific factors that control OM interactive effects at the level of individual bacteria and/or communities of bacteria have not been elucidated.

Members of the Roseobacter clade of marine bacteria are among the most numerically abundant and active members of the coastal bacterial communities, and several representative strains have been isolated from Southeastern US estuaries (*e.g. 19–21*). Success of the lineage has largely been attributed to metabolic diversity, including growth on a wide range of plant-derived aromatic compounds characteristic of t-DOM (*22–25*). Growth assays are supported by genome analyses which indicate Roseobacters often possess multiple catabolic pathways for aromatic compound degradation (*26*). Given their abundance, metabolic activity, and ability to oxidize aromatic monomers, members of the Roseobacter clade are ideal lab cultivars to examine how representative members of the estuarine community may undergo interactive effects to degrade t-DOM. As a first step, laboratory mesocosm experiments were conducted with individual strains and a constructed community of Roseobacters to determine the potential roles of (i) concentration and (ii) chemical form of labile organic matter in eliciting an interactive response by these bacteria to naturally derived organic matter from a southeastern blackwater river. The ability of mixtures of OM with distinct chemical characteristics to support microbial respiration and growth, along with the resulting growth dynamics, provides mechanistic insight into the microbial processing of this material.

III. MATERIALS AND METHODS

Strains, media, and growth conditions

Roseobacter strains *Sagittula stellata* sp. E37, *Citreicella* sp. SE45, *Phaeobacter* sp. Y4I, *Roseovarius nubinhibens* ISM, *Sulfitobacter* sp. EE-36, and *Sulfitobacter* sp. NAS-14.1 were routinely grown on an aromatic basal medium (ABM) containing 8.7 μM KCl, 8.7 μM $CaCl_2$, 43.5 μM $MgSO_4$, and 174 μM NaCl with 225 nM K_2HPO_4, 13.35 μM NH_4Cl, 71 mM Tris-HCl (pH 7.5), 68 μM Fe-EDTA, trace metals and trace vitamins. The strains were incubated at 30°C, shaking, in the dark. Suwannee River natural organic matter (NOM) collected and characterized by the International Humic Substance Society (IHSS, St. Paul, MN) was used as a representative t-DOM. ^{13}C NMR estimates of carbon distribution provided by IHSS show that Suwannee NOM comprised of roughly 25% aromatic residues. NOM was held at a constant concentration of 2 mM-C for all experiments.

Four different forms of labile organic matter (LOM) (sodium acetate, casamino acids + tryptophan, coumarate, and tryptone) were added at four concentrations (400, 40, 4, and 1 μM-C). These concentrations were selected after initial experimentation using a LOM concentration gradient of 400 μM-C to 20 nM-C. All glassware used was combusted at 450° C for at least four hours to remove trace organic carbon. All experiments utilized cultures preconditioned on 2 mM-C *p*-hydroxybenzoic acid to match the *in situ* carbon concentration of the Suwannee River NOM.

Experimental treatments

All experiments assessed interactive effects of organic matter by comparing microbial growth or respiration in a treatment containing both labile and recalcitrant organic matter to the sum of growth or respiration in treatments containing only one of those two carbon sources. There were a total of four treatments: No C (No carbon addition control), LOM (labile organic matter), NOM (Suwannee River natural organic matter), and mix (LOM + NOM treatments) (Table 3.1). The No C controls lacked both LOM and NOM, serving as

a control for bacterial growth on medium alone. The LOM treatment consisted of LOM under the same conditions as the corresponding mix treatment. The NOM treatment contained 2 mM-C Suwannee River NOM as the sole carbon source. The mix treatment had both 2 mM-C NOM and one of four concentrations of the different LOMs. The microbial seeding density for all experiments was ~ $1x10^4$ cells mL^{-1}. For the constructed community inoculum, equal representation of each strain was targeted.

For each treatment, viable cell abundance and community composition were measured. As we were motivated to understand the ability of different OM mixtures to support the growth of marine bacteria, viable counts were monitored rather than direct counts, which do not readily distinguish between living and dead cells. Viable counts have the additional advantage over direct counts that it is easy to distinguish between Roseobacter strains (see below). Due to the impracticability of obtaining all of the necessary samples from a single set of experimental samples, two parallel sets of the same experiment were performed. A set of incubations for viable counts was first performed and the results from those incubations were used to inform the conditions selected for incubation in a respirometer. For the viable cell abundance and community composition experiment, culture aliquots were collected on days 0, 1, 2, 4, 7, 10 and 14. Community composition was determined by colony morphology, as each strain of Roseobacter in the community had unique, readily identifiable colony morphology (Figure 3.1). Respiration was monitored in a separate set of microcosms using a Micro-Oxymax respirometer (Columbus Instruments, Columbus, OH), in which cumulative CO_2 production was measured by infrared absorbance continuously throughout the incubation.

Data analysis

To assess interactive effects of mixed substrate treatments, the sum of the cell density or CO_2 production in the LOM and NOM treatments was calculated and termed "composite", which represents the case in which rates of LOM and NOM metabolism are independent. This case would represent zero interactive response to mixed substrate regimes. The extent

and nature (synergistic or antagonistic) of any interactive response was determined through comparison of the "composite" and the mix treatments.

All data analysis was performed using the R statistical platform and visualized using the ggplot2 package (*27*, *28*). Raw data and scripts are posted at http://github.com/lnmquigley/roseo_priming_2018. Viable counts were log-transformed and sub-setted by day. For each day, a three-way ANOVA was performed to determine whether differences in viable counts were being driven by treatment, concentration or source of LOM. Because the experimental design was unbalanced, two three-way ANOVAs were performed on the final time point in the respirometer incubations in order to determine the factors influencing CO_2 accumulation. Additionally, rates were calculated during exponential CO_2 production, and three-way ANOVAs were employed to identify factors influencing the rate of CO_2 production. For all ANOVAs, Fisher's least significant difference was used as a post hoc test and p-values were adjusted to correct for the false discovery rate using the Benjamini-Hochberg correction (*29*).

In order to calculate α diversity in the constructed community experiments, Shannon entropy was calculated for each culture, which was then exponentially transformed into true diversity, also known as effective species number (*30*). A three-way ANOVA was performed to determine the relationship between effective species number and treatment, concentration and source of LOM. The *p*-values obtained from the Fisher's least significant difference were adjusted using the Benjamini-Hochberg correction to account for multiple comparisons. A Bray-Curtis dissimilarity matrix was calculated using all constructed community cultures for each day. In order to determine sources of variation (treatment, concentration, and/or source of LOM) within the Bray-Curtis dissimilarity matrix, a permutational MANOVA was employed using the Adonis function in the R package vegan (*31*).

IV. RESULTS

Prior results demonstrated that Southeastern US coastal microbial communities can be primed by labile substrates, but that the observed PE is transient and can be either positive or negative, depending upon the priming agent employed (*11*). Thus, in order to better understand the factors that may control interactive effects in these communities, we assessed the influence of labile carbon concentration and chemical identity on the growth dynamics and respiration of monocultures of two coastal bacterial species, *Sagittula stellata* E-37 and *Citreicella* sp. SE45, as well as a constructed community of six coastal bacteria, provided an environmentally relevant and natural source of organic matter (NOM). Strains E-37 and SE45 were both isolated from Southeastern coastal waters, belong to the Roseobacter lineage of bacteria that are abundant in these systems and have demonstrated abilities to degrade plant-derived recalcitrant compounds (*32*, *33*). The constructed community of six bacteria included these two strains, plus four additional Roseobacter strains: *Phaeobacter* sp. Y4I, *Roseovarius nubinhibens* ISM, *Sulfitobacter* sp. EE-36, and *Sulfitobacter* sp. NAS-14.1. Of the latter four, two (Y4I and EE-36) were also isolated from Southeastern US coastal waters, one from North Atlantic off-shore waters (NAS-14.1) and one (ISM) from the Caribbean Sea (*34*, *35*). This community was used to assess the interactions of mixed species cultures and mixed substrate regimes. The six representative isolates were selected based on the number (1-6) and type of aromatic carbon catabolism pathways present in their genomes (Table 3.2).

A fully factorial experimental design was employed. Sixteen LOM conditions were tested: four substrates, ranging from relatively simple to chemically complex (sodium acetate, coumarate, casamino acids + tryptophan, and tryptone, in order of increasing chemical complexity) at four concentrations (1, 4, 40, and 400 μM-C; Table 1). Sources of LOM were chosen to represent a gradient of chemical complexities that are differentially processed by microbes: sodium acetate and casamino acids + tryptophan are likely shunted directly into central metabolism; tryptone is a mixture of oligo-peptides and, coumarate is an aromatic monomer derived from lignin (*36*). Cleavage of the aromatic ring requires

specific pathways that are found in a limited number of microbes and are most often subject to catabolite repression (*37*, *38*). Of the six bacterial isolates tested, only *Sagittula stellata* sp. E-37 and *Citreicella* sp. SE45 possess the ability use coumarate as a sole carbon source (Table 3.2).

Substrate preferences vary between individual strains

To assess the extent to which each LOM type and concentration could support the growth of the tested coastal bacteria, we monitored viable counts of monocultures of *Sagittula stellata* sp. E-37 and *Citreicella* sp. SE45 as a function of organic matter treatment. Viable cell densities for SE45 and E-37 increased two to three orders of magnitude within the first 24 hours of incubation, depending on the concentration of LOM provided (Figure 3.2). In both strains, LOM type and concentration interacted significantly to drive viable counts at each time point (three-way ANOVA, n=5, $p<0.001$, Tables 3.3 and 3.4), with the single exception of E-37 on Day 14 (Table 3.4). For all four LOM types, the two lowest concentrations of LOM (1 and 4 μM) did not support reliable growth of either of the two monocultures over the course of the experiment, relative no carbon added controls. With the exeption of E-37 provided 40 μM tryptone, neither of the two bacterial isolates showed consistently robust growth at 40μM on the remaining LOM substrates. For all LOM types, the highest concentration of labile carbon (400 μM) showed statistically significant enhanced growth of both the strains (7-15x greater than No C). A general trend emerged for all cultures in which cell viability increased rapidly at the start of the experiment and was followed by a decline in cell viability beginning around or after Day 4. For SE45, viable cells remained significantly higher than no carbon controls throughout the course of the experiment (at least 3-fold higher). In contrast, E-37 demonstrated a more rapid decline in viability; viable counts in those cultures were indistinguishable from no carbon controls by Day 10, or earlier. Modest increases in viable cell counts seen on Day 14 are attributed to cannibalism of deceased sibling cells. Viable count data indicate that both monocultures are able to use a small fraction of NOM in the absence of any LOM. This is supported by respiration data that indicate that up to 10% of added NOM is respired by Day 7 (Figure 3.3).

Each strain demonstrated unique and apparent preferences for the four different LOM types. Given the boom and bust growth dynamics described above, we focused on maximal viable counts within the first 48 hrs of the experiment for all LOM types at the highest concentration (400 μM). E-37 reached the highest cell densities on coumarate, nearly ten-fold higher viable counts compared to no carbon controls (2.3×10^7 +/- 6.28×10^6 vs 2.86×10^6 +\- 9.34×10^5), and lowest on acetate (5.18×10^6 +/- 1.58×10^6). It grew equally well on casamino acids and tryptone. SE45 grew equally well on all substrates except casamino acids, for which its viable counts were ~50% of the other three substrates within the first few days of the experiment (Figure 3.2).

Individual strains show differential responses to mixed organic matter treatments

For the mixed substrate experiments, NOM was held at a constant concentration of 2 mM-C, consistent with OC concentrations in Georgia coastal estuaries (*16*). To assess interactive growth responses, mixed substrate treatments (mix), which included a source of LOM and NOM in the same treatment, were compared to a composite class of data: the additive response of the LOM alone and NOM alone treatments. This allowed us to assess synergistic or antagonistic interactions of LOM and NOM on bacterial growth in the mixed treatments.

The individual strains displayed differing response to the various treatments. SE45 reached the highest viable cell densities in the mix treatments (LOM + NOM) with the highest LOM concentrations (400 μM-C; Figure 3.2). Final cell densities increased with increasing LOM concentrations. While E-37 viable cell densities generally tracked with LOM concentrations, the differences in maximum cell densities across LOM type and concentration were less than an order of magnitude, compared to on average 10-fold difference in SE45 treatments between 400 μM-C and the lower concentrations (Figure 3.2). E-37 cell viabilities at the conclusion of the experiment always fell below Day 1 cell densities for the same treatment (Figure 3.2B).

While both strains demonstrated a notable growth response (statistically significant from composite data) to the mixed substrate treatments in the majority of the treatments (12 or 14 of 16), the effect was always transient. Both synergistic (positive) and antagonistic (negative) responses were observed, and the responses were species-specific. A significant synergistic response was seen for SE45 on all four LOM substrates at the highest concentration (400 μM-C), however, this was displayed at different time points for the different LOMs (Figure 3.2, Table 3.5). Conversely, antagonistic interactions (i.e., composite cell densities significantly higher than those in the mixtures) were observed for all LOM types at 4 μM-C (Figure 3.2, Table 3.5) with this strain. Inconsistent trends were observed in other LOM concentration treatments. E-37 also displayed a significant response to all four LOM substrates at in the highest concentrations, but the effect was negative on one substrate (tryptone; Figure 3.2, Table 3.5). Growth of E-37 was negatively influenced at some point during the experiment for all concentrations of tryptone, expect the lowest (1 μM–C). While a synergistic response was observed with coumarate at the highest concentration, antagonistic responses were observed with this substrate at the three lower concentrations. When E-37 displayed a significant growth response on casamino acids, it was always positive.

Due to the differential responses of the two strains to different concentrations of casamino acids, additional experiments were performed to monitor respiration at all concentrations of this LOM. Respiration assays were also performed on cultures provided acetate and coumarate at the highest LOM concentration (400 μM-C) to provide comparative information on the influence different chemical compositions of LOM to OM mineralization. Respiration data largely supported the viable count data and, as a result of automated sampling, provide higher temporal resolution (Figure 3.3). The response by SE45 to mixed substrate conditions when measured via respiration matched the viable count results for 1, 4, and 400 μM-C casamino acids. However, mixed and composite CO_2 production data were indistinguishable from each other with cultures provided 400 μM-C coumarate and 40 μM-C casamino acids and, despite the fact that these treatments exhibited significant synergistic and antagonistic responses, respectively, when assayed by viable

count (Figure 3.3). SE45 produced less CO_2 in the mixed treatment than the composite when provided 400 μM-C acetate (Figure 3.3), which contrasts with the viable count results in which a synergistic response occurred (Figure 3.2). CO_2 production in NOM alone treatments was statistically indistinguishable from mixed OM treatments when SE45 was provided low concentrations of casamino acids (1 and 4 μM). However, it was significantly lower than the mixed treatments at 40 μM-C casamino acids (three-way ANOVA, n=3, $p<0.001$) and all LOM sources at 400 μM-C (three-way ANOVA, n=3, $p<0.001$, Table 3.6). At low concentrations of casamino acids the mix and composite treatments of E-37 were indistinguishable (Figure 3.3A). The low concentration mixed treatments for E-37 all had significantly higher rates of CO_2 production (~2-10 fold) than their corresponding LOM alone treatments (Figure 3.3A). E-37 displayed a synergistic response when stimulated with 400 μM-C acetate, casamino acids and coumarate, yielding CO_2 evolution rates that were 2.8-7.4 fold higher than with corresponding LOM alone treatments (Figure 3.3B).

Constructed community displays similar dynamics to single strains under mixed conditions

Given the differential response of individual strains to homogenous and mixed substrate conditions, we next tested a constructed community that included both of these strains to assess interactions amongst community members with different metabolic capabilities. Similar to the single strain experiments, concentration and source of the labile carbon addition interacted significantly to determine cell densities at each time point in the 14-day experiment (Figure 3.4, Table 3.7). The community responses generally mirrored those of SE45 monocultures. For each source of LOM, the cell densities produced at 400 μM-C were significantly greater than those at all lower LOM concentrations (three-way ANOVA, n=5, $p<0.001$ for all time points). For mixed NOM + LOM substrate experiments, the community demonstrated a synergistic growth response to all LOM sources at 400 μM-C, and tryptone at 40 μM-C and 4 μM-C (Figure 3.4, Table 3.8). The community displayed a significant reduction in viable counts when supplied with each LOM source at 1 μM-C; the intervening concentrations showed varying responses. The six-member constructed

community was best able to utilize tryptone for growth; the three other LOM types produced ~25% of viable cells (Figure 3.4).

No synergistic responses were observed in the constructed community when respiration was used as the measure of microbial activity. However, significant antagonistic responses were observed in 40 μM-C casamino acids treatment, as well as significantly lower CO_2 production rates (1.45 fold) compared to the LOM treatment (three-way ANOVA, n=3, $p<0.001$), corroborating some of the antagonistic results from the viable count-based approach (Figures 3.2 and 3.5). CO_2 production rates were 1.3 and 1.45-fold higher in the mixed treatments than the LOM alone treatments for the low concentrations (1 and 4 μM-C) of casamino acids treatments (three-way ANOVA, n=3, $p<0.001$) and were statistically indistinguishable at the highest LOM concentrations (Figure 3.5).

LOM type drives microbial community composition

We next accessed the influence of concentration and source of LOM on community composition in the 6-member culture. Species diversity decreased with increasing LOM concentration in both single and mixed substrate treatments. At the highest LOM concentration, mesocosms were dominated by a single strain: either SE45 on coumarate or Y4I on the other three LOM types (Figure 3.4). Treatment (mix or composite), LOM concentration, and LOM source interacted significantly to influence species diversity for all time points, with the exception of Day 2 where only LOM concentration and source interacted significantly (three-way ANOVA, n=5, $p< 0.002$ for all time points) (Figure 3.6, Table 3.9). LOM concentration, LOM source, and treatment interacted significantly to drive differences between communities throughout the course of the incubation (permutational MANOVA, $p<0.05$). Treatments using coumarate as LOM source resulted in a community distinct from the other sources of LOM at 400 μM-C (Figure 3.4C). Coumarate communities were characterized by increased abundances of SE45, comprising up to 84-90% of the community, compared to the other sources of LOM, where communities were dominated by strain Y4I (up to 85-98% of the community) (Figure 3.4).

Mixed LOM + NOM treatments had increased abundances in E-37 and SE45 compared to LOM treatments (Figure 3.4).

V. DISCUSSION

Whether PE is quantitatively important in aquatic ecosystems is an area of current study and debate. Field and lab studies have shown that, depending on the precise circumstance, labile organic matter can speed, slow, or have no effect on the oxidation of recalcitrant organic matter in aquatic environments (*11*, *12*, *39–41*). Given these inconsistencies in the literature, we set out to perform simple and controlled laboratory experiments to identify key mechanistic underpinnings of PE with an explicit focus on the interactive effects of distinct OM pools on microbial metabolism. As coastal salt marsh microbial communities are both subject to predictive pulses of differentially sourced OM and inherently complex (*e.g. 23*, *24*), the use of environmentally relevant and culturable representatives from these communities provides a tractable system for obtaining foundational knowledge of the underlying mechanisms of interactive effects on microbial processing of OM. Here, we used cultured representatives from a lineage of coastal marine bacteria that are known to dominate and be active in coastal estuaries (*42*, *43*). These bacteria were provided a natural and environmentally relevant source of recalcitrant organic matter, natural organic matter (NOM) derived from a river that feeds Southeastern US coastal estuaries, to assess the microbial metabolic response to mixtures of labile and recalcitrant OM in two ways: by measuring viable cell abundance and by measuring CO_2 emissions. These experiments revealed the importance of labile substrate concentration and chemical composition in dictating the growth dynamics of representative marine bacteria in the presence of natural organic matter. We quantify species-specific responses to mixed substrate regimes and document how microbial community composition may shift in response to priming relevant conditions.

Interactive effects are often transient

Previous studies provide evidence for the transience of interactive effects in aquatic ecosystems. For example, a positive PE, lasting approximately a day, was observed in a

single freshwater isolate of *Acinetobacter* provided diatom-derived DOC and trehalose (*41*). Similarly a week-long positive PE was observed when a estuarine microbial community was provided protein in mesocosm studies (*11*). While reports of interactive effects in aquatic systems are limited, their apparently transient nature suggests appropriate temporal resolution in experimental design is essential in assessing aquatic OM interactive effects. We note that studies in which temporal resolution is relatively low (i.e. weekly sampling) tend not to observe interactive effects, compared to those with higher temporal resolution, where such effects are evident (*11*, *44*, *45*).

Our data with cultured bacteria provide further evidence of the transience of interactivity in OM degradation and the timeframes are consistent with what has been reported previously in the literature for both individual microbial isolates and communities (*11*, *41*). Synergistic interactive effects of the labile and recalcitrant C sources on microbial growth were detectable either within the first few days of our incubations and/or as the microbial populations started to decline towards the end of the experimental period. With few exceptions, synergistic interactions did not persist beyond a two to four day timeframe. It has previously been reported that PE happens relatively quickly after the addition of an LOM source (*11*), yet in the experiments reported here, we observed an additional, temporally distinct and synergistic interaction 10-14 days into the experiment. This was evident with both the single strains and the constructed community. This later phase apparent synergistic interaction may arise as a result of cannibalism of deceased sibling cells from the initial growth phase early in the experiment. Alternatively, this response may indicate the microbial community experiences a stabilizing effect from the mixed carbon regime of LOM and NOM. While cell densities in treatments with NOM alone stay relatively consistent throughout the incubation, most of the LOM alone treatments demonstrate severe decline in cell densities, which serves to drive down the composite values used for comparisons with mix treatments to quantitatively assess interactive effects. Cell densities in the mix treatments did not decline as precipitously as those in the composite profiles. The stabilizing effect seen in the mix compared to the composites may arise from the ability of the bacteria to access additional components of NOM, enabled by

LOM catabolism, a mechanism posited by Guenet and colleagues (*8*). Another possible explanation for the stabilizing effect seen in the mix cultures compared to LOM alone is that the catabolism of the LOM source may result in toxic by-products which result in a less precipitous decline in the mix treatments due to the large background of recalcitrant carbon. In some instances, the number of viable cells in the mix treatments begin to rebound towards the later stages of the experiment. The mixed carbon regime provided by the mix treatment yields conditions favorable for microbial adaptations, such as the proliferation of growth advantage in stationary phase (GASP) mutants (*46*), which could utilize previously unavailable components of the NOM. Additional experiments are needed to specifically address the contribution of microbial adaptation to the observed trends, and whether such responses would be invoked in natural settings.

Some inconsistencies between interactive effects in the viable counts and the PE in the respiration data were observed. These discrepancies can provide information on the growth efficiencies of these bacteria under different substrate regimes or incubation conditions. Cultures had to remain static in the respirometer and it is likely that biofilms developed in these conditions. Roseobacters are prolific in natural marine biofilms (*47*, *48*). The physiological states of bacteria growing in biofilms are dramatically different from those grown planktonically (*49*), and this could account for the observed variation.

Interactive effects are species-specific

While there is overlap between the carbon substrate conditions that prime SE45, E-37 and the constructed community, each inoculum experienced synergistic OM interactivity under a unique set of conditions. For example, SE45 demonstrated a synergistic response to mixtures of NOM and 400 μM-C tryptone, a treatment in which E-37 responded antagonistically. The differential ability of SE45 and E-37 to undergo synergistic interactive effects through the addition of tryptone suggests that the expression and/or activity of peptidases and oligopeptide permeases could be an important factor in the onset of interactive effects. While monocultures of E-37 ultimately reach similar cell densities as all other members of the community, E-37 displays a considerably longer lag phase

relative to the other strains when grown on 2 mM-C tryptone (Figure 3.7). Given the transient nature of priming, it is plausible that the delayed growth on tryptone prevents E-37 from interacting synergistically with tryptone to degrade NOM.

In agreement with our earlier report that a natural estuarine microbial community was positively primed by the addition of a globular protein (bovine serum albumin) (*11*), the constructed community analyzed in this study underwent a synergistic interactive effect in the presence tryptone, an assortment of peptides. However, timing of the response differed: it was delayed in the constructed community with tryptone (occurring during the second week of incubation) compared to an immediate priming response by the natural community provided protein. While there are many factors that could contribute to this apparent temporal disconnect, the relatively low strain diversity of the constructed community may be a key driver. By day 1, the constructed community was dominated by a single strain: Y4I comprised 98% of the community in this treatment. Y4I belongs to the genus *Phaeobacter,* members of which were recently shown to bloom in the presence of Arctic riverine, dissolved organic matter (*25*). Additionally, we earlier observed that acetate (at 500 μM-C) repressed the ability of a estuarine microbial community to degrade phytoplankton necromass (*11*). However, in the current experiments all bacterial inocula were positively primed by the addition of acetate, at the highest concentration (400 μM-C). Collectively, these findings demonstrate that the conditions that result in positive priming are species-specific and thus dictated by the composition and metabolic potential of a community.

Carbon sources shape the composition and diversity of the constructed community

While scant information exists on how priming influences community composition, studies that indicate riverine DOM structures the composition of microbial communities along the river-estuary continuum provide a useful comparative framework (*45*, *50*). One report using an estuarine community incubated with riverine DOM and casamino acids saw no evidence for PE and only minor alterations in microbial community composition (*45*). In contrast, we observed that the composition of our constructed microbial community was

influenced significantly both by the carbon sources present (e.g. LOM, NOM, or mix) and the concentrations and sources of the LOM. Several of the strains in our constructed community have been previously shown to simultaneously catabolize aromatic compounds via two different ring cleaving pathways, the benzoyl Co-A and protocatechuate pathways, and derive a beneficial effect when grown on a mixture of carbon substrates compared to either substrate presented alone, with total carbon concentrations held constant (*51*). The metabolic synergy between these two aromatic carbon catabolism pathways may also be a mechanism for PE that has been previously overlooked.

Our studies reveal that structure of the constructed communities is determined by the concentration of LOM provided, regardless of type. As the concentration of LOM increases, the diversity within the community decreases. This stands in contrast to some prior findings in which increasing amounts of autochthonous carbon resulted in increased degradation of allochthonous carbon with little to no effect on bacterial community composition (*52*). This decrease in diversity was most pronounced in the highest LOM additions (400 μM-C), where a single strain (Y4I) dominated all, but the coumarate, treatments. The shorter lag phase and faster growth rate of Y4I relative to other members of the community when grown on labile substrates may have allowed Y4I to gain a foothold in the community. This possibility is supported by the fact that the numerical dominance of Y4I began as early as day 1 in the incubations, after which it either increased in terms of relative abundance or maintained its numerical dominance in the community (Figure 3.4). The stark contrast in community composition between those provided coumarate compared to the other LOM types is likely due to the unique ability of SE45 and E-37 to utilize coumarate as a carbon source. For the coumarate treatments, SE45, and E-37 to a lesser extent, become the most numerically abundant organisms. These two strains are expected to be the members of the constructed community most adept at aromatic carbon catabolism. Given they are both ligninolytic they are likely better tuned to access the aromatic carbon moieties characteristic of NOM (*32*, *33*). Additionally, SE45 reached higher cell densities in the constructed community in the presence of both NOM and 400 μM-C coumarate compared to its growth on these substrates in monoculture, suggesting

SE45 is interacting synergistically with other members of the constructed community to degrade NOM.

Implications for priming effects in natural microbial communities

In this study, individual strains and a constructed community of Roseobacters exhibited different interactive effects under identical growth conditions. Addition of acetate, which negatively primed a natural salt march community previously (*11*), interacted synergistically in all inocula in this study when provided at concentrations of 40 μM-C or higher for the single strains and 400 μM-C for the community. Conversely, addition of proteinaceous OM positively primed the natural community, but interacted antagonistically with one of the single strains, E-37. Inconsistencies between studies in reported PE should not be surprising in light of these results. Given the rapid turnover of LOM, the transience of PE, and the ephermal nature of pulses of LOM to coastal salt marshes and estuaries it is likely that PE in these systems is highly variable in space and time. Ultimately, a detailed understanding of the nature and sources of LOM to estuaries, as well as the molecular mechanisms that driving priming, will be necessary to understand the controls on microbial oxidation of terrestrial organic carbon in estuaries.

VI. ACKNOWLEDGMENTS

We thank Terry Hazen for the use of the respirometer and Melanie Mayes and Hannah Woo for training on the instrument.

VII. REFERENCES

1. J. I. Hedges, R. G. Keil, R. Benner, in *Organic Geochemistry* (1997), vol. 27, pp. 195–212.
2. R. L. Vannote, G. W. Minshall, K. W. Cummins, J. R. Sedell, C. E. Cushing, The River Continuum Concept. *Can. J. Fish. Aquat. Sci.* **37**, 130–137 (1980).
3. L. Sun, E. M. Perdue, J. L. Meyer, J. Weis, Use of elemental composition to predict bioavailability of dissolved organic matter in a Georgia river. *Limnol. Oceanogr.* **42**, 714–721 (1997).
4. A. Mannino, H. R. Harvey, Terrigenous dissolved organic matter along an estuarine gradient and its flux to the coastal ocean. *Org. Geochem.* **31**, 1611–1625 (2000).
5. C. L. Osburn *et al.*, Optical Proxies for Terrestrial Dissolved Organic Matter in Estuaries and Coastal Waters. *Front. Mar. Sci.* **2** (2016), doi:10.3389/fmars.2015.00127.
6. N. D. Ward *et al.*, Degradation of terrestrially derived macromolecules in the Amazon River. *Nat. Geosci.* **6** (2013), doi:10.1038/ngeo1817.
7. T. S. Bianchi, The role of terrestrially derived organic carbon in the coastal ocean: A changing paradigm and the priming effect. *Proc. Natl. Acad. Sci.* **108**, 19473–19481 (2011).
8. B. Guenet, M. Danger, L. Abbadie, G. Lacroix, Priming effect: Bridging the gap between terrestrial and aquatic ecology. *Ecology*. **91**, 2850–2861 (2010).
9. Y. Kuzyakov, J. K. Friedel, K. Stahr, Review of mechanisms and quantification of priming effects. *Soil Biol. Biochem.* **32** (2000), pp. 1485–1498.
10. E. Blagodatskaya, Y. Kuzyakov, Mechanisms of real and apparent priming effects and their dependence on soil microbial biomass and community structure: Critical review. *Biol. Fertil. Soils*. **45** (2008), pp. 115–131.
11. A. D. Steen, L. N. Quigley, A. Buchan, Evidence for the Priming Effect in a Planktonic Estuarine Microbial Community Andrew. *Front. Mar. Sci.* (2016), doi:10.3389/fmars.2016.00006.
12. N. Catalán, A. M. Kellerman, H. Peter, F. Carmona, L. J. Tranvik, Absence of a

priming effect on dissolved organic carbon degradation in lake water. *Limnol. Oceanogr.* **60**, 159–168 (2015).

13. D. S. Jenkinson, R. H. Fox, J. H. Rayner, Interactions between fertilizer nitrogen and soil nitrogen—the so-called 'priming' effect. *J. Soil Sci.* **36**, 425–444 (1985).
14. T. S. Bianchi, The role of terrestrially derived organic carbon in the coastal ocean: a changing paradigm and the priming effect. *Proc. Natl. Acad. Sci. U. S. A.* **108**, 19473–81 (2011).
15. M. M. Bengtsson, K. Attermeyer, N. Catalán, Interactive effects on organic matter processing from soils to the ocean: are priming effects relevant in aquatic ecosystems? *Hydrobiologia* (2018), doi:10.1007/s10750-018-3672-2.
16. J. J. Alberts, M. Takács, in *Organic Geochemistry* (1999), vol. 30, pp. 385–395.
17. R. G. Wiegart, B. J. Freeman, Tidal marshes of the southeastern Atlantic coast: a community profile. *U.S. Fish Wildl. Serv.* **85**, 1–80 (1990).
18. G. A. Hyndes *et al.*, Mechanisms and ecological role of carbon transfer within coastal seascapes. *Biol. Rev.* **89**, 232–254 (2014).
19. J. M. Gonzalez, M. A. Moran, Numerical dominance of a group of marine bacteria in the alpha-subclass of the clas Proteobacteria in coastal seawater. *Appl. Environ. Microbiol.* **63**, 4237–4242 (1997).
20. J. M. González, R. P. Kiene, M. A. Moran, Transformation of sulfur compounds by an abundant lineage of marine bacteria in the α-subclass of the class Proteobacteria. *Appl. Environ. Microbiol.* **65**, 3810–3819 (1999).
21. R. N. Slightom, A. Buchan, Surface colonization by marine roseobacters: Integrating genotype and phenotype. *Appl. Environ. Microbiol.* **75** (2009), pp. 6027–6037.
22. X. Mou, S. Sun, R. A. Edwards, R. E. Hodson, M. A. Moran, Bacterial carbon processing by generalist species in the coastal ocean. *Nature*. **451**, 708–711 (2008).
23. M. A. Moran *et al.*, Ecological genomics of marine roseobacters. *Appl. Environ. Microbiol.* **73**, 4559–4569 (2007).
24. P. M. Medeiros *et al.*, Microbially-Mediated Transformations of Estuarine Dissolved Organic Matter. *Front. Mar. Sci.* **4** (2017),

doi:10.3389/fmars.2017.00069.

25. R. E. Sipler *et al.*, Microbial Community Response to Terrestrially Derived Dissolved Organic Matter in the Coastal Arctic. *Front. Microbiol.* **8**, 1018 (2017).
26. R. J. Newton *et al.*, Genome characteristics of a generalist marine bacterial lineage. *ISME J.* **4**, 784–798 (2010).
27. R Core team, R Core Team. *R A Lang. Environ. Stat. Comput. R Found. Stat. Comput. , Vienna, Austria. ISBN 3-900051-07-0, URL http//www.R-project.org/.* **55** (2015), pp. 275–286.
28. H. Wickham, ggplot 2 Version 1. *Media*. **35**, 211 (2009).
29. Y. Benjamini, Y. Hochberg, Controlling the false discovery rate: a practical and powerful approach to multiple testing. *J. R. Stat. Soc.* **57**, 289–300 (1995).
30. L. Jost, Partitioning diversity into independent alpha and beta components. *Ecology*. **88**, 2427–2439 (2007).
31. J. Oksanen *et al.*, vegan: Community Ecology Package. *R Packag. ver. 2.4–3* (2017), p. 282.
32. J. M. Gonzalez, F. Mayer, M. a Moran, R. E. Hodson, W. B. Whitman, Sagittula stellata gen. nov., sp. nov., a lignin-transforming bacterium from a coastal environment. *Int. J. Syst. Bacteriol.* **47**, 773–780 (1997).
33. A. M. Frank, Aerobic bacterial transformations of lignin-derived aromatic compounds (2016) (available at http://trace.tennessee.edu/utk_graddiss/3652).
34. W. N. Cude *et al.*, Production of the antimicrobial secondary metabolite indigoidine contributes to competitive surface colonization by the marine roseobacter Phaeobacter sp. strain Y4I. *Appl. Environ. Microbiol.* **78**, 4771–80 (2012).
35. A. Buchan, L. S. Collier, E. L. Neidle, M. A. Moran, Key aromatic-ring-cleaving enzyme, protocatechuate 3,4-dioxygenase, in the ecologically important marine Roseobacter lineage. *Appl. Environ. Microbiol.* **66**, 4662–4672 (2000).
36. J. I. Hedges, R. A. Blanchette, K. Weliky, A. H. Devol, Effects of fungal degradation on the CuO oxidation products of lignin: A controlled laboratory study. *Geochim. Cosmochim. Acta*. **52**, 2717–2726 (1988).
37. S. Dal, I. Steiner, U. Gerischer, Multiple operons connected with catabolism of

aromatic compounds in Acinetobacter sp. strain ADP1 are under carbon catabolite repression. *J. Mol. Microbiol. Biotechnol.* **4**, 389–404 (2002).

38. R. Mazzoli *et al.*, Degradation of aromatic compounds by Acinetobacter radioresistens S13: Growth characteristics on single substrates and mixtures. *Arch. Microbiol.* **188**, 55–68 (2007).
39. E. Gontikaki, B. Thornton, T. Cornulier, U. Witte, Occurrence of priming in the degradation of lignocellulose in marine sediments. *PLoS One*. **10** (2015), doi:10.1371/journal.pone.0143917.
40. M. M. Bengtsson *et al.*, No evidence of aquatic priming effects in hyporheic zone microcosms. *Sci. Rep.* **4** (2014), doi:10.1038/srep05187.
41. T. S. Bianchi *et al.*, Positive priming of terrestrially derived dissolved organic matter in a freshwater microcosm system. *Geophys. Res. Lett.* **42**, 5460–5467 (2015).
42. A. Buchan, J. M. González, M. A. Moran, Overview of the marine Roseobacter lineage. *Appl. Environ. Microbiol.* **71** (2005), pp. 5665–5677.
43. I. Bakenhus *et al.*, Composition of total and cell-proliferating bacterioplankton community in early summer in the North Sea - roseobacters are the most active component. *Front. Microbiol.* **8** (2017), doi:10.3389/fmicb.2017.01771.
44. N. Catalán, A. M. Kellerman, H. Peter, F. Carmona, L. J. Tranvik, Absence of a priming effect on dissolved organic carbon degradation in lake water. *Limnol. Oceanogr.* **60**, 159–168 (2015).
45. M. Blanchet *et al.*, When riverine dissolved organic matter (DOM) meets labile DOM in coastal waters: changes in bacterial community activity and composition. *Aquat. Sci.* (2017), doi:10.1007/s00027-016-0477-0.
46. E. R. Zinser, R. Kolter, Mutations Enhancing Amino Acid Catabolism Confer a Growth Advantage in Stationary Phase. *J. Bacteriol.* **181**, 5800–5807 (1999).
47. H. Dang, C. R. Lovell, Bacterial primary colonization and early succession on surfaces in marine waters as determined by amplified rRNA gene restriction analysis and sequence analysis of 16S rRNA genes. *Appl. Environ. Microbiol.* **66**, 467–475 (2000).
48. H. Dang, T. Li, M. Chen, G. Huang, Cross-ocean distribution of Rhodobacterales

bacteria as primary surface colonizers in temperate coastal marine waters. *Appl. Environ. Microbiol.* **74**, 52–60 (2008).

49. J. W. Costerton, Z. Lewandowski, D. E. Caldwell, D. R. Korber, H. M. Lappin-Scott, Microbial Biofilms. *Annu. Rev. Microbiol.* **49**, 711–745 (1995).
50. S. Langenheder, V. Kisand, E. S. Lindström, J. Wikner, L. J. Tranvik, Growth dynamics within bacterial communities in riverine and estuarine batch cultures. *Aquat. Microb. Ecol.* **37**, 137–148 (2004).
51. C. A. Gulvik, A. Buchan, Simultaneous Catabolism of Plant-Derived Aromatic Compounds Results in Enhanced Growth for Members of the Roseobacter Lineage. *Appl. Environ. Microbiol.* **79**, 3716–3723 (2013).
52. K. Attermeyer *et al.*, Enhanced bacterial decomposition with increasing addition of autochthonous to allochthonous carbon without any effect on bacterial community composition. *Biogeosciences*. **11**, 1479–1489 (2014).

VIII. APPENDIX: TABLES

Table 3.1. Organic carbon composition of the comparative treatments groups used to test for interactive effects.

Comparative treatment group	LOM[a]	NOM[b]	mix[c]
400 μM-C	400 μM-C LOM	2 mM-C NOM	400 μM-C LOM (16.67%) 2 mM-C NOM (83.33%)
40 μM-C	40 μM-C LOM	2 mM-C NOM	40 μM-C LOM (1.67%) 2 mM-C NOM (98.33%)
4 μM-C	4 μM-C LOM	2 mM-C NOM	4 μM-C LOM (0.17%) 2 mM-C NOM (99.83%)
1 μM-C	1 μM-C LOM	2 mM-C NOM	1 μM-C LOM (0.04%) 2 mM-C NOM (99.96%)

[a] labile organic matter, potential priming agent (either acetate, casamino acids + tryptophan, coumarate, or tryptone) added at one of four concentrations.

[b] natural organic matter (recalcitrant organic matter).

[c] experimental interactive effect conditions. Values in parentheses indicate the relative contribution of LOM and NOM to the total organic carbon pool.

Table 3.2. Genomic evidence for aromatic carbon catabolism pathways present in Roseobacter strains used in this study.

Aromatic catabolism pathway	Isolate					
	Citreicella sp. SE45[a]	*Phaeobacter* sp. Y4I[b]	*Roseovarius nubinhibens* ISM[b]	*Sagittula stellata* E-37[b]	*Sulfitobacter* sp. EE-36[b]	*Sulfitobacter* sp. NAS-14.1[b]
β-ketoadipate (protocatechuate)	+	+	+	+	+	+
Gentisate	+	-	-	+	-	-
Benzoyl-CoA	-	-	-	+	-	-
Phenylacetic acid	+	+	-	+	+	+
Homoprotocatechuate	-	+	-	+	-	-
Homogentisate	+	+	-	+	-	-

[a] genomic data derived from Chua & Buchan, in prep.

[b] genomic data derived from Buchan & Gonzalez, 2010 and Newton et al., 2010.

Table 3.3. ANOVA Tables for each three-way ANOVA performed for SE45 cell density by day.

Day	ANOVA Table
1	

	Df	Sum Sq	Mean Sq	F value	Pr(>F)
Treatment	1	0.14	0.145	3.866	0.05143
Concentration	3	46.41	15.470	413.565	< 2e-16
Carbon	3	0.90	0.300	8.011	6.19e-05
Treatment:Concentration	3	1.75	0.582	15.556	1.10e-08
Treatment:Carbon	3	0.46	0.154	4.110	0.00804
Concentration:Carbon	9	3.49	0.388	10.372	6.39e-12
Treatment:Concentration:Carbon	9	2.21	0.246	6.566	1.14e-07
Residuals	128	4.79	0.037		

2					
	Df	Sum Sq	Mean Sq	F value	Pr(>F)
Treatment	1	0.40	0.397	14.620	0.000211
Concentration	3	51.95	17.318	638.473	< 2e-16
Carbon	3	2.15	0.715	26.378	3.75e-13
Treatment:Concentration	3	0.96	0.320	11.812	7.92e-07
Treatment:Carbon	3	0.03	0.010	0.351	0.788349
Concentration:Carbon	9	3.22	0.358	13.203	1.90e-14
Treatment:Concentration:Carbon	9	0.31	0.034	1.271	0.259552
Residuals	119	3.23	0.027		

4					
	Df	Sum Sq	Mean Sq	F value	Pr(>F)
Treatment	1	0.67	0.666	28.833	3.70e-07
Concentration	3	32.28	10.760	465.940	< 2e-16
Carbon	3	0.75	0.250	10.836	2.23e-06
Treatment:Concentration	3	0.59	0.196	8.500	3.50e-05
Treatment:Carbon	3	0.47	0.156	6.738	0.000299
Concentration:Carbon	9	5.08	0.564	24.423	< 2e-16
Treatment:Concentration:Carbon	9	0.70	0.078	3.361	0.001020
Residuals	125	2.89	0.023		

7					
	Df	Sum Sq	Mean Sq	F value	Pr(>F)
Treatment	1	0.003	0.003	0.100	0.752828
Concentration	3	18.786	6.262	210.239	< 2e-16
Carbon	3	0.501	0.167	5.606	0.001219
Treatment:Concentration	3	0.387	0.129	4.332	0.006084
Treatment:Carbon	3	1.031	0.344	11.539	9.82e-07
Concentration:Carbon	9	3.736	0.415	13.939	2.23e-15
Treatment:Concentration:Carbon	9	1.001	0.111	3.734	0.000347
Residuals	126	3.753	0.030		

10					
	Df	Sum Sq	Mean Sq	F value	Pr(>F)
Treatment	1	0.020	0.020	0.643	0.424108
Concentration	3	15.930	5.310	172.504	< 2e-16
Carbon	3	0.643	0.214	6.959	0.000232
Treatment:Concentration	3	1.206	0.402	13.060	1.88e-07
Treatment:Carbon	3	0.399	0.133	4.321	0.006221
Concentration:Carbon	9	1.131	0.126	4.083	0.000133
Treatment:Concentration:Carbon	9	0.843	0.094	3.042	0.002571
Residuals	122	3.755	0.031		

14					
	Df	Sum Sq	Mean Sq	F value	Pr(>F)
Treatment	1	0.217	0.2170	4.739	0.031419
Concentration	3	9.323	3.1078	67.872	< 2e-16
Carbon	3	2.528	0.8427	18.405	6.48e-10
Treatment:Concentration	3	1.183	0.3942	8.609	3.14e-05
Treatment:Carbon	3	0.192	0.0638	1.394	0.247777
Concentration:Carbon	9	1.714	0.1904	4.158	0.000107
Treatment:Concentration:Carbon	9	0.420	0.0467	1.020	0.428257
Residuals	122	5.586	0.0458		

Table 3.4. ANOVA Tables for each three-way ANOVA performed for E-37 cell density by day.

Day	ANOVA table					
1		Df	Sum Sq	Mean Sq	F value	Pr(>F)
	Treatment	1	0.004	0.004	0.269	0.60469
	Concentration	3	28.549	9.516	649.373	< 2e-16
	Carbon	3	1.715	0.572	38.999	< 2e-16
	Treatment:Concentration	3	0.231	0.077	5.257	0.00192
	Treatment:Carbon	3	0.620	0.207	14.102	6.09e-08
	Concentration:Carbon	9	3.846	0.427	29.159	< 2e-16
	Treatment:Concentration:Carbon	9	1.185	0.132	8.983	2.67e-10
	Residuals	121	1.773	0.015		
2		Df	Sum Sq	Mean Sq	F value	Pr(>F)
	Treatment	1	0.017	0.017	0.466	0.49587
	Concentration	3	15.543	5.181	139.414	< 2e-16
	Carbon	3	4.327	1.442	38.814	< 2e-16
	Treatment:Concentration	3	0.419	0.140	3.755	0.01266
	Treatment:Carbon	3	0.633	0.211	5.682	0.00111
	Concentration:Carbon	9	2.536	0.282	7.581	7.93e-09
	Treatment:Concentration:Carbon	9	0.412	0.046	1.233	0.28075
	Residuals	126	4.682	0.037		
4		Df	Sum Sq	Mean Sq	F value	Pr(>F)
	Treatment	1	0.190	0.190	2.547	0.11314
	Concentration	3	11.964	3.988	53.593	< 2e-16
	Carbon	3	5.806	1.935	26.010	4.70e-13
	Treatment:Concentration	3	0.263	0.088	1.177	0.32142
	Treatment:Carbon	3	1.062	0.354	4.758	0.00359
	Concentration:Carbon	9	3.548	0.394	5.297	4.38e-06
	Treatment:Concentration:Carbon	9	2.056	0.228	3.070	0.00238
	Residuals	121	9.004	0.074		
7		Df	Sum Sq	Mean Sq	F value	Pr(>F)
	Treatment	1	2.255	2.255	57.171	7.73e-12
	Concentration	3	0.294	0.098	2.486	0.0637
	Carbon	3	11.767	3.922	99.457	< 2e-16
	Treatment:Concentration	3	0.142	0.047	1.200	0.3126
	Treatment:Carbon	3	1.493	0.498	12.618	2.97e-07
	Concentration:Carbon	9	5.829	0.648	16.422	< 2e-16
	Treatment:Concentration:Carbon	9	2.880	0.320	8.113	2.13e-09
	Residuals	124	4.890	0.039		
10		Df	Sum Sq	Mean Sq	F value	Pr(>F)
	Treatment	1	0.006	0.0056	0.101	0.7513
	Concentration	3	5.987	1.9957	35.790	< 2e-16
	Carbon	3	9.430	3.1432	56.370	< 2e-16
	Treatment:Concentration	3	1.624	0.5414	9.709	8.91e-06
	Treatment:Carbon	3	2.209	0.7364	13.206	1.71e-07
	Concentration:Carbon	9	4.080	0.4534	8.131	2.56e-09
	Treatment:Concentration:Carbon	9	1.112	0.1235	2.216	0.0255
	Residuals	118	6.580	0.0558		
14		Df	Sum Sq	Mean Sq	F value	Pr(>F)
	Treatment	1	0.110	0.110	2.995	0.0861
	Concentration	3	20.854	6.951	189.836	< 2e-16
	Carbon	3	3.376	1.125	30.733	7.69e-15
	Treatment:Concentration	3	0.212	0.071	1.926	0.1290
	Treatment:Carbon	3	1.602	0.534	14.582	3.62e-08
	Concentration:Carbon	9	1.500	0.167	4.551	3.55e-05
	Treatment:Concentration:Carbon	9	0.724	0.080	2.197	0.0267
	Residuals	121	4.431	0.037		

Table 3.5. Probability values[a] for monoculture interactive effect experimental data[ab].

	LOM Concentration			
LOM Source	**1 µM-C**	**4 µM-C**	**40 µM-C**	**400 µM-C**
Acetate	SE45 *Days 1,4,7* *p < 0.02*	SE45 *Days 2, 4* *p < 0.05*	SE45 **Days 2, 4, 7** ***p* < 0.02**	SE45 **Days 2, 7, 10** ***p* < 0.001**
	E-37 *Day 1* *p < 0.05*	E-37 *Days 7* *p < 0.001*	E-37 **Days 10, 14** ***p* < 0.02**	E-37 **Days 1, 2, 4, 10, 14** ***p* < 0.01**
Casamino Acids	SE45 **Day 10 *p* < 0.02** **Day 14 *p* < 0.03**	SE45 *Days 1, 2, 10* *p < 0.04*	SE45 *Day 1* *p < 0.04*	SE45 *Day 4 p < 0.001* **Day 7 *p* < 0.001**
	E-37 No significant Difference	E-37 **Days 1, 4, 14** ***p* < 0.05**	E-37 **Days 2, 14** ***p* < 0.02**	E-37 **Day 14** ***p* < 0.02**
Coumarate	SE45 No Significant Difference	SE45 *Days 1, 2, 4, 10* *p < 0.0*	SE45 *Day 2 p < 0.02* *Day 7 p < 0.03*	SE45 **Day 2** ***p* < 0.02**
	E-37 *Day 1 p < 0.02*	E-37 *Day 1, 4, 10, 14* *p < 0.03*	E-37 *Day 10 p < 0.05*	E-37 **Days 1, 10** ***p* < 0.03**
Tryptone	SE45 No Significant Difference	SE45 *Days 1, 2, 4* *p < 0.01*	SE45 *Days 1, 4, 7* *p < 0.03*	SE45 **Day 1 *p* < 0.0001**
	E-37 No Significant Difference	E-37 *Day 10 p < 0.01*	E-37 *Days 1, 7, 10* *p < 0.04*	E-37 *Days 1, 4, 7, 14* *p < 0.03*

[a] For each day, a three-way ANOVA was performed to determine whether differences in cell densities were being driven by treatment, concentration or source of LOM. *p*-values are adjusted to correct for the false discovery rate using the Benjamini-Hochberg correction.

[b] Synergistic interactive effect *p*-values are **bolded;** antagonistic interactive effect *p*-values are *italicized.*

Table 3.6. Average amount of CO_2 (µg) respired at the final time point for each treatment.

Priming Condition	composite	LOM	NOM	PRI
SE45 400 µM-C Acetate	1153.63±364.827	963.717±415.236	189.913±51.34	826.507±221.183
SE45 1 µM-C Casamino Acids	73.392±120.376	-116.52±125.775	189.913±51.34	262.938±62.971
SE45 4 µM-C Casamino Acids	300.515±109.887	63.31±31.565	158.66±168.965	190.108±84.88
SE45 40 µM-C Casamino Acids	591.737±130.242	354.532±227.549	158.66±168.965	695.018±358.06
SE45 400 µM-C Casamino Acids	1283.077±76.017	1045.872±53.908	158.66±168.965	550.017±155.514
SE45 400 µM-C Coumarate	974.442±42.406	784.529±61.918	189.913±51.34	777.093±161.755
E-37 400 µM-C Acetate	750.155±127.131	426.021±147.197	324.124±175.099	3972.297±94.832
E-37 1 µM-C Casamino Acids	162.746±74.709	8.503±5.228	154.243±78.244	227.88±86.904
E-37 4 µM-C Casamino Acids	134.837±17.065	-19.406±72.831	154.243±78.244	32.691±16.461
E-37 40 µM-C Casamino Acids	158.124±83.591	3.882±39.58	154.243±78.244	141.597±34.703
E-37 400 µM-C Casamino Acids	522.587±241.107	198.453±134.404	324.124±175.099	2817.886±13.645
E-37 400 µM-C Coumarate	1706.554±17.47	1289.158±78.092	324.124±175.099	3473.37+122.556
Constructed Community 400 µM-C Acetate	838.134±49.201	525.051±15.697	313.084±33.88	612.5 ±14.195
Constructed Community 1 µM-C Casamino Acids	591.669±16.165	293.568±20.93	298.101±4.8	542.647±27.325
Constructed Community 4 µM-C Casamino Acids	1000.828±32.324	702.726±28.378	298.101±4.8	1085.364±28.646
Constructed Community 40 µM-C Casamino Acids	1395.324±18.685	1097.223±23.485	298.101±4.8	723.123±40.75
Constructed Community 400 µM-C Casamino Acids	429.31±39.803	116.226±6.911	313.084±33.88	257.371±24.349
Constructed Community 400 µM-C Coumarate	1368.75±85.465	1055.666±73.568	313.084±33.88	952.786±23.311

Table 3.7. ANOVA Tables for each three-way ANOVA performed for the constructed community cell densityby day.

Day	ANOVA Table
1	

	Df	Sum Sq	Mean Sq	F value	Pr(>F)
Treatment	1	1.185e+11	1.185e+11	0.017	0.89602
Concentration	3	1.616e+16	5.386e+15	779.351	< 2e-16
Carbon	3	5.357e+15	1.786e+15	258.377	< 2e-16
Treatment:Concentration	3	8.469e+13	2.823e+13	4.085	0.00836
Treatment:Carbon	3	4.262e+13	1.421e+13	2.056	0.10956
Concentration:Carbon	9	1.266e+16	1.407e+15	203.509	< 2e-16
Treatment:Concentration:Carbon	9	9.517e+13	1.057e+13	1.530	0.14447
Residuals	124	8.570e+14	6.911e+12		

2					
	Df	Sum Sq	Mean Sq	F value	Pr(>F)
Treatment	1	4.666e+13	4.666e+13	2.004	0.160
Concentration	3	1.809e+16	6.032e+15	259.014	<2e-16
Carbon	3	3.011e+15	1.004e+15	43.106	<2e-16
Treatment:Concentration	3	1.146e+14	3.819e+13	1.640	0.185
Treatment:Carbon	3	4.151e+13	1.384e+13	0.594	0.620
Concentration:Carbon	9	8.992e+15	9.991e+14	42.903	<2e-16
Treatment:Concentration:Carbon	9	1.691e+14	1.879e+13	0.807	0.611
Residuals	101	2.352e+15	2.329e+13		

4					
	Df	Sum Sq	Mean Sq	F value	Pr(>F)
Treatment	1	4.026e+10	4.026e+10	0.003	0.95598
Concentration	3	8.482e+15	2.827e+15	214.882	< 2e-16
Carbon	3	3.295e+15	1.098e+15	83.482	< 2e-16
Treatment:Concentration	3	6.241e+13	2.080e+13	1.581	0.19732
Treatment:Carbon	3	1.543e+14	5.142e+13	3.908	0.01045
Concentration:Carbon	9	8.542e+15	9.491e+14	72.132	< 2e-16
Treatment:Concentration:Carbon	9	3.956e+14	4.395e+13	3.340	0.00108
Residuals	125	1.645e+15	1.316e+13		

7					
	Df	Sum Sq	Mean Sq	F value	Pr(>F)
Treatment	1	5.033e+13	5.033e+13	5.902	0.016597
Concentration	3	4.782e+15	1.594e+15	186.894	< 2e-16
Carbon	3	1.219e+15	4.063e+14	47.648	< 2e-16
Treatment:Concentration	3	1.778e+14	5.925e+13	6.948	0.000236
Treatment:Carbon	3	1.985e+13	6.617e+12	0.776	0.509620
Concentration:Carbon	9	3.138e+15	3.487e+14	40.884	< 2e-16
Treatment:Concentration:Carbon	9	8.561e+13	9.513e+12	1.115	0.357067
Residuals	121	1.032e+15	8.528e+12		

10					
	Df	Sum Sq	Mean Sq	F value	Pr(>F)
Treatment	1	1.178e+14	1.178e+14	12.658	0.000532
Concentration	3	6.171e+15	2.057e+15	221.110	< 2e-16
Carbon	3	2.062e+15	6.874e+14	73.895	< 2e-16
Treatment:Concentration	3	5.647e+14	1.882e+14	20.234	1.00e-10
Treatment:Carbon	3	2.959e+14	9.865e+13	10.604	2.99e-06
Concentration:Carbon	9	5.634e+15	6.260e+14	67.292	< 2e-16
Treatment:Concentration:Carbon	9	6.062e+14	6.736e+13	7.241	2.14e-08
Residuals	123	1.144e+15	9.303e+12		

14					
	Df	Sum Sq	Mean Sq	F value	Pr(>F)
Treatment	1	7.619e+13	7.619e+13	15.55	0.000144
Concentration	3	4.007e+15	1.336e+15	272.65	< 2e-16
Carbon	3	1.438e+15	4.795e+14	97.88	< 2e-16
Treatment:Concentration	3	3.158e+14	1.053e+14	21.48	6.01e-11
Treatment:Carbon	3	1.636e+14	5.453e+13	11.13	2.07e-06
Concentration:Carbon	9	3.337e+15	3.708e+14	75.69	< 2e-16
Treatment:Concentration:Carbon	9	4.453e+14	4.948e+13	10.10	4.33e-11
Residuals	106	5.193e+14	4.899e+12		

Table 3.8. Probability values[a] for constructed community interactive effect experimental data[b].

	LOM Concentration			
LOM Source	**1 µM-C**	**4 µM-C**	**40 µM-C**	**400 µM-C**
Acetate	*Days 1, 4, 7 $p < 0.05$*	*Days 1, 10, 14 $p < 0.04$*	*Day 10 $p < 0.01$*	**Days 4, 10, 14 $p < 0.05$**
Casamino Acids	*Days 1, 2, 4, 7, 10, 14 $p < 0.005$*	No Significant Difference	*Days 1, 14 $p < 0.001$*	*Day 4 $p < 0.01$* **Day 10 $p < 0.006$**
Coumarate	*Days 1, 2, 7, 10, 14 $p < 0.001$*	No Significant Difference	No Significant Difference	**Days 1, 7 $p < 0.001$**
Tryptone	*Days 1, 2, 7, 10, 14 $p < 0.001$*	*Days 1, 4 $p < 0.04$*	**Day 10 $p < 0.001$**	**Days 10, 14 $p < 0.003$**

[a] For each day, a three-way ANOVA was performed to determine whether differences in cell densities were being driven by treatment, concentration or source of LOM. *p*-values are adjusted to correct for the false discovery rate using the Benjamini-Hochberg correction.

[b] Synergistic interactive effect *p*-values are **bolded;** antagonistic interactive effect *p*-values are *italicized.*

Table 3.9. ANOVA tables for each three-way ANOVA performed for constructed community alpha diversity estimates by day.

Day	ANOVA Table				
1		Df	Sum Sq	Mean Sq	F value	Pr(>F)
	Treatment	1	1.89	1.89	8.115	0.005141
	Concentration	3	110.94	36.98	158.782	< 2e-16
	Carbon	3	28.73	9.58	41.123	< 2e-16
	Treatment:Concentration	3	0.64	0.21	0.922	0.432564
	Treatment:Carbon	3	1.73	0.58	2.479	0.064284
	Concentration:Carbon	9	16.19	1.80	7.725	5.8e-09
	Treatment:Concentration:Carbon	9	8.51	0.95	4.062	0.000138
	Residuals	124	28.88	0.23		
2		Df	Sum Sq	Mean Sq	F value	Pr(>F)
	Treatment	1	0.39	0.39	1.037	0.310547
	Concentration	3	125.41	41.80	110.947	< 2e-16
	Carbon	3	13.83	4.61	12.235	4.71e-07
	Treatment:Concentration	3	1.60	0.53	1.418	0.240679
	Treatment:Carbon	3	0.58	0.19	0.516	0.671937
	Concentration:Carbon	9	13.47	1.50	3.973	0.000182
	Treatment:Concentration:Carbon	9	3.29	0.37	0.971	0.467301
	Residuals	122	45.97	0.38		
4		Df	Sum Sq	Mean Sq	F value	Pr(>F)
	Treatment	1	0.00	0.003	0.015	0.904
	Concentration	3	59.15	19.718	103.707	< 2e-16
	Carbon	3	7.13	2.377	12.500	3.39e-07
	Treatment:Concentration	3	4.75	1.583	8.328	4.34e-05
	Treatment:Carbon	3	1.05	0.348	1.832	0.145
	Concentration:Carbon	9	10.01	1.112	5.851	8.91e-07
	Treatment:Concentration:Carbon	9	9.34	1.037	5.456	2.67e-06
	Residuals	124	23.58	0.190		
7		Df	Sum Sq	Mean Sq	F value	Pr(>F)
	Treatment	1	0.37	0.365	3.344	0.0699
	Concentration	3	39.20	13.066	119.573	< 2e-16
	Carbon	3	5.25	1.752	16.030	7.74e-09
	Treatment:Concentration	3	1.19	0.398	3.639	0.0148
	Treatment:Carbon	3	1.04	0.348	3.186	0.0263
	Concentration:Carbon	9	6.13	0.681	6.232	3.36e-07
	Treatment:Concentration:Carbon	9	4.19	0.465	4.258	8.15e-05
	Residuals	121	13.22	0.109		
10		Df	Sum Sq	Mean Sq	F value	Pr(>F)
	Treatment	1	10.731	10.731	125.149	< 2e-16
	Concentration	3	30.257	10.086	117.623	< 2e-16
	Carbon	3	7.102	2.367	27.608	1.01e-13
	Treatment:Concentration	3	1.474	0.491	5.730	0.00105
	Treatment:Carbon	3	0.191	0.064	0.743	0.52814
	Concentration:Carbon	9	4.403	0.489	5.705	1.36e-06
	Treatment:Concentration:Carbon	9	3.389	0.377	4.391	5.46e-05
	Residuals	123	10.547	0.086		
14		Df	Sum Sq	Mean Sq	F value	Pr(>F)
	Treatment	1	19.789	19.789	215.291	< 2e-16
	Concentration	3	17.150	5.717	62.191	< 2e-16
	Carbon	3	25.118	8.373	91.088	< 2e-16
	Treatment:Concentration	3	5.414	1.805	19.635	1.88e-10
	Treatment:Carbon	3	1.483	0.494	5.379	0.001640
	Concentration:Carbon	9	10.376	1.153	12.543	6.26e-14
	Treatment:Concentration:Carbon	9	2.833	0.315	3.425	0.000867
	Residuals	122	11.214	0.092		

IX. APPENDIX: FIGURES

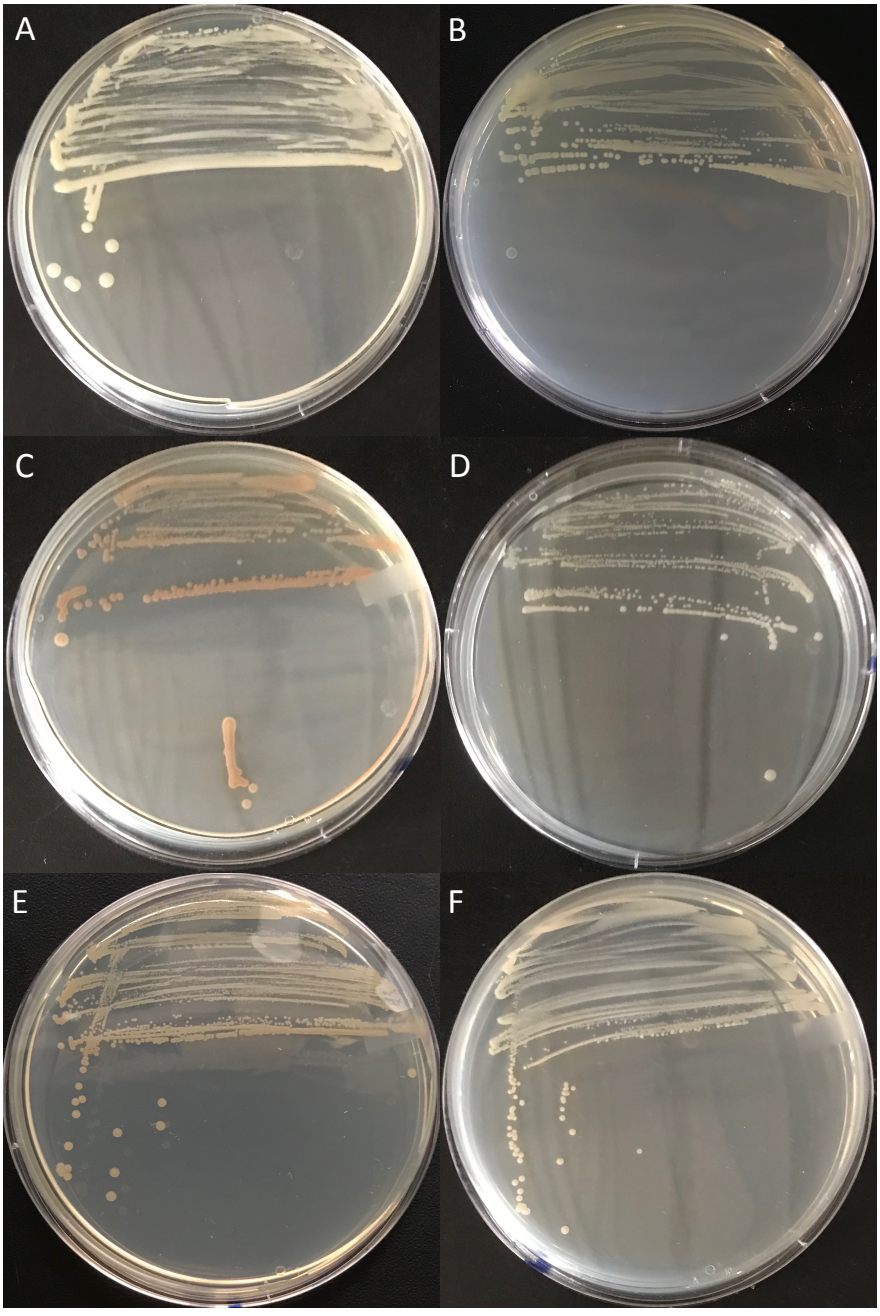

Figure 3.1. Colony morphologies of the bacterial isolates used in the constructed community.

A. *Citreicella* sp. SE45 B. *Phaeobacter* sp. Y4I C. *Roseovarius nubinhibens* ISM D. *Sagittula stellata* E-37 E. *Sulfitobacter* sp. EE-36 F. *Sulfitobacter* sp. NAS-14.1

Figure 3.2. Biomass produced in μg-C for all inocula.

Cell density (CFU/mL) was converted to biomass in μg-C by multiplying by a conversion factor for the amount of C in a bacterial cell (149 fg-C) and the volume of culture in the experiment (10 mL). Points represent the mean (n=3-5); error bars represent one standard deviation from the mean. Seeding densities for A. SE45, B. E-37, and C. constructed community were 1.51×10^4 CFU/mL ($\pm 5.1 \times 10^3$), 4.23×10^4 CFU/mL ($\pm 9 \times 10^3$), and 7.01×10^3 CFU/mL ($\pm 2.6 \times 10^3$), respectively.

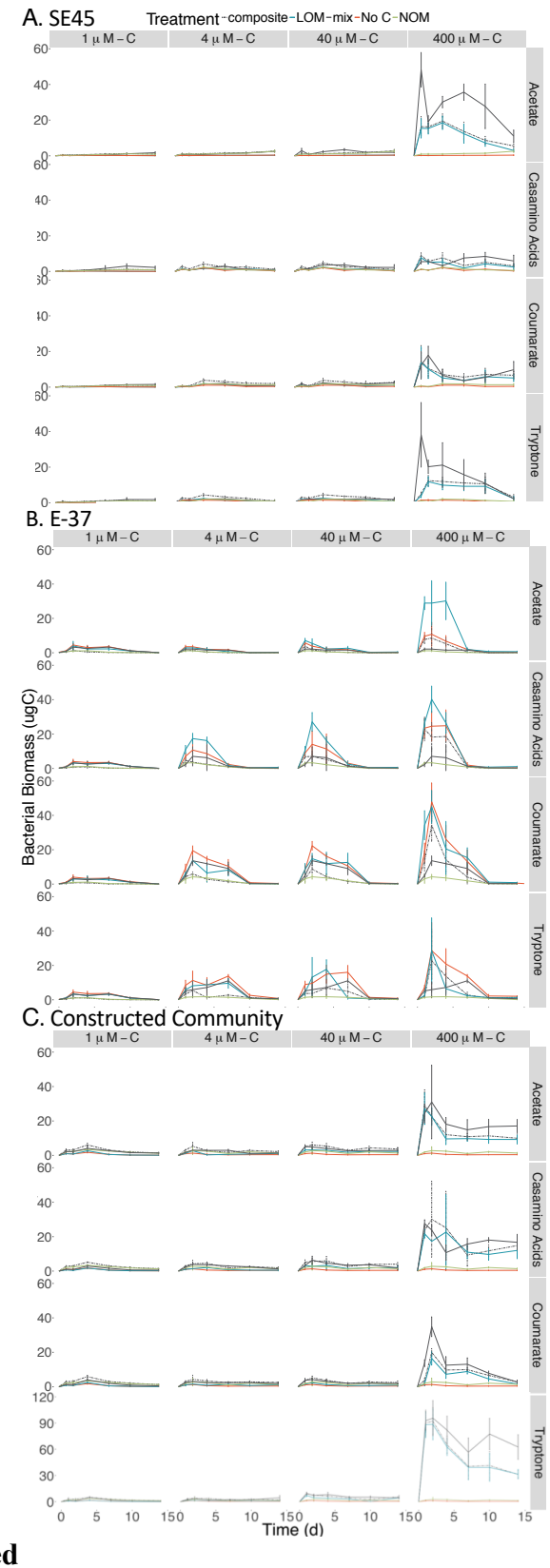

Figure 3.2. Continued

Figure 3.3. CO_2 production from SE45 and E-37 monocultures when provided low concentrations of casamino acids and 400 µM-C acetate, casamino acids, and coumarate.

Composite data are shown in grey; PRI data in orange. Panel A contains data for the low concentrations of casamino acids, and Panel B contains data for 400 µM-C acetate, casamino acids, and coumarate. The average of the No C control was subtracted from all replicates. Points represent the mean (n=2-3); error bars represent one standard deviation from the mean. Red plus signs indicate a significant positive priming effect ($p < 0.05$), blue minus signs indicate a negative priming effect ($p < 0.05$). The seeding densities for SE45 and E-37 were 3.05×10^4 CFU/mL ($\pm 7.97 \times 10^3$) and 1.43×10^4 CFU/mL ($\pm 4.71 \times 10^3$), respectively.

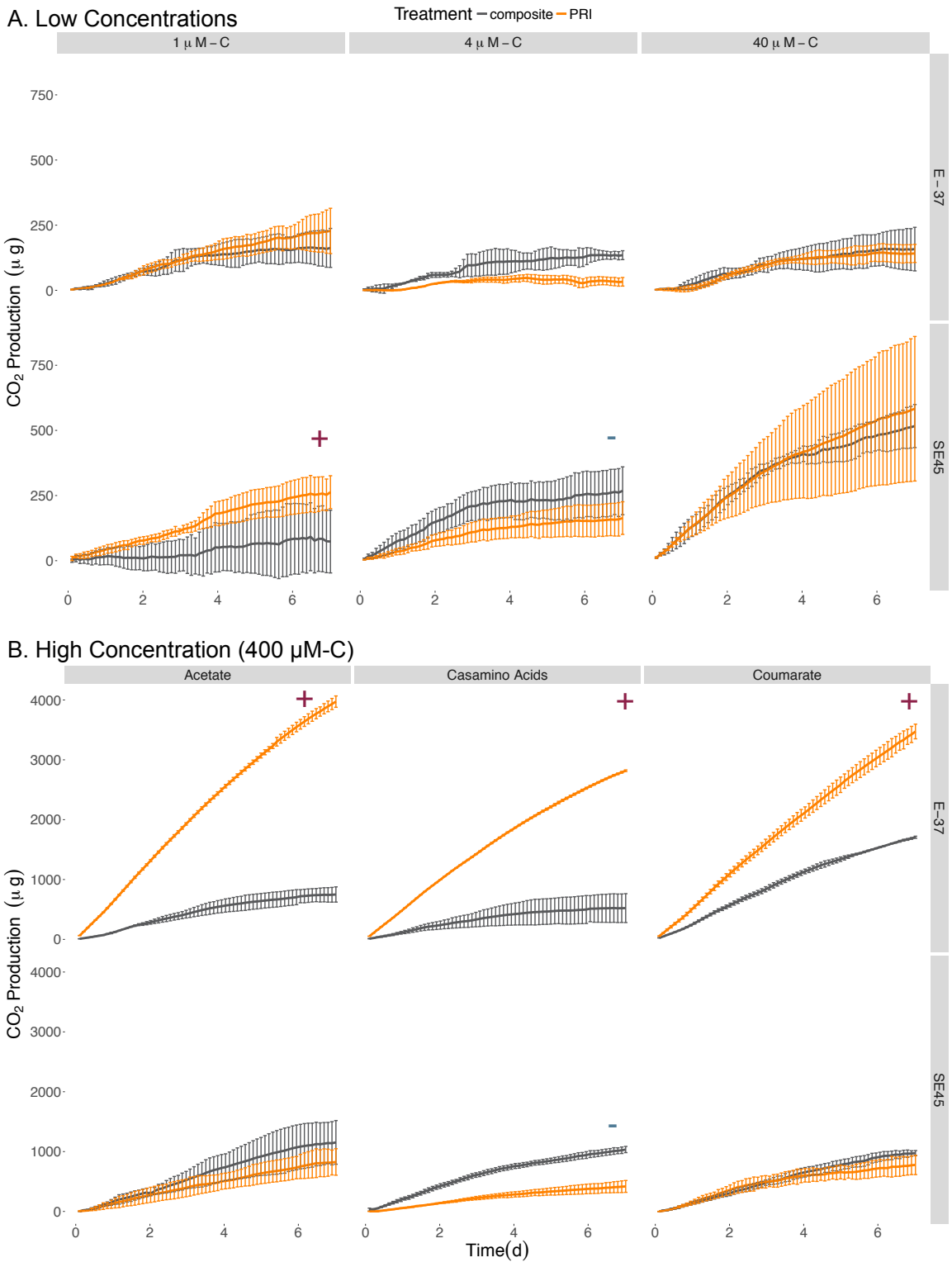

Figure 3.3. Continued

Figure 3.4. Viable counts and community composition of the constructed communities from LOM and mix treatments: acetate, casamino acids, coumarate and tryptone.

Individual strains are color-coded according to the key. Points represent the mean (n=3-5) while error bars represent one standard deviation from the mean. Red plus signs indicate a significant synergistic interactive effect ($p < 0.05$), blue minus signs indicate an antagonistic interactive effect ($p < 0.05$). The community composition is displayed in relative abundance with the LOM treatment displayed above its corresponding mix treatment. Seeding density for the constructed community was 7.01×10^3 CFU/mL ($\pm 2.6 \times 10^3$.

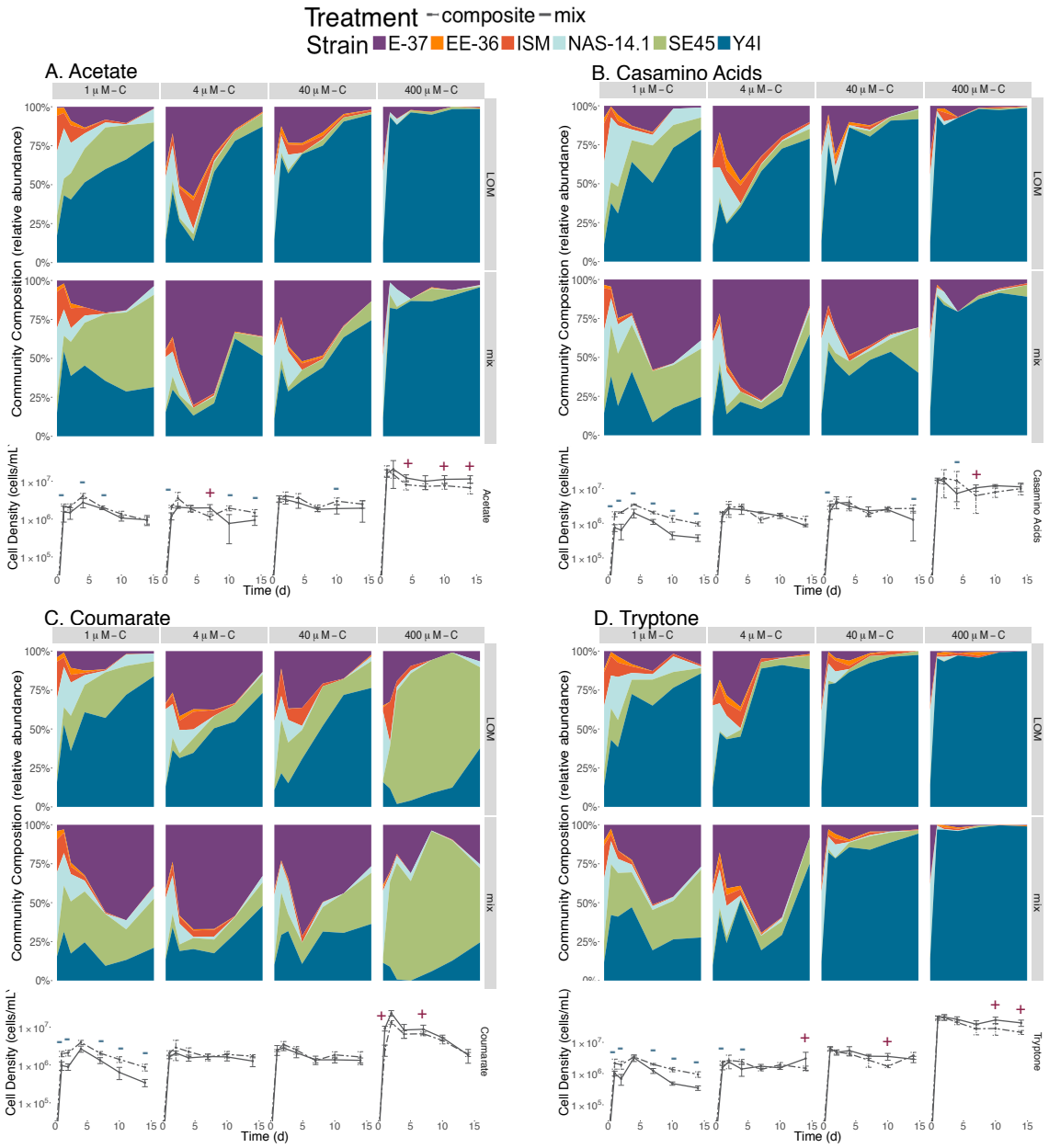

Figure 3.4. Continued

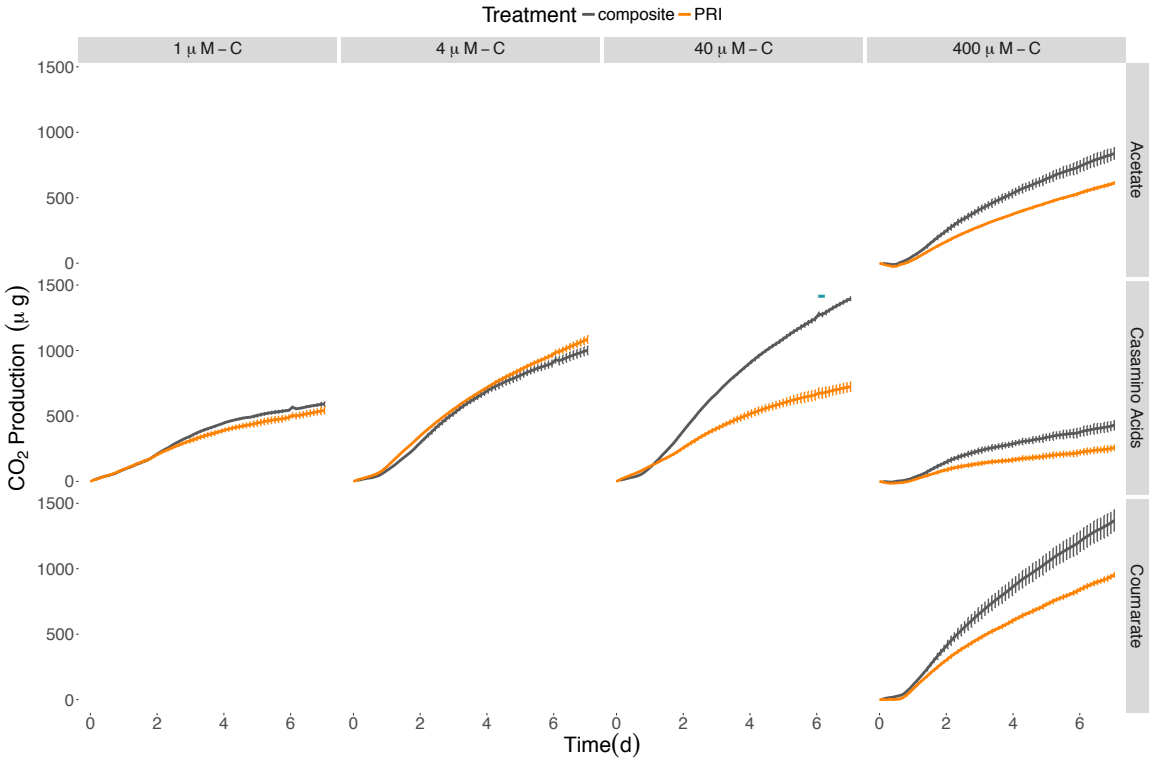

Figure 3.5. CO_2 production from the constructed community when provided different sources and concentrations of LOM.

Composite data are shown in grey; PRI data in orange. The average of the No C control was subtracted from all replicates. Points represent the mean (n=2-3) while error bars represent one standard deviation from the mean. Red plus signs indicate a significant positive priming effect ($p < 0.05$) and blue minus signs indicate a negative priming effect ($p < 0.05$). The seeding density was 5.13 x 10^3 CFU/mL (± 3.73 x 10^3).

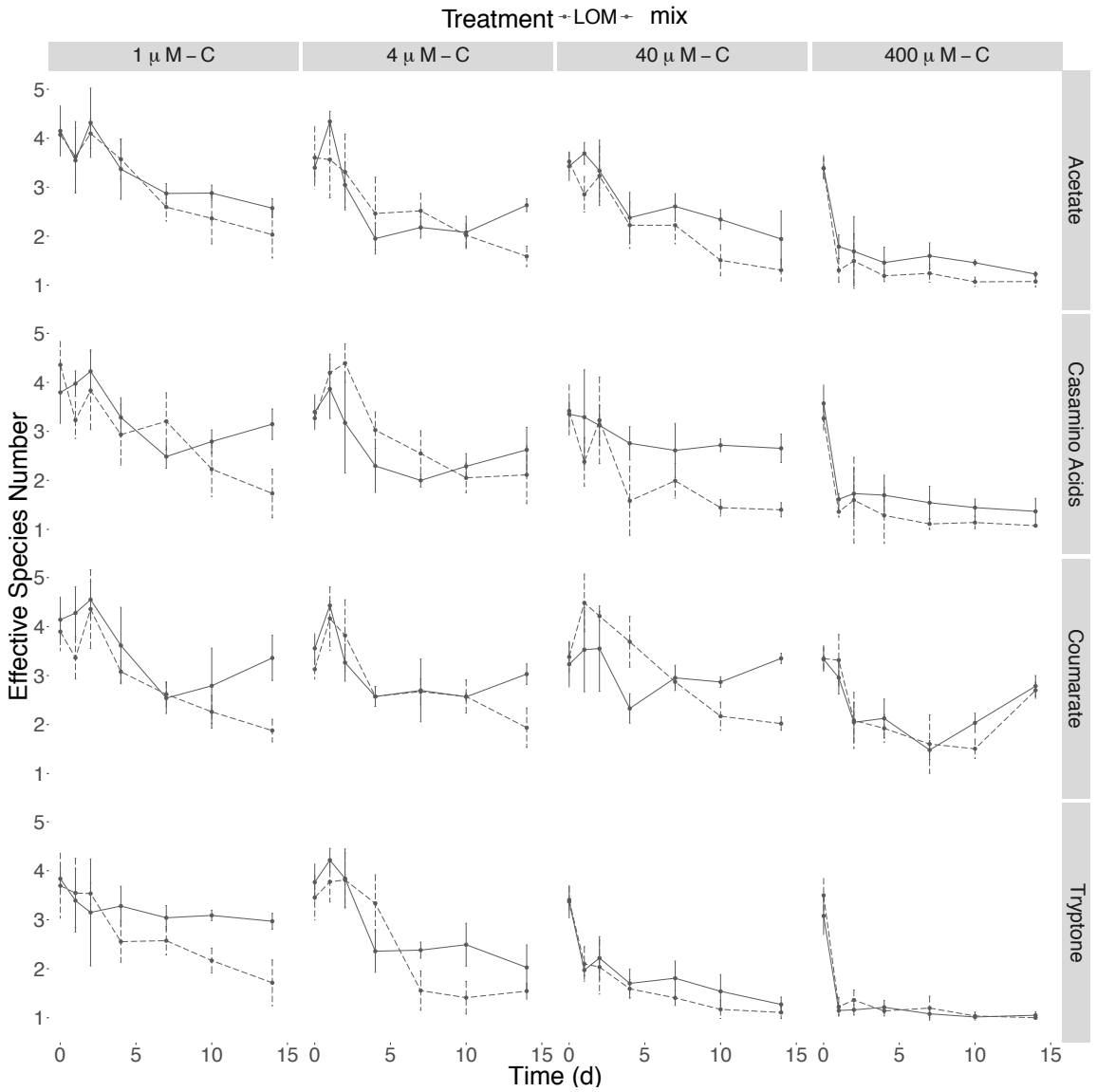

Figure 3.6. Alpha diversity of constructed community under interactive effect conditions.

Shannon entropy was calculated for each replicate at each time point. Shannon entropy was converted to Hill numbers or effective species number. Points represent the average of 3-5 replicates, and error bars represent one standard deviation from the mean. Dashed lines represent the LOM cultures while the solid lines represent the mixed carbon cultures.

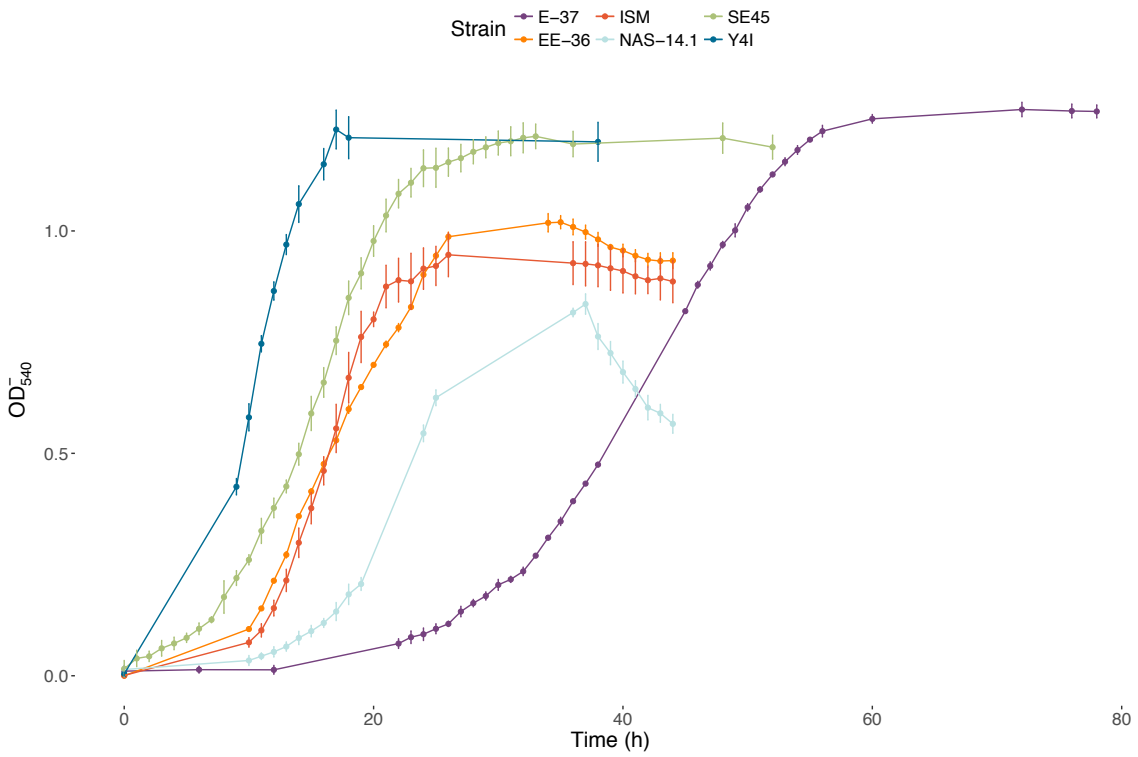

Figure 3.7. Growth curves of the strains used in this study when grown as monocultures in minimal media supplemented with 2 mM-C tryptone.

Points represent the mean of three biological replicates and error bars represent one standard deviation from the mean.

CHAPTER FOUR - THE INFLUENCE OF TIDAL CYCLES ON THE DEGRADATION OF TERRESTRIALLY-DERIVED, DISSOLVED ORGANIC MATTER IN A TEMPERATE SALT MARSH.

AUTHOR CONTRIBUTIONS

Nine individuals significantly contributed to this chapter: Lauren Quigley, Bridget S. O'Banion, Christina Codden, Megan Thompson, Zachary Tait, Thais Bittar, Aron Stubbins, Andrew D. Steen, and Alison Buchan. Conceived the experiment: AS, ADS, AB. Collected and analyzed environmental data: CC, ZT, AS. Collected and analyzed measurements of bulk biological activity: MT, ZT, TB. Collected and extracted nucleic acids: LQ, AB. Analyzed community sequencing data: LQ. Wrote the manuscript: LQ, CC, AS, TB, AB.

I. ABSTRACT

Terrestrially-derived, dissolved organic matter (t-DOM) constitutes one of the largest pools of reduced carbon on Earth with approximately $2.5x10^{14}$ g-C flowing into the coastal oceans annually. This pool of carbon is largely composed of vascular plant detritus in the form of humic and fulvic acids which are enriched in aromatic moieties, contributing to their resistance to biodegradation. However, most chemical tracers diagnostic of t-DOM (e.g. lignin-derived phenols) are removed before reaching the open oceans, suggesting that this material is transformed in coastal margins. In order to gain a more mechanistic understanding of how these communities degrade t-DOM we generated paired metagenomes and metatranscriptomes from the surface water of a salt marsh and collected data on the amount and quality of dissolved organic carbon (DOC) flowing through the marsh over a period of 26 hours (two full tidal cycles and one diel cycle). We found that DOC, lignin, cell density, and bacterial production all significantly influence clustering in the metatranscriptomic functional profile. Metatranscriptomic analysis indicated that the microbial community was actively using specific pathways for degradation of select components of t-DOM. In particular, transcripts showing greatest homology to *boxB*, the ring-cleaving gene of the benzoyl-CoA pathway found in some marine bacteria, class II lignin-modifying peroxidases, and lytic polysaccharide monooxygenases were enriched in estuarine communities throughout the diel cycle. The community composition of the microbes contributing genes and transcripts to these enzymes varied between enzyme class but were conserved across the tidal cycle, with some overlap in taxonomic affiliation between *boxB* and the lignin peroxidase gene sets. These data suggest functional niches within the microbial community to transform different components of t-DOM.

II. INTRODUCTION

Saltmarsh-dominated estuarine systems are of critical importance to the global carbon cycle as they are hotspots of net primary productivity and are intermediaries in the flux of dissolved and particulate organic matter from terrestrial to marine environments (*1*). The salt marshes of the Southeastern United States are dominated by a monoculture of the cordgrass *Spartina alterniflora* and have among the highest net primary productivity rates on Earth ranging from 0.2 to 2.25 kg C m^{-2} yr^{-1} (*2*, *3*). Given there are very few metazoan grazers in these systems, the majority of carbon turnover in these systems is mediated by microbial communities. Thus, these systems excellent models for the study of study microbial decomposers (*2*, *4*, *5*).

The rivers flowing through Southeastern US coastal marshes carry 400 to 2300 μM of dissolved organic carbon (DOC), approximately 75% of which is terrestrially-derived, dissolved organic matter (t-DOM) (*6*). T-DOM is highly enriched in aromatic moieties, which is largely derived from vascular plant detritus (*7*). However, very low concentrations of t-DOM are found in the open oceans, suggesting that the majority of t-DOM is removed in coastal margins (*8*, *9*). While photodegradation and burial contribute to this removal, t-DOM is biodegraded in the coastal margins (*10*). The mechanisms by which the microbial community transforms components of this carbon pools are largely unknown. However, it is likely the tidal cycle plays a role as the tidal amplitude in these systems is 2-3 m and there is a large shift from a more marine influenced microbial community and dissolved organic matter (DOM) pool at high tide to a more riverine influenced system at low tide. The lack of studies examining estuarine communities over the tidal cycle contributes to this knowledge gap.

The vast majority of studies focused on microbial carbon transformations in coastal transitions employ a spatial sampling regime that follows a salinity gradient from fresh to marine water. To our knowledge, there are only two studies that have employed a static sampling program to examine the microbial community of a coastal marsh over the course

of a tidal cycle; both studies focus solely on community composition (*11*, *12*). Salinity gradient studies have shown taxonomically distinct communities between riverine and marine communities; estuaries represent a transition zone where these two communities mix and potentially interact (*13*, *14*). We hypothesize that the degradation of t-DOM results from the combined metabolic efforts of microbes from riverine and marine communities.

The carbon in coastal salt marshes is highly enriched in aromatic moieties because of the t-DOM flowing in from riverine systems and the fresh *S. alterniflora* biomass being produced in the marsh. Soluble degradation products of *S. alterniflora* decay constitute up to 44% of the C in the bulk DOC pool in these systems, roughly half of which is lignin (*15*). Given that the degradation products of vascular plant decay dominate the DOC pool we have chosen to focus on the gene expression profiles of genes encoding aromatic carbon catabolism and carbohydrate metabolism functions. Traditionally, fungi are thought to be predominantly responsible for breaking down the high molecular weight (HMW) fraction of plant matter into lower molecular weight compounds which are then available to both bacteria and fungi (*16*). Previous work done in these systems has shown that bacteria also contribute to the breakdown of HMW lignin and that bacteria and fungi co-occur on decaying *S. alterniflora* biomass (*17*, *18*). The datasets described here will provide a more comprehensive understanding on how the degradation of recalcitrant, plant-derived C occurs in these systems, specifically by allowing us to tie function to taxonomic groups. Further, we will be able to assess if and how the tidal cycle influences these processes.

In this study, we assess the inventory of microbial genes and their expression over a semidiurnal tide cycle in Groves Creek Marsh, GA. The analyses address three main questions: 1) How does microbial community structure and function change as a result of tidal stage? 2) How does tidal stage influence t-DOM concentration in the marsh and consequently the microbial signatures of t-DOM degradation? 3) What other metabolic pathways are the microbial community using to degrade t-DOM?

III. MATERIALS AND METHODS

Study Site

Groves Creek Marsh (31.972, -81.028), a temperate salt marsh fringing Skidaway Island, GA served as the field site for this observational study. Samples were collected every two hours and four minutes to evenly sample across two tidal cycles and one diurnal cycle. Time points refer to a specific sampling interval over the 26-hour time course. Tidal amplitude in these systems is between two and three meters. Environmental and summary data are provided in Table 4.1.

Microbial community analysis sample collection

July 16-17, 2014, microbial cells from surfaces water were collected by filtration. All samples were collected from the surface water by pumping water into a 20 L carboy. Water was first filtered through a GF/D glass fiber filter (~2.7 μM pore size, Whatman, GE Healthcare Life Sciences, Marlborough, MA); 500 mLs of the filtrate was passed through a 0.22 μM pore size, 47 mm diameter filter (Millipore, Burlington, MA). Filtration was completed within 30 min of sample collection. After filtration all filters were placed in cryovials and flash frozen in liquid nitrogen. The samples were stored at -80 C until processing.

Microbial community analysis sample processing

For all samples the filters were thawed and placed in a 2 mL tube with 0.3 g glass and zirconia beads (0.2 g glass and 0.1 g zirconia), 0.75 mL CTAB extraction buffer, 0.75 mL phenol:chloroform:isoamyl alcohol (25:24:1, pH 8), internal standards (*19*), proteinase K, 10% SDS, and lysozyme for DNA extractions. Samples were vortexed for 10 min to lyse the cells. For metatranscriptomic samples the tubes were centrifuged for 10 min at 10,000 rpm and 4° C. The lysates were transferred to a sterile 1.5 mL microcentrifuge tube and mixed with 0.75 mL chloroform:isoamyl alcohol (24:1). The aqueous phase was added to a sterile 1.5 mL microcentrifuge with $MgCl_2$, sodium acetate, and isopropanol. This solution was incubated at -80° C for 1.5 hours and then centrifuged at 4° C for 45 min at

10,000 rpm. The supernatant was discarded and the RNA was washed with 70% EtOH twice. Following RNA extraction Turbo DNase was used to remove residual DNA. For metagenomic samples the lysate was centrifuged at 5,000 rpm for 5 min and washed twice with 0.5 mL of chloroform:isoamyl alcohol by centrifugation at 15,000 rpm for 5 min. The upper aqueous phase was incubated with isopropanol at room temperature for 2 hrs. The DNA was precipitated by centrifugation at 10,000 rpm for an hour and washed with 70% EtOH twice.

All sequencing, assembly, and annotation was performed by the DOE Joint Genome Institute. JGI generated 16S rRNA libraries, metagenomes, and metatranscriptomes. Plate-based DNA library preparation for Illumina sequencing was performed on the PerkinElmer Sciclone NGS robotic liquid handling system using Kapa Biosystems library preparation kit. DNA was sheared to 300 base pairs (bp) using the Covaris LE220 focused-ultrasonicator and size selected using SPRI beads (Beckman Coulter). The fragments were treated with end-repair, A-tailing, and ligation of Illumina compatible adapters (IDT, Inc) containing a unique molecular index barcode for each sample library. qPCR was used to determine the concentration of the libraries and were sequenced on the Illumina HiSeq-2500 to yield 150 bp paired-end reads at the DOE Joint Genome Institute. Quality filtered metagenomic sequences for each sample were assembled with metaSPAdes (version 3.10.1; (*20*) and all contigs >200 bp were uploaded and annotated by the Integrated Microbial Genomes (IMG) pipeline (*21*). For metatranscriptomes, a plate-based RNA sample preparation was performed on the PerkinElmer Sciclone NGS robotic liquid handling system using the Illumina Ribo-Zero rRNA Removal Kit (bacteria) and the TruSeq Stranded Total RNA HT sample prep kit following the protocol outlined by Illumina. Total RNA starting material consisted of 100 ng per sample and included 10 cycles of PCR for library amplification. Illumina sequencing was performed as described for metagenome samples.

Quality filtered metatranscriptomic sequences for each sample were assembled with Megahit (version 1.10.6, *32*), and all contigs > 200 bp were annotated as described for the

metagenome samples. Datasets which had assemblies for which the N50 was greater than three standard deviations from mean were not included in further analyses (Tables 4.2 and 4.3) Resultant assemblies were combined with coding sequences (CDS) using bedtools2 (version 2.27.0, *33*) in order to generate an assembly with CDS embedded. Quality controlled raw reads were mapped to the assembly with gene features using bowtie2 (version 2.2.9, *34*). Coverage information on the number of reads mapping to each contig was generated using pileup in the BBmap suite of tools. The coverage information was used to normalize read counts to account for the length of reads and the length of CDS. Read counts within KEGG ortholog groups (KO) were summed and normalized as read counts per million mapped to KO-annotated contigs (genes per million [GPM], transcripts per million [TPM], *35*, *36*). GPM and TPM were also used in taxonomic analyses.

Community sequencing data analysis

All data analysis and visualization was performed using the R statistical platform and ggplot2 package (*27*, *28*). Metacoder was used to plot taxonomic trees showing changes in community composition between low tide and high tide (*29*). All multivariate statistics and ordination were performed with Vegan (*30*). DESeq2 was used to calculate significant differences between KO functions and taxonomic lineages present at high versus low tide (*31*). Taxonomic lineages and KEGG ortholog groups that appeared at only a single time point were removed from analyses, and only those annotations which were a 75% or greater match to the reference were used in analyses. Assemblies were aligned to a database for automated Carbohydrate-active enzyme annotation (dbCAN) using the sequence aligner DIAMOND (*32*, *33*). Only alignments which had an e-value less than $1x10^{-6}$, an alignment length of greater than or equal to 30 amino acids, and a percentage of identical match greater than or equal to 75. For the purposes of these analyses we used a conservative definition of actively transcribed in which the TPM for a given gene had to be greater than the corresponding GPM. Raw data and scripts are posted at http://github.com/lnmquigley.

Environmental and summary data collection

All plastic and glassware were pre-cleaned by rinsing 5 times with ultrapure water (MilliQ, Millipore, Burlington, MA), soaking in pH 2 ultrapure water (2 ppt 6N hydrochloric acid), re-rinsing 5 times with ultrapure water. Once dry, glassware was baked at 450°C for 8 hours.

Samples were collected from approximately 1 m depth using a hand deployed Niskin bottle. Samples for dissolved constituents were filtered on site through 0.2 μm Polycap filters within minutes of collection and then transported to the laboratory for further processing. Samples for flow cytometry were transported to the laboratory and fixed using 25% glutaraldehyde. Samples for additional microbial analyses were returned to the laboratory, which was within 10 minutes' drive of the field site. Salinity was measured for discrete samples collected in the field using a handheld multiparameter probe (YSI, Pro2030). Depth was recorded using a YSI 600OMS V2 Optical Monitoring Sonde deployed on the creek bed.

Dissolved organic carbon concentrations

Following filtration, sample aliquots were transferred to pre-combusted 40 mL glass vials, acidified to pH 2 (hydrochloric acid), and analyzed for non-purgable organic carbon using a Shimadzu TOC-VCPH analyzer fitted with a Shimadzu ASI-V autosampler. In addition to potassium hydrogen phthalate standards, aliquots of deep seawater reference material, Batch 10, Lot# 05-10, from the Consensus Reference Material (CRM) Project were analyzed to check the precision and accuracy of the DOC analyses. Analyses of the CRM deviated by <5% from the reported value for these standards (41 to 44 mM-DOC; http://yyy.rsmas.miami.edu/groups/biogeochem/Table1.htm). Routine minimum detection limits in the investigator's laboratory using the above configuration are 2.8±0.3 μM-C and standard errors are typically 1.7±0.5% of the DOC concentration (*34*). Lignin was measured using the cupric oxide oxidation method (*35*) and dissolved black carbon was measured using the BPCA method (*36*–*38*).

Colored dissolved organic matter

Filtered samples (non-acidified) were placed in a 1 cm quartz absorbance cell situated in the light path of an Agilent 8453 ultraviolet-visible spectrophotometer and CDOM absorbance spectra were recorded from 190 to 800 nm. Ultrapure water provided a blank. Blank corrected absorbance spectra were corrected for offsets due to scattering and instrument drift by subtraction of the average absorbance between 700 and 800 nm (*39*). Data output from the spectrophotometer were in the form of dimensionless absorbance (i.e. optical density, OD) and were subsequently converted to the Napierian absorption coefficient, *a* (m^{-1}) (*40*). If sample absorbance (OD) exceeded 2 at 250 nm, samples were diluted tenfold with ultrapure water and reanalyzed. Specific UV absorbance at 254 nm ($SUVA_{254}$; L mg-C^{-1} m^{-1}), an indicator of DOM aromaticity defined as the Decadic absorption coefficient at 254 nm (m^{-1}) normalized to DOC (mg-C L^{-1}) (*41*) was calculated along with spectral slope over the range 275 to 295 nm ($S_{275\text{-}295}$) (*42*). Spectral slope values are reported as positive values.

Nutrient analysis

Single samples for inorganic nutrient analysis were filtered through combusted 0.7 µm GF/F filters. The filtrate was collected into acid-washed polycarbonate bottles and immediately frozen at -20°C. Samples were analyzed for NO_x, NH_4, PO_4 and SiO_2 using a Lachat Quickchem FIA+ 8000 nutrient analyzer, following established colorimetric protocols (*43*, *44*).

Bacterial Production

Bacterial production was determined by tritiated leucine (^{3}H-leucine) incorporation (*45*). 1.5 mL of sample was placed into 2 mL centrifuge tubes. Killed controls consisted of samples fixed at the start of the incubations by the addition of 100% trichloroacetic acid (TCA; final concentration 1:15 TCA:sample by volume). Triplicate live samples and the killed controls were incubated in the dark for approximately 2 hours (exact time was used in rate calculations for each incubation) after the addition of ^{3}H-leucine (final concentration 40 nM). Incubation temperatures were within 5°C of in situ water temperatures at the time

of sample collection. Live samples were fixed by the addition TCA to the same concentration at the end of incubations. Once killed, samples were frozen at -20°C until further processing. Once samples were ready to be analyzed, they were centrifuged for 15 minutes and the supernatant decanted. 1 mL of 5% TCA solution was then added to the centrifuge tubes before re-centrifugation for 5 minutes and decanting. 1 mL of 80% ethanol solution was then added to the centrifuge tubes before re-centrifugation for 5 minutes and decanting. Tubes were then left to dry for >12 hours to ensure all ethanol had evaporated. 1 mL of scintillation cocktail (Ecoscint) was then added before samples were vortex mixed for 10 seconds. Tubes were then placed in to a liquid scintillation counter (Beckman LS-6500) overnight and measured disintegrations per minute (DPM) for live samples were corrected using DPM recorded for killed controls. Bacterial production was then calculated from leucine incorporation rates (pmol leucine uptake L^{-1} hr^{-1}) (*46*).

Microbial abundances

Duplicate samples of unfiltered water were collected for flow cytometric analysis, preserved with 0.1% glutaraldehyde solution (final concentration) and frozen at -80°C. Blanks consisted of a 0.2 µm-filtered water aliquot. Microbial communities were analyzed using a flow cytometer (BD FACSCalibur) equipped with a 15 mW air-cooled argon-ion laser tuned for blue excitation (ex 488 nm) and a red diode laser (ex 635 nm), with emission (em) detectors at 535, 585 and 650 nm, and forward (FSC) and side scatter (SSC) light detectors. Runs were calibrated with fluorescent polystyrene beads (1 µm, Spherotech) added to each sample to account for instrument reproducibility and fluorescence reference. Samples were pre-screened with a 52 µm mesh to preclude the introduction of larger particles into the flow cell. Sample volumes were estimated by sample weight before and after each run. Data were acquired using BD Cell Quest Pro software (v. 4.0.1) and analyzed with FlowJo software (v.10)

Samples for analysis of heterotrophic bacteria were vortexed to disrupt bacterial assemblages and particle-attached bacteria, 10-fold diluted and stained with Sybr Green I,

a nucleic acid (NA) binding stain (*47*). Total heterotrophic bacteria abundances represented the whole bacterioplankton community.

IV. RESULTS

Thirteen samples were taken every two hours for a total of 26 hours in order to resolve how tidal cycle influences t-DOM degradation in a coastal salt marsh. This sampling period lasted two complete tidal cycles and one diurnal cycle. Seven of the samples were collected at high tide (1-3, 7-9, 13) and six at low tide (4-6, 10-12). Eight samples were collected during the day (1-5, 11-13), while five were collected at night (6-10).

Planktonic microbial community composition across tidal cycle

The community composition in both the metagenomes and metatranscriptomes varies across tidal cycle. DESeq2 analyses reveal that eukaryotes and viruses are significantly more abundant at low tide, and archaea are significantly more abundant at high tide (Figures 4.1 and 4.2). While there are differences between the domains across tidal cycles, the distinction between communities at high and low tide becomes less discernable at higher taxonomic resolutions (Figure 4.3). For example, in the bacterial metagenomes α-Proteobacteria are more abundant at low tide, but many orders within α-Proteobacteria are significantly more abundant at high tide (e.g. Rhizobiales, Rhodospiralles, and Sphingomonadales; Figure 4.2B). Two different methods of assessing community composition from the same DNA samples yielded divergent patterns of community composition. The metagenomes and 16S libraries both show ε-Proteobacteria as being more abundant at low tide, Thaumarcheota and Verrucomicrobia as more abundant at high tide, and variable responses to tidal stage within γ-Proteobacteria. However, some taxa demonstrate variable responses to tidal stage between the metagenomes and 16S rRNA libraries, such as Euryarcheota, Rhodobacterales, and Rhodocyclales. Furthermore, Cyanobacteria are missing from the 16S rRNA but present in the metagenomes, while Actinobacteria are present in the metagenomes and largely absent in the 16S rRNA. The phyla Verrucomicrobia, Actinobacteria, and Bacteroidetes display similar abundance

patterns in the mRNA and DNA pools across tidal cycles. Cyanobacteria and β-Proteobacteria are more abundant at different stages of the tidal cycle in the metagenomes and metatranscriptomes.

Community function across tidal cycles

Tidal stage significantly structures the microbial community function in the metagenomes, but not in the metatranscriptomes (Figure 4.4, PERMANOVA, metagenome: $p < 0.016$, R^2=0.245; metatranscriptome: $p < 0.057$, R^2=0.165). The only other environmental parameter that significantly explains the clustering for the metagenomes is salinity (p <0.035, R^2=0.535), while the concentration of DOC, lignin, cell density, and bacterial production all significantly influence the clustering of the metatranscriptomes based on functionality (p <0.05, R^2= 0.955, 0.955, 0.925, 0.924, respectively). All of the environmental parameters that structure the microbial community functionality strongly correlate with depth, with the exception of lignin and DOC which only weakly correlate with depth (Table 4.5; Spearman's correlation, cell density: -0.832, bacterial production: -0.809, salinity: 0.606, DOC: -0.375, and lignin: -0.28). These data suggest that microbial community functioning in the marsh is dependent on the tidal stage. Furthermore, the metatranscriptomes appear to show a diel pattern in clustering with dawn, dusk, and night samples (5-11) clustering away from day samples (1-4; 12-13). This diel pattern is not maintained in the metagenome NMDS.

Additionally, analyses were conducted with DESeq2 to identify transcripts annotated to KEGG ontology (KO) number, which represents a group of similar sequences assingned to a function, that were differentially expressed between tidal stages, of which 769 transcripts were significantly more abundant at low tide while 686 were more significantly abundant at high tide. These analyses were performed by comparing high tide transcript levels to low tide, which results in KO numbers with positive logΔ being more abundant at high tide and those with a negative logΔ being more abundant at low tide. The transcripts that were significantly more abundant at low tide were genes associated with environmental information processing and metabolism, while high tide transcripts were

enriched in KO functions related to genetic information processing (Figure 4.5; Tables 4.5 and 4.6). Of the 50 transcripts significantly most enriched at high tide, 15 were annotated to metabolism. While most of the metabolism transcripts were annotated to central metabolism, three were involved in the degradation of plant-derived carbon, *cbh1* (cellulose 1,4-beta-cellobiosidase), *hbaB* (hydroxybenzoyl-CoA reductase), and *etbC* (dihydroxyethylbenzene 1,2-dioxygenase) (*cbh1* logΔ -3.74, $p < 0.05$; *hbaB* logΔ -2.76, $p < 0.01$; *etbC* logΔ -2.74, $p < 0.05$ Table 4.5). The amount of aromatic carbon is the most dilute in the marsh at high tide (Table 4.1), so it is surprising that transcripts involved in the degradation of cellulose and benzoate are more abundant at high tide.

Given the anticipated importance of the concentration of lignin in structuring the functional clustering of both the metatranscriptomes (Figure 4.4B), and the increased expression of select aromatic carbon catabolism genes at high tide, when the amount of aromatic carbon is at its lowest in the marsh, we chose to take a targeted approach to examine aromatic carbon catabolism over the tidal cycle.

Aromatic carbon degradation within the marsh based on KEGG and EC annotation

Despite the fact that these marshes contain high concentrations of lignin and contain known fungal and bacterial decomposers of lignin (*17*, *48*), we found no genes or transcripts for laccases and lignin peroxidases, with the sole exception of dye-decolorizing peroxidases which average 0.419 +/- 0.04 TPM for four metatranscriptomic samples and 3.06 +/- 1.69 GPM for all metagenomic samples (Figure 4.6). All of the genes and transcripts were from members of the Candidatus genus *Aquiluna* within the phylum Actinobacteria. Members of this genus are exclusively found in aquatic ecosystems (*49*, *50*).

We examined gene and transcript abundance for genes encoding the ring-cleaving enzymes for four aerobic, aromatic carbon degradation pathways which are commonly found in soil microbial communities degrading organic carbon (*51–53*): benzoyl-CoA (*boxB*), catechol (*catA*), gentisate (*genA*), and protocatechuate (*pcaHG*). Of the ring-cleaving genes for these four pathways, only the *boxB* gene encoding the β subunit of benzoyl-CoA 2,3-

epoxidase was actively transcribed (TPM/GPM > 1), indicating that ring-cleavage predominantly proceeds through the benzoyl-CoA pathway in this system (Figure 4.7A). Additionally, *boxB* had the highest gene abundance of the aerobic ring-cleaving genes, followed by *pcaHG* and *genA*, while *catA* had the lowest gene abundance (Figure 4.7). Members of the family Rhodobacteriaceae are responsible for almost all of the *genA* and *pcaHG* and half of the *boxB* genes in the system (Figure 4.7). The remaining *boxB* genes are from unclassified Euryarcheota Marine Group II, and almost all of the *catA* genes are from the family Oscillatoriaceae, specifically one genus Lyngbya, which is responsible for harmful algal blooms off the coast of the Florida (*54*, *55*). Thus, the vast majority of the ring-cleaving genes in this system belong to marine lineages of bacteria and archaea. While the catechol, gentisate, and protocatechuate pathways are not actively being expressed, the transcripts from the *catA, genA,* and *pcaH* are from the marine families Rhodobacteriaceae and Oscillatoriaceae; however, organisms from freshwater, marine, and soil systems appear to be contributing to the *boxB* transcripts (Figure 4.8). The bacterial family most actively transcribing *boxB* is the unclassified Rhodospiriillales, which was dominated by a single OTU that is most closely related to the homologous gene from *Rhodospirillales bacterium* URHD0088 (78.42% of *boxB* transcripts), a metagenome amplified genome from North African soils.

Genes and transcripts for carbohydrate-active enzymes (CAZys)

Carbohydrates in the form of cellulose and hemicellulose can account for up to 75% of the dry weight of *Spartina alterniflora* (*56*) and cellulose 1,4-β-cellobiosidase was one of the most significantly and differentially expressed genes at high tide suggesting that carbohydrate degradation is occurring concurrently with aromatic carbon degradation. In order to more completely assess the prevalence of enzymes relevant to the degradation of plant-derived carbohydrates we performed an alignment to the dbCAN database. The dbCAN database is a manually curated collection of signature domains for each CAZy family and includes published metagenomic CAZyme genes with the goal of discovering novel CAZyme catalysts (*32*). This represents a departure from KEGG and EC annotations which requires experimental evidence of functionality with characterized sequence data.

The genes and transcripts for CAZys across the tidal cycle are fairly equal, averaging 1474.095 +/- 241.98 GPM and 1361.165 +/- 231.309 TPM. While the gene and transcripts numbers show temporal variation, they are not significantly explained by tidal stage. CAZys are broadly subdivided into six groups: auxiliary activities (AA), which are oxidoreductases that are either ligninolytic enzymes or lytic polysaccharide monooxygenases (LPMO), glycoside hydrolases (GH), glycosyltransferases (GT), carbohydrate esterases (CE), polysaccharide lyases (PL), and non-catalytic carbohydrate binding modules (CBM). Of these enzyme classes GH and GT are the most abundant in the metagenomes at 29.5 and 36.5% of the CAZy pool, respectively (Figure 4.9A). Of these classes, PL is the least abundant occurring only in nine metagenomic samples and never constituting more than 0.01% of the CAZy pool. In the metatranscriptomic samples, CE is the most abundant CAZy class and 5-fold more abundant than in metagenomes. The number of AA genes and transcripts is approximately the same at 16.5% of the metatranscriptomes and 15.1% of the metagenomes.

The distribution of domains contributing CAZy genes and transcripts is largely limited to bacteria and eukaryota with viruses and archaea making up less than a percent of the total gene and transcript pool (Figure 4.9B). Bacteria contribute 85.8% of the CAZy genes while eukaryota make up 13.6%. However, in the metatranscriptomes eukaryotic relative abundance increases to 20.3% of the CAZy transcripts suggesting that eukaryotes are more actively transcribing genes encoding CAZys. Eukaryotic transcripts for CAZys are significantly more abundant at low tide (t-test, $p < 0.05$), while bacterial transcripts show temporal variation they are not significantly influenced by the tidal cycle.

The AA consist of eight families of ligninolytic enzymes and three families of LPMOs. Contrary to KEGG and EC annotations, we found evidence for three families of ligninolytic enzymes and two families of LPMOs in our samples with alignment to dbCAN. Of these, only two families appear to be actively expressed (TPM/GPM > 1) across the tidal cycle, AA2 or class II lignin-modifying peroxidases and AA10 or LPMOs, while the 1,4-benzoquinone reductases had roughly equal number of genes and transcripts (Figure

4.10). Eukaryotes almost exclusively contributed the genes and transcripts for the LPMOs, with only one family of Bacteria (Oxalobacteraceae) making up greater than 1% of the community (Figure 4.11). For the class II lignin-modifying peroxidases and 1,4-benzoquinone reductases, only genes and transcripts mapped to Bacteria were identified in our libraries (Figures 4.12 and 4.13).

Additionally, there are a greater number of bacterial families contributing genes and transcripts to the class II lignin-modifying peroxidases and 1,4-benzoquinone reductases compared to the ring-cleaving genes. For the *boxB, catA, genA*, and *pcaH* ring-cleaving genes ten, four, six, and five bacterial families contributed greater than 1% of the genes, respectively. Five families had multiple ring-cleaving genes that were mapped to them (Figure 4.6). The 1,4-benzoquinone reductase genes and transcripts came from 15 families, three of which (Burkholderiaceae, Comamonadaceae, and Erythrobacteraceae) overlap with those possessing ring-cleaving genes. The class II lignin-modifying peroxidases were mapped to 26 families, five of which (Burkholderiaceae, Comamonadaceae, Rhodobacteraceae, unclassified δ-Proteobacteria, and Flavobacteraceae) overlap with those identified has contributing to the ring-cleaving gene pool. Overall, the ring-cleaving gene pool was enriched in OTUs that mapped to α-Proteobacteria, while the class II lignin-modifying peroxidases and 1,4-benzoquinone reductases community appear to belong to members of the γ-Proteobacteria. Of the 49 recognized enzymes in the CAZys database that are predicated to target plant or algal detritus (*57*), ten were present in the majority of both the metagenomic and metatranscriptomic samples. These CAZys were contributed from the GH, GT, CE, and CBM classes. Of these ten only one was actively expressed, GH19 (Figure 4.14). GH19 is annotated as a chitinase/lysozyme and is exclusively secreted by prokaryotic members of the marsh community. GH19 follows the same temporal pattern of transcription as the class II lignin-modifying peroxidases.

V. DISCUSSION

Community composition across tidal cycle

The structure of the salt marsh microbial community changes significantly over the tidal cycle with eukaryotes and viruses being more abundant at low tide and archaea at high tide with various classes of bacteria being more abundant at high tide (e.g. α-Proteobacteria) or low tide (e.g. γ-Proteobacteria). It is possible that as the marsh becomes more marine at high tide, the eukaryotes and viruses are diluted by the marine community which is largely composed of bacteria and archaea. The 16S rRNA amplicon libraries, metagenomes, and metatranscriptomes all reveal taxa that are differentially abundant across the tidal cycle. Bacterial orders which are significantly more abundant at high tide compared to low tide include Rhizobiales, Rhodospirillales, and unclassified Verrucomicrobia. There are no orders which are significantly more abundant at low tide across all datasets. The community composition within the 16S rRNA gene and metagenome datasets show differences in both presence and absence of specific microbial groups and variation across tidal cycles. For example, the phyla Actinobacteria and Cyanobacteria are largely absent from the 16S rRNA amplicon datasets, but present in the metagenomes. Furthermore, the Euryarcheota are more abundant at low tide in the 16S rRNA dataset but at high tide in the metagenomes. It is difficult to determine if these differences are driven by the determining community composition from a marker gene compared to functional genes or due to the use of different databases to assign taxonomy to the OTU clusters (SILVA) and the CDS (GOLD). Additionally, both techniques of assessing community composition have inherent biases; however, extraction bias is unlikely to have played a role as the DNA for both datasets came from the same extraction. Primer biases coupled with PCR biases, along with variable 16S rRNA copy numbers within genomes could lead to the differential abundances seem between the metagenomes and 16S rRNA libraries. Further, the community composition in the metagenomes was calculated from read-length and sequencing-depth normalized datasets generated from taxonomic assignments to CDS. This methodology is biased towards organisms with larger genome sizes. Considering the biases inherent in both techniques, it is not surprising that the 16S rRNA libraries and metagenomes do not show

similar community composition profiles, although the community composition results between the 16S rRNA genes and the CDS likely would have been much more similar had the 16S rRNA genes from the metagenomes been analyzed.

Differential representation of microbial taxa in metagenomes and metatranscriptomes helps elucidate genetic potential from activity. While some phyla show similar abundance patterns at high or low tide, including the Actinobacteria and Bacteroidetes in both the metagenomes and metatranscriptomes, β-Proteobacteria are more abundant at high tide in the metagenomes and at low tide in the metatranscriptomes and Cyanobacteria are more abundant at low tide in the metagenomes and at high tide in the metatranscriptomes. The differential contribution of these taxa to the mRNA and DNA pools at high and low tide suggest that while organisms may contribute more genes at a given tide, they are more active at another. Furthermore, the community composition in both the metagenomes and metatranscriptomes demonstrate the importance of assessing community composition at the finest taxonomic resolution feasible. For example, in the metagenomes α-Pproteobacteria are more abundant at low tide than high tide, but this abundance pattern is being driven by one order, Pelagibacterales, while in the metatranscriptomes α-Proteobacteria are more abundant at high tide, but the Rhodobacterales order are more abundant at low tide (Figure 4.2). These data underscore the necessity of assessing community composition at the most resolved taxonomic classification that is achievable.

Community function across tidal cycle

The tidal cycle influences the community function as assessed by both the metagenomes and the metatranscriptomes. Both datasets show tighter clustering of low tide samples and a looser clustering of high tide samples (Figure 4.4), suggesting that the functions at low tide are more conserved. Comparing the relative abundance of genes and transcripts that are significantly more abundant at high or low tide reveals that genes and transcripts for environmental processing, such as transporters, and metabolism are more abundant at low tide. Given that the highest concentrations of DOC and total dissolved nitrogen (TDN) occur at low tide, it is unsurprising that the functions which are significantly more abundant

at low tide are enriched in genes for transporters and metabolism. At high tide, genes and transcripts annotated to genetic information processing are enriched in the pool of significantly differentially abundant genes. Genes involved in transcription and translation fall into this category (*58*), suggesting that the high tide community may be more active in responding to pulses of nutrients compared to a low tide community which experiences higher concentrations of DOC and TDN. If the microbial community at high tide is more actively transcribing mRNA and translating protein to respond to pulses of nutrients this could explain the more disparate clustering within the metatranscriptomes.

Degradation of plant-derived C characteristic of t-DOM

The marshes of the Southeastern United States receive and produce high amount of plant-derived carbon (*2*, *6*), suggesting that the degradation of plant-derived carbon and the aromatic moieties that they are enriched in are key ecological functions in these systems. Furthermore, previous results from these salt marsh systems suggest that both bacteria and fungi degrade HMW plant-derived C, (*17*, *18*) which differs from soil systems where fungi are thought to almost exclusively produce the enzymes active against the HMW portion of plant matter (*59*). These data enabled us to determine how these two microbial groups degrade plant-derived C and showed clear functional niches for these processes in the planktonic portion of marsh water in which bacteria and archaea exclusively provide ring-cleaving enzymes and peroxidases and eukaryotes, a small fraction of which were fungi, produce enzymes active against cellulose and hemicellulose.

Of the four major aerobic, ring-cleaving pathways only the ring-cleaving genes for the benzoyl-CoA pathway, *boxAB*, were actively expressed, which we define as a higher number of transcripts than genes. The benzoyl-CoA pathway was only recently described and is postulated to be an important pathway for the degradation of plant-derived carbon with increasing reports of its presence in environmental studies (*51*, *60*, *61*). Marine microbes from multiple lineages (Rhodobacteriaceae, Euryarcheota MG II, and Oscillatoriaceae) are responsible for almost all of the ring-cleaving genes within the marsh; however, the microbial community contributing to the mRNA pool for these same genes

is much more diverse, particularly for *boxB,* the most actively expressed ring-cleaving gene. Transcripts for *boxB* were mapped to organisms originating in marine, freshwater, and soil systems. If these taxonomic assignments are valid, this finding suggests that interactions between freshwater and marine microbial community may contribute to microbial degradation of t-DOM in these coastal margins. Furthermore, previous studies have shown that *boxB* is taxonomically constrained to Actinobacteria and Proteobacteria (*61*, *62*); however, no *boxB* genes or transcripts were mapped to Actinobacteria. While the majority of boxB transcripts mapped to members of the class α-Proteobacteria, approximately 25% of the genes and 10% of the transcripts mapped to Euryarcheota Marine Group II (MGII). These data along with recent reports of Bathyarcheota in estuarine sediments growing on lignin monitored through gene copy numbers (*63*), suggest that archaea may play a previously overlooked role in the degradation of t-DOM and could be important decomposers of plant-derived carbon.

Additionally, we looked for the presence of enzymes that degrade lignin in our KEGG and enzyme commission (EC) annotations (lignin peroxidase EC 1.11.1.14, manganese-dependent peroxidase EC 1.11.113 and KO:K20205, versatile peroxidase EC 1.11.1.16, dye-decolorizing peroxidase EC 1.11.1.19 and KO:K15733, and laccases EC 1.10.3.2 and KO:K05909). Of these enzymes we only found evidence for the dye-decolorizing peroxidases which ranged from 0.37-0.44 TPM in four samples of the metatranscriptomes and 0.95-7.2 GPM in all metagenomic samples. The low gene and transcript numbers for the dye decolorizing peroxidases and the absence of other classes of lignin-degrading enzymes was surprising given these systems are known hot spots of the breakdown of recalcitrant organic matter (*18*, *64*). However, the vast majority of laccases and lignin-peroxidases have been characterized in fungi (*59*, *65*, *66*). Previous studies in these systems suggest that the bacteria remineralize more lignin than the fungi (*17*), yet the enzymes by which bacteria transform lignin are not well characterized. Accurate annotation of bacterial lignin-degrading enzymes first requires experimental evidence of functionality with characterized sequence data, thus the limited detection of lignin-degrading enzymes in our system more than likely stems from a lack of accurate functional annotation. Furthermore,

our metagenomes and metatranscriptomes were generated from marsh water that was pre-filtered through a GF/D filter (~ 2.7 μM pore size), which excludes some of the particle-attached community due to retention on the prefilter. It is likely that through our prefiltration we are missing some of the metabolic potential for these functions.

Furthermore, all genes and transcripts for the dye-decolorizing peroxidases belonged to the order Micrococcales within the Actinobacteria. Actinobacteria did not contribute any genes or transcripts to the pool of aromatic monomer ring-cleaving genes detected within the marsh (Figure 5.5), suggesting that the niches of lignin degradation and aromatic monomer cleavage may be filled by different communities of bacteria within the marsh.

Distribution and community composition of CAZys

Of the CAZys that target plant-derived C and appear in the majority of the metagenomes and metatranscriptomes, three are actively expressed: AA2 – class II lignin-modifying peroxidases, AA10 – LPMOs, and GH19 – chitinases/lysozymes. Analyses with KEGG and EC annotations revealed only a limited number of transcripts and genes for dye-decolorizing peroxidases and no genes and transcripts for any other class of lignin peroxidase, while alignment to dbCAN resulted in twice the number of genes for lignin-modifying peroxidases (6.84 +/- 2.54 GPM compared to 3.06 +/- 1.69 GPM) and a 50-fold increase in the number of transcripts (22.91 +/-8.75 compared to 0.419 +/- 0.04). Furthermore, the phylogenetic diversity within in genes and transcripts revealed by dbCAN was far greater than those of the KEGG annotations; 26 families were represented in the dbCAN genes and transcripts while only one order was represented in the KEGG genes and transcripts. While the phylum Actinobacteria was represented in both the KEGG and dbCAN annotations the orders were different with Micrococcales in the KEGG annotations and Corynebacteriales and Streptomycetales in the dbCAN annotations. The discrepancies between these two annotation methods likely stems from KEGG annotations requiring experimental evidence of function in a laboratory setting before being added to the database while dbCAN contains signature domains for every CAZyme family and incorporates CAZy sequences published in metagenomic datasets.

Comparison of the communities contributing genes and transcripts for ring-cleaving genes for aromatic monomers (KEGG annotation), class II lignin-modifying reductases, and LPMOs reveal three distinct microbial communities. The ring-cleaving genes for aromatic monomers are largely composed of bacteria from the class α-Proteobacteria along with archaea (MGII) in the *boxB* community. Class II lignin-modifying peroxidase genes and transcripts are provided by six phyla of bacteria but tend to fluctuate between γ-Proteobacteria, specifically Pseudomonadaceae, and α-Proteobacteria (Pelagibacteraceae, Rhodobacteraceae, and Rhizobiaceae). This temporal fluctuation in community composition is not significantly influenced by the tidal cycle. There is some overlap between the families of α-Proteobacteria contributing ring-cleaving genes for aromatic monomers and class II lignin-modifying peroxidases. Finally, eukaryotes contribute the vast majority of genes and transcripts for LPMOs. Only one family of bacteria constitutes greater than 1% of the population in the genes (Oxalobacteraceae; 2.3%), while no family of bacteria contributes more than 1% of the transcripts. These observations suggest that there are functional niches for the degradation of t-DOM within the marsh.

Furthermore, of the ten secreted CAZys predicted to target plant-derived C only one was actively expressed, GH19 a predicted chitinase/lysozyme. GH19 showed the same temporal pattern of expression as the class II lignin-modifying peroxidases suggesting that these enzymes may be co-expressed. The bacteria may be secreting the chitinases as a competitive measure against the fungi in order to access the lignin as it is active against the chitin in the cell walls of fungi (*67*). Antagonism between bacteria and fungi when grown on plant-derived C has been well-documented (*18*, *68*) and may serve to explain why only bacteria are contributing genes and transcripts for the lignin peroxidases in the planktonic portion of the microbial community. Additionally, both GH19 and the class II lignin-modifying peroxidase transcripts decline precipitously in samples collected at night, which indicates a potential synergistic interaction between photo and biodegradation of plant-derived C in the marsh. Taken as a whole these data suggest that there are functional niches for the degradation of t-DOM in coastal salt marshes that are conserved across the tidal cycle, while expression of only one class of t-DOM degrading genes, the ring-cleaving

genes of aromatic monomers, is significantly influenced by the tidal cycle. Most delignification studies consider the metabolic efforts of either the bacterial or fungal community, and when bacteria and fungi are considered together the community composition and bulk loss of lignin are measured (*17*, *64*). These approaches prevent the identification of functional niches within the degradation of plant-derived C, which likely influence the ability of the community to perform this ecological function. Studies examining the contribution of bacteria along, fungi alone, and the whole community in these systems have found that the whole community remineralizes the most plant-derived C (*17*, *64*), further bolstering the idea that domain-level functional niches for t-DOM degradation exist in these systems.

VI. ACKNOWLEDGMENTS

We would like to thank Drs. Mary Ann Moran and Alexey Vorobev for their RNA extraction protocol without which we would have been unable to complete this work. We also acknowledge and thank Drs. Byron Crump and Jérôme Payet for their bioinformatics pipeline and help with its implementation. Additionally, we thank Yi Ting Huang and Katherine Moccia for their help with sample collection.

This work was supported by a grant from the National Science Foundation [OCE-1357242] awarded to AB, ADS, AS and sequencing was conducted by the U.S. Department of Energy Joint Genome Institute, a DOE Office of Science User Facility, is supported by the Office of Science of the U.S. Department of Energy under Contract No. DE-AC02-05CH11231 through a community sequencing project awarded to AB, ADS, AS.

VII. REFERENCES

1. C. S. Hopkinson, in *Coastal-Offshore Ecosystem Interactions* (ed. 22, 1988), pp. 122–154.
2. R. G. Wiegart, B. J. Freeman, Tidal marshes of the southeastern Atlantic coast: a community profile. *U.S. Fish Wildl. Serv.* **85**, 1–80 (1990).
3. G. A. Hyndes *et al.*, Mechanisms and ecological role of carbon transfer within coastal seascapes. *Biol. Rev.* **89**, 232–254 (2014).
4. R. J. Aspden, S. Vardy, D. M. Paterson, Salt Marsh Microbial Ecology: Microbes Benthic Mats and Sediment Movements. *Salt Marsh Microb. Ecol.*, 115–136 (2004).
5. S. C. Pennings, M. D. Bertness, in *Marine Community Ecology* (2001; http://www.sillimanlab.com/pdf/Bertness_Chapter11.pdf), pp. 289–316.
6. J. J. Alberts, M. Takács, in *Organic Geochemistry* (1999), vol. 30, pp. 385–395.
7. A. Mannino, H. R. Harvey, Terrigenous dissolved organic matter along an estuarine gradient and its flux to the coastal ocean. *Org. Geochem.* **31**, 1611–1625 (2000).
8. J. I. Hedges, R. G. Keil, R. Benner, in *Organic Geochemistry* (1997), vol. 27, pp. 195–212.
9. C. L. Osburn *et al.*, Optical Proxies for Terrestrial Dissolved Organic Matter in Estuaries and Coastal Waters. *Front. Mar. Sci.* **2** (2016), doi:10.3389/fmars.2015.00127.
10. N. D. Ward *et al.*, Degradation of terrestrially derived macromolecules in the Amazon River. *Nat. Geosci.* **6** (2013), doi:10.1038/ngeo1817.
11. A. Chauhan, J. Cherrier, H. N. Williams, Impact of sideways and bottom-up control factors on bacterial community succession over a tidal cycle. *Proc. Natl. Acad. Sci.* **106**, 4301–4306 (2009).
12. P. J. Kearns, D. Holloway, J. H. Angell, S. G. Feinman, J. L. Bowen, Effect of short-term, diel changes in environmental conditions on active microbial communities in a salt marsh pond. *Aquat. Microb. Ecol.* **80**, 29–41 (2017).
13. C. S. Fortunato, B. C. Crump, Microbial gene abundance and expression patterns across a river to ocean salinity gradient. *PLoS One* (2015),

doi:10.1371/journal.pone.0140578.

14. B. C. Crump, C. S. Hopkinson, M. L. Sogin, J. E. Hobbie, Microbial Biogeography along an Estuarine Salinity Gradient: Combined Influences of Bacterial Growth and Residence Time. *Appl. Environ. Microbiol.* **70**, 1494–1505 (2004).
15. M. Moran, R. Hodson, Contributions of degrading Spartina alterniflora lignocellulose to the dissolved organic carbon pool of a salt marsh. *Mar. Ecol. Prog. Ser. Oldend.* **62**, 161–168 (1990).
16. G. Janusz *et al.*, Lignin degradation: Microorganisms, enzymes involved, genomes analysis and evolution. *FEMS Microbiol. Rev.* **41** (2017), pp. 941–962.
17. R. Benner, M. A. Moran, R. E. Hodson, Biogeochemical cycling of lignocellulosic carbon in marine and freshwater ecosystems: Relative contributions of procaryotes and eucaryotes. *Limnol. Oceanogr.* **31**, 89–100 (1986).
18. A. Buchan *et al.*, Dynamics of Bacterial and Fungal Communities on Decaying Salt Marsh Grass. *Appl Env. Microbiol*. **69**, 6676–6687 (2003).
19. B. M. Satinsky, S. M. Gifford, B. C. Crump, M. A. Moran, Use of Internal Standards for Quantitative Metatranscriptome and Metagenome Analysis. *Enzymology*. **531**, 237–250 (2013).
20. A. Bankevich *et al.*, SPAdes: A New Genome Assembly Algorithm and Its Applications to Single-Cell Sequencing. *J. Comput. Biol.* **19**, 455–477 (2012).
21. M. Huntemann *et al.*, The standard operating procedure of the DOE-JGI Metagenome Annotation Pipeline (MAP v.4). *Stand. Genomic Sci.* **11** (2016), doi:10.1186/s40793-016-0138-x.
22. D. Li, C. M. Liu, R. Luo, K. Sadakane, T. W. Lam, MEGAHIT: An ultra-fast single-node solution for large and complex metagenomics assembly via succinct de Bruijn graph. *Bioinformatics*. **31**, 1674–1676 (2015).
23. A. R. Quinlan, I. M. Hall, BEDTools: A flexible suite of utilities for comparing genomic features. *Bioinformatics*. **26**, 841–842 (2010).
24. B. Langmead, S. L. Salzberg, Fast gapped-read alignment with Bowtie 2. *Nat. Methods*. **9**, 357–359 (2012).
25. G. P. Wagner, K. Kin, V. J. Lynch, Measurement of mRNA abundance using RNA-

seq data: RPKM measure is inconsistent among samples. *Theory Biosci.* **131**, 281–285 (2012).

26. M. R. Gradoville, B. C. Crump, R. M. Letelier, M. J. Church, A. E. White, Microbiome of Trichodesmium colonies from the North Pacific Subtropical Gyre. *Front. Microbiol.* **8** (2017), doi:10.3389/fmicb.2017.01122.
27. R Core team, R Core Team. *R A Lang. Environ. Stat. Comput. R Found. Stat. Comput. , Vienna, Austria. ISBN 3-900051-07-0, URL http//www.R-project.org/.* **55** (2015), pp. 275–286.
28. H. Wickham, ggplot 2 Version 1. *Media*. **35**, 211 (2009).
29. Z. S. L. Foster, T. J. Sharpton, N. J. Grünwald, Metacoder: An R package for visualization and manipulation of community taxonomic diversity data. *PLoS Comput. Biol.* **13** (2017), doi:10.1371/journal.pcbi.1005404.
30. J. Oksanen *et al.*, vegan: Community Ecology Package. *R Packag. ver. 2.4–3* (2017), p. 282.
31. M. I. Love, S. Anders, W. Huber, *Differential analysis of count data - the DESeq2 package* (2014; http://biorxiv.org/lookup/doi/10.1101/002832%5Cnhttp://dx.doi.org/10.1186/s13059-014-0550-8), vol. 15.
32. L. Huang *et al.*, DbCAN-seq: A database of carbohydrate-active enzyme (CAZyme) sequence and annotation. *Nucleic Acids Res.* (2018), doi:10.1093/nar/gkx894.
33. B. Buchfink, C. Xie, D. H. Huson, Fast and sensitive protein alignment using DIAMOND. *Nat. Methods* (2015), doi:10.1038/nmeth.3176.
34. A. Stubbins, T. Dittmar, Low volume quantification of dissolved organic carbon and dissolved nitrogen. *Limnol. Oceanogr. Methods* (2012), doi:10.4319/lom.2012.10.347.
35. L. Sun, R. G. M. Spencer, P. J. Hernes, R. Y. Dyda, K. Mopper, A comparison of a simplified cupric oxide oxidation HPLC method with the traditional GC-MS method for characterization of lignin phenolics in environmental samples. *Limnol. Oceanogr. Methods* (2015), doi:10.1002/lom3.10001.
36. T. Dittmar, B. Koch, N. Hertkorn, G. Kattner, A simple and efficient method for the

solid-phase extraction of dissolved organic matter (SPE-DOM) from seawater. *Am. Soc. Limnol. Oceanogr.* (2008).

37. Y. Ding, K. M. Cawley, C. N. da Cunha, R. Jaffé, Environmental dynamics of dissolved black carbon in wetlands. *Biogeochemistry* (2014), doi:10.1007/s10533-014-9964-3.
38. D. B. Wiedemeier *et al.*, Characterization, Quantification and Compound-specific Isotopic Analysis of Pyrogenic Carbon Using Benzene Polycarboxylic Acids (BPCA). *J. Vis. Exp.* (2016), doi:10.3791/53922.
39. A. Stubbins, C. S. Law, G. Uher, R. C. Upstill-Goddard, Carbon monoxide apparent quantum yields and photoproduction in the Tyne estuary. *Biogeosciences* (2011), doi:10.5194/bg-8-703-2011.
40. C. Hu, F. E. Muller-Karger, R. G. Zepp, Absorbance, absorption coefficient, and apparent quantum yield: A comment on common ambiguity in the use of these optical concepts. *Limnol. Oceanogr.* (2002), doi:10.4319/lo.2002.47.4.1261.
41. J. L. Weishaar *et al.*, Evaluation of specific ultraviolet absorbance as an indicator of the chemical composition and reactivity of dissolved organic carbon. *Environ. Sci. Technol.* (2003), doi:10.1021/es030360x.
42. J. R. Helms *et al.*, Absorption spectral slopes and slope ratios as indicators of molecular weight, source, and photobleaching of chromophoric dissolved organic matter. *Limnol. Oceanogr.* (2008), doi:10.4319/lo.2008.53.3.0955.
43. USEPA, Methods for Chemical Analysis of Water and Wastes. *Environ. Prot.* (1983).
44. P. J. Mann *et al.*, Controls on the composition and lability of dissolved organic matter in Siberia's Kolyma River basin. *J. Geophys. Res. Biogeosciences* (2012), doi:10.1029/2011JG001798.
45. D. C. Smith, F. Azam, A simple, economical method for measuring bacterial protein synthesis rates in seawater using tritiated-leucine. *Mar. Microb. Food Webs* (1992).
46. X. A. G. Moran, J. M. Gasol, M. Estrada, C. Pedros-Alio, Dissolved and particulate primary production and bacterial production in offshore antarctic waters during austral summer:coupled or uncoupled? *Mar. Ecol. Prog. Ser.* (2001),

doi:10.3354/meps222025.

47. D. Marie, F. Partensky, S. Jacquet, D. Vaulot, Enumeration and cell cycle analysis of natural populations of marine picoplankton by flow cytometry using the nucleic acid stain SYBR Green I. *Appl. Environ. Microbiol.* (1997), doi:10.1111/j.1365-294X.2009.04480.x.

48. J. M. Gonzalez, F. Mayer, M. a Moran, R. E. Hodson, W. B. Whitman, Sagittula stellata gen. nov., sp. nov., a lignin-transforming bacterium from a coastal environment. *Int. J. Syst. Bacteriol.* **47**, 773–780 (1997).

49. I. Kang *et al.*, Genome sequence of "Candidatus Aquiluna" sp. Strain IMCC13023, a marine member of the actinobacteria isolated from an arctic fjord. *J. Bacteriol.* (2012), , doi:10.1128/JB.00586-12.

50. M. W. Hahn, Description of seven candidate species affiliated with the phylum Actinobacteria, representing planktonic freshwater bacteria. *Int. J. Syst. Evol. Microbiol.* (2009), doi:10.1099/ijs.0.001743-0.

51. D. Garrido-Sanz, J. Manzano, M. Martín, M. Redondo-Nieto, R. Rivilla, Metagenomic analysis of a biphenyl-degrading soil bacterial consortium reveals the metabolic roles of specific populations. *Front. Microbiol.* (2018), doi:10.3389/fmicb.2018.00232.

52. J. Widada *et al.*, Molecular detection and diversity of polycyclic aromatic hydrocarbon-degrading bacteria isolated from geographically diverse sites. *Appl. Microbiol. Biotechnol.* (2002), doi:10.1007/s00253-001-0880-9.

53. C. F. Feist, G. D. Hegeman, Phenol and benzoate metabolism by Pseudomonas putida: regulation of tangential pathways. *J. Bacteriol.* (1969).

54. Montoya. Haydee, Algal and cyanobacterial saline biofilms of the Algal and cyanobacterial saline biofilms of the Grande Coastal Lagoon , Lima , Peru. *Nat. Resour. Environ. Issues* (2009).

55. K. Sharp *et al.*, Phylogenetic and chemical diversity of three chemotypes of bloom-forming Lyngbya species (cyanobacteria: Oscillatoriales) from reefs of southeastern Florida. *Appl. Environ. Microbiol.* (2009), doi:10.1128/AEM.02656-08.

56. R. E. Hodson, R. R. Christian, A. E. Maccubbin, Lignocellulose and lignin in the

salt marsh grass Spartina alterniflora: initial concentrations and short-term, post-depositional changes in detrital matter. *Mar. Biol.* **81**, 1–7 (1984).

57. W. D. Orsi, T. A. Richards, W. R. Francis, Predicted microbial secretomes and their target substrates in marine sediment. *Nat. Microbiol.* (2018), doi:10.1038/s41564-017-0047-9.
58. M. Kanehisa, The KEGG databases at GenomeNet. *Nucleic Acids Res.* (2002), doi:10.1093/nar/30.1.42.
59. M. Dashtban, H. Schraft, T. A. Syed, W. Qin, Fungal biodegradation and enzymatic modification of lignin. *Int. J. Biochem. Mol. Biol.* (2010).
60. J. Gescher, A. Zaar, M. Mohamed, H. Schägger, G. Fuchs, Genes coding for a new pathway of aerobic benzoate metabolism in Azoarcus evansii. *J. Bacteriol.* (2002), doi:10.1128/JB.184.22.6301-6315.2002.
61. C. A. Gulvik, Ecology and Physiology of Aerobic Aromatic Catabolism in Roseobacters (2013).
62. D. Pérez-Pantoja, R. Donoso, H. Junca, D. González, H. Pieper, in *Handbook of Hydrocarbon and Lipid Microbiology* (2009).
63. T. Yu *et al.*, Growth of sedimentary Bathyarchaeota on lignin as an energy source. *Proc. Natl. Acad. Sci. U. S. A.*, 201718854 (2018).
64. R. Benner, S. Y. Newell, A. E. Maccubbin, R. E. Hodson, Relative contributions of bacteria and fungi to rates of degradation of lignocellulosic detritus in salt-marsh sediments. *Appl. Environ. Microbiol.* **48**, 36–40 (1984).
65. J. C. Sigoillot *et al.*, Fungal Strategies for Lignin Degradation. *Adv. Bot. Res.* **61**, 263–308 (2012).
66. K. E. Hammel, D. Cullen, Role of fungal peroxidases in biological ligninolysis. *Curr. Opin. Plant Biol.* (2008), , doi:10.1016/j.pbi.2008.02.003.
67. W. De Boer *et al.*, Anti-fungal properties of chitinolytic dune soil bacteria. *Soil Biol. Biochem.* (1997), doi:10.1016/S0038-0717(97)00100-4.
68. C. Mille-Lindblom, L. J. Tranvik, Antagonism between bacteria and fungi on decomposing aquatic plant litter. *Microb. Ecol.* (2003), doi:10.1007/s00248-002-2030-z.

VIII. APPENDIX: TABLES

Table 4.1. Summary and environmental conditions for sampling intervals during the July 2014 diel field campaign

Time point	1	2	3	4	5	6	7
Time	7/16/14 11:00	7/16/14 13:00	7/16/14 15:00	7/16/14 17:00	7/16/14 19:00	7/16/14 21:15	7/16/14 23:15
tide	High	High	High	Low	Low	Low	High
Temperature (°C)	29	29	30.1	30.7	30.7	30.4	29.2
Depth (m)	4	4.4	3.7	2.2	1.9	3.1	4
Salinity (ppt)	29.5	30.6	29.7	29.5	29.5	29.5	29.7
Cell Density (cells/mL)	$6.35x10^{6}$	$1.03x10^{6}$	$6.81x10^{6}$	$9.96x10^{6}$	$7.7x10^{6}$	$1.01x10^{7}$	$5.34x10^{6}$
Bacterial Production (mmol/h)	$7.64x10^{-7}$	$7.29x10^{-7}$	$1.39x10^{-6}$	$1.71x10^{-6}$	$1.83x10^{-6}$	$1.57x10^{-6}$	$8.07x10^{-7}$
DOC (μm)	257.64	249.43	357.35	282.96	287.56	284.6	262.66
TDN (μm)	19.88	17.27	44.38	18.88	18.96	19.57	19.27
DOC/TDN	12.96	14.44	8.05	14.99	15.16	14.54	13.63
a254/DOC	0.074	0.068	0.049	0.074	0.075	0.075	0.0710
Lignin mg 1 / mg OC	0.320	0.280	0.240	0.292	0.315	0.2689	0.2798

Time point	8	9	10	11	12	13
Time	7/17/14 1:15	7/17/14 3:30	7/17/14 5:30	7/17/14 7:30	7/17/14 9:30	7/17/14 11:45
tide	High	High	Low	Low	Low	High
Temperature (°C)	29.1	28.8	28.8	28.6	28.8	29.2
Depth (m)	4.5	3.7	2.3	1.8	2.9	4
Salinity (ppt)	30.7	29.7	29.4	29.4	29.5	29.6
Cell Density (cells/mL)	$6.12x10^{6}$	$6.57x10^{6}$	$8.76x10^{6}$	$9.85x10^{6}$	$9.3x10^{6}$	$6.1x10^{6}$
Bacterial Production (mmol/h)	$7.25x10^{-7}$	$1.11x10^{-6}$	$1.31x10^{-6}$	$1.13x10^{-6}$	$1.09x10^{-6}$	$5.09x10^{-7}$
DOC (μm)	231.5	260.06	294.86	282.91	475.08	308.13
TDN (μm)	16.44	18.77	21	22.2	88.14	30.66
DOC/TDN	14.08	13.85	14.04	12.74	5.39	10.05
a254/DOC	0.068	0.066	0.073	0.071	0.046	0.062
Lignin mg 1 / mg OC	0.274	0.202	0.269	0.324	0.041	0.052

Table 4.2. Metagenome sequencing statistics

Sample	Illumina paired-end reads	Paired-end reads remaining after QC	Contigs assembled	Weighted-average contig length (N50)	Reads aligning to assembly[a]
1	189,013,848	180,501,510	1,253,561	1,155 bp	145,892,580 (80.83)
2	140,665,208	139,026,258	874,598	1,348 bp	111,812,630 (80.43)
3	223,997,266	221,845,582	1,472,396	1,059 bp	188,544,096 (84.99)
4	219,681,294	218,545,060	1,248,411	1,163 bp	185,890,433 (85.06)
5A	226,017,752	224,361,702	1,244,732	1,211 bp	189,167,028 (84.31)
5C	217,715,922	216,568,866	1,246,595	1,146 bp	185,942,209 (85.86)
6	200,925,514	198,883,764	1,263,359	1,085 bp	165,847,150 (83.39)
7	225,417,792	223,429,644	1,492,667	1,102 bp	186,297,959 (83.38)
9A	214,677,540	212,732,118	1,329,794	1,180 bp	171,547,952 (80.64)
9B	187,211,648	180,596,430	1,003,417	1,312 bp	146,656,287 (81.21)
10	230,949,626	228,956,740	1,329,507	1,173 bp	192,369,696 (84.02)
11	229,938,350	228,061,836	1,507,675	1,115 bp	190,628,841 (83.59)
12A	250,665,800	246,023,032	1,574,289	1,165 bp	205,376,340 (83.48)
12B	218,849,272	214,849,912	1,468,314	1,111 bp	177,503,692 (82.62)
13A	265,087,680	261,399,186	1,576,715	1,234 bp	215,769,880 (82.54)
13B	204,428,282	195,394,452	1,195,005	1,244 bp	159,497,823 (81.63)

[a]Values in parentheses represent percentages

Table 4.3. Metatranscriptome sequencing statistics

Sample	Illumina paired-end reads	Paired-end reads remaining after QC	Contigs assembled	Weighted-average contig length (N50)	Reads aligning to assembly[a]
1	125,451,862	101,398,452	801,560	591 bp	91,566,907 (90.3)
2	148,524,602	116,726,522	661,035	592 bp	107,627,329 (92.21)
3	69,299,818	53,802,970	556,084	609 bp	47,783,381 (88.81)
5B	99,310,818	59,698,470	554,002	608 bp	53,777,322 (90.08)
5C	102,593,816	64,047,020	610,658	639 bp	57,868,041 (90.35)
6	89,990,976	66,083,314	604,808	600 bp	60,237,079 (91.15)
7	145,221,882	106,339,590	865,884	618 bp	96,006,672 (90.28)
8	90,300,750	66,082,344	606,721	611 bp	59,419,857 (89.92)
9A	106,922,802	74,680,938	713,222	611 bp	67,892,656 (90.91)
9B	106,166,008	93,593,776	1,023,625	755 bp	80,867,534 (86.40)
10	145,918,538	90,883,140	734,483	615 bp	83,544,393 (91.93)
11	134,676,690	91,790,984	798,201	602 bp	84,559,059 (92.12)
12A	104,172,002	68,547,096	659,468	611 bp	62,701,910 (91.47)
12B	75,422,074	61,015,260	623,846	628 bp	53,207,869 (87.20)
13A	149,403,230	107,593,086	877,592	630 bp	99,254,797 (92.25)
13C	79,376,410	63,282,348	587,564	606 bp	55,952,799 (88.42)

[a]Values in parentheses present percentages

Table 4.4. Environmental data Spearman's ρ correlation matrix[a]

Variable	(1)	(2)	(3)	(4)	(5)	(6)	(7)	(8)	(9)	(10)
(1) a254/DOC	-	-	-	-	-	-	-	-	-	-
(2) Bacterial production	0.492	-	-	-	-	-	-	-	-	-
(3) Cell density	0.396	0.696	-	-	-	-	-	-	-	-
(4) Depth	0.349	0.809	-0.832	-	-	-	-	-	-	-
(5) Dissolved organic carbon (DOC)	N.D.	0.118	0.389	-0.375	-	-	-	-	-	-
(6) DOC/TDN	N.D.	0.514	0.0475	-0.199	N.D.	-	-	-	-	-
(7) Salinity	0.278	0.441	-0.541	0.606	0.051	-0.12	-	-	-	-
(8) Temperature	0.366	0.326	-0.084	0.0188	0.097	0.48	0.483	-	-	-
(9) Total dissolved nitrogen (TDN)	0.313	0.140	0.317	-0.198	0.845	0.802	0.072	0.168	-	-
(10) Lignin	N.D	0.405	0.07	-0.28	N.D.	0.603	0.067	0.207	0.474	-

[a]Correlations were not determined (N.D.) for environmental data between data types which were used to normalize each other (e.g. Lignin is reported as mg lignin/100 mg organic carbon, thus, a correlation was not determined between lignin and dissolved organic carbon)

Table 4.5. Transcripts (50) with the greatest, significant log fold change between tidal stage associated with high tide

KO_number	KO_name	base mean	log fold change	padj[a]	group_1[b]
KO:K02322	DPB1, *polD2*; DNA polymerase II large subunit	243.6539653	-2.797715395	0.000462	Metabolism
KO:K02599	NOTCH1; Notch 1	223.2387744	-2.789383283	4.09E-05	Human Diseases
KO:K15553	*ssuA*; sulfonate transport system substrate-binding protein	220.2136293	-6.287570118	1.63E-06	Environmental Information Processing
KO:K03389	*hdrB*; heterodisulfide reductase subunit B	175.6199005	-3.322104648	3.13E-07	Metabolism
KO:K09482	gatD; glutamyl-tRNA(Gln) amidotransferase subunit D	136.7047244	-2.616032927	4.60E-08	Genetic Information Processing
KO:K11089	TROVE2, SSA2; 60 kDa SS-A/Ro ribonucleoprotein	115.9843735	-2.868526578	0.007222	Human Diseases
KO:K15554	*ssuC*; sulfonate transport system permease protein	111.3250911	-5.091014602	8.63E-06	Environmental Information Processing
KO:K01387	*colA*; microbial collagenase	102.9258025	-2.779936184	0.00404	Environmental Information Processing
KO:K01225	CBH1; cellulose 1,4-beta-cellobiosidase	84.94936023	-3.743698983	0.042830	Metabolism
KO:K03390	*hdrC*; heterodisulfide reductase subunit C	83.47155842	-4.375449589	2.05E-06	Metabolism
KO:K05565	*mnhA*, *mrpA*; multicomponent Na+:H+ antiporter subunit A	75.20253892	-3.711508013	0.002055	Environmental Information Processing
KO:K12527	*ygfK*; putative selenate reductase	72.46551573	-3.251139892	0.009413	Metabolism
KO:K00635	E2.3.1.20; diacylglycerol O-acyltransferase	67.686491	-2.787423606	0.028588	Metabolism
KO:K19577	*ydhP*; MFS transporter, DHA1 family, inner membrane transport protein	57.42377336	-3.955965084	0.026882	Environmental Information Processing
KO:K13922	*pduP*; propionaldehyde dehydrogenase	55.55795621	-2.728775426	0.003239	Metabolism
KO:K07557	*tgtA2*; archaeosine synthase	55.51496932	-2.985477405	0.001489	Unclassified
KO:K13529	*ada-alkA*; AraC family transcriptional regulator, regulatory protein	50.29551327	-3.26303606	0.000121	Genetic Information Processing
KO:K16927	*cbrT*; energy-coupling factor transport system substrate-specific component	42.48622667	-3.047325958	0.003645	Environmental Information Processing
KO:K09716	*dtd*A, GEK1; D-aminoacyl-tRNA deacylase	35.29316943	-2.930695269	0.028150	Genetic Information Processing
KO:K07464	*cas*4; CRISPR-associated exonuclease Cas4	32.23655585	-3.46705863	0.009104	Cellular Processes

Table 4.5. Continued

KO_number	KO_name	base mean	log fold change	padj[a]	group_1[b]
KO:K14751	*etbC*; 2,3-dihydroxyethylbenzene 1,2-dioxygenase	30.61569435	-2.748813772	0.001263	Metabolism
KO:K11325	K11325; L-cysteine/cystine lyase	29.17656146	-2.825189204	0.013913	Unclassified
KO:K04795	*flpA*; fibrillarin-like pre-rRNA processing protein	27.07112302	-2.608796242	0.039019	Genetic Information Processing
KO:K03802	*cphA*; cyanophycin synthetase	25.84486546	-2.97572404	0.006699	Unclassified
KO:K02107	ATPVG, ahaH, atpH; V/A-type H+/Na+-transporting ATPase subunit G/H	23.80823524	-2.729967081	0.025178	Metabolism
KO:K15981	CYP125A; cholest-4-en-3-one 26-monooxygenase	23.35010398	-5.532642382	0.006198	Metabolism
KO:K01746	E4.3.1.4; formiminotetrahydrofolate cyclodeaminase	23.22980242	-3.889521086	0.001476	Metabolism
KO:K04479	K04479; DNA polymerase IV (archaeal DinB-like DNA polymerase)	23.17990634	-5.274259912	0.010655	Genetic Information Processing
KO:K17244	*chiE*; putative chitobiose transport system substrate-binding protein	22.345463	-3.330666351	0.025870	Environmental Information Processing
KO:K07318	K07318; adenine-specific DNA-methyltransferase	22.31975419	-2.901127711	0.012568	Cellular Processes
KO:K01707	*kdgD*; 5-dehydro-4-deoxyglucarate dehydratase	20.36196978	-4.115802846	0.001850	Metabolism
KO:K18958	whiB7; WhiB family transcriptional regulator	20.3022685	-3.829275369	0.039939	Genetic Information Processing
KO:K07165	*fecR*; transmembrane sensor	19.56703687	-5.837839385	0.001139	Unclassified
KO:K07463	K07463; archaea-specific RecJ-like exonuclease	18.36930872	-3.629209593	0.019572	Unclassified
KO:K14059	int; integrase	17.48694471	-3.568547776	0.006332	Unclassified
KO:K07254	atrm56; tRNA (cytidine56-2'-O)-methyltransferase	17.33583569	-3.900625765	0.041324	Genetic Information Processing
KO:K16444	*gtfB, gtfE*; vancomycin aglycone glucosyltransferase	17.19763121	-4.478737689	0.014463	Metabolism
KO:K07092	K07092; uncharacterized	16.96127843	-3.447096079	0.000977	Unclassified
KO:K05827	*lysX*; [lysine-biosynthesis-protein LysW]	15.7013713	-2.564483474	0.021468	Metabolism
KO:K10979	ku; DNA end-binding protein Ku	13.66015818	-4.714983167	0.041324	Genetic Information Processing
KO:K04107	*hcrC, hbaB*; 4-hydroxybenzoyl-CoA reductase subunit gamma	13.55276756	-2.760278936	0.008275	Metabolism
KO:K00693	GYS; glycogen synthase	13.34302733	-6.13069238	0.00010	Environmental Information Processing

Table 4.5. Continued

KO_number	KO_name	base mean	log fold change	padj[a]	group_1[b]
KO:K16681	CRB; protein crumbs	12.80376421	-5.210480101	0.01779	Environmental Information Processing
KO:K07651	*resE*; two-component system, OmpR family, sensor histidine kinase ResE	12.55236283	-2.632050765	0.03702	Environmental Information Processing
KO:K01788	*nanE*; N-acylglucosamine-6-phosphate 2-epimerase	12.52248453	-4.603813917	0.02034	Metabolism
KO:K03224	*yscN, sctN, hrcN;* ATP synthase in type III secretion protein N	12.28411521	-6.010703224	8.05E-05	Environmental Information Processing
KO:K02245	comGC; competence protein ComGC	11.75919296	-6.781634688	0.01300	Environmental Information Processing
KO:K19290	*alg8*; mannuronan synthase	11.0405142	-3.212659344	0.03499	Metabolism
KO:K14414	*rtcR*; transcriptional regulatory protein RtcR	10.96947215	-2.849870812	0.02603	Genetic Information Processing
KO:K03196	*virB11, lvhB11*; type IV secretion system protein VirB11	8.952008022	-6.393962032	0.00018	Environmental Information Processing

[a]padj is the Benjamini-Hochberg corrected p-value associated with the log-fold change between tidal cycles.

[b]group_1is a hierarchical functional category into which KO numbers are sorted. Group_1 represents the broadest functional category.

Table 4.6. Transcripts (50) with the greatest, significant log fold change between tidal stage associated with low tide

KO_number	KO_name	base mean	log fold change	padj[a]	group_1[b]
KO:K08676	tri; tricorn protease	2766.0340	2.014418047	9.27E-05	Metabolism
KO:K15559	RTT103; regulator of Ty1 transposition protein 103	1529.0854	2.080639102	0.001581	Genetic Information Processing
KO:K11000	CALS; callose synthase	1155.0558	4.325802976	0.004924	Metabolism
KO:K13412	CPK; calcium-dependent protein kinase	1138.9511	2.549715797	0.000924	Metabolism
KO:K17069	MET17; O-acetylhomoserine/O-acetylserine sulfhydrylase	904.10206	3.823016375	0.020414	Metabolism
KO:K12472	EPS15; epidermal growth factor receptor substrate 15	843.82103	2.221604092	0.004726	Genetic Information Processing
KO:K09272	SSRP1; structure-specific recognition protein 1	759.52337	3.874850668	0.000653	Genetic Information Processing
KO:K00814	GPT, ALT; alanine transaminase	619.35729	2.361649477	0.008415	Metabolism
KO:K10544	*xylH*; D-xylose transport system permease protein	571.33215	2.037486626	0.003676	Environmental Information Processing
KO:K01188	E3.2.1.21; beta-glucosidase	364.43115	2.274707885	0.007240	Metabolism
KO:K08794	CAMK1; calcium/calmodulin-dependent protein kinase	313.15882	1.984476287	3.00E-06	Organismal Systems
KO:K01161	E3.1.25.1; deoxyribonuclease	307.02752	2.331113214	1.73E-10	Unclassified
KO:K03015	RPB7, POLR2G; DNA-directed RNA polymerase II subunit RPB7	303.42481	2.465467283	0.010655	Genetic Information Processing
KO:K14563	NOP1, FBL; rRNA 2'-O-methyltransferase fibrillarin	299.74978	2.53222202	0.012729	Genetic Information Processing
KO:K17491	SMEK, PPP4R3; protein phosphatase 4 regulatory subunit 3	229.15241	2.048366165	0.034039	Organismal Systems
KO:K17398	DNMT3A; DNA (cytosine-5)-methyltransferase 3A	222.39847	2.602598504	0.041324	Genetic Information Processing
KO:K08488	STX7; syntaxin 7	219.68135	2.041627933	0.000373	Genetic Information Processing
KO:K12881	THOC4, ALY; THO complex subunit 4	213.21571	2.063998352	0.001145	Human Diseases
KO:K17279	REEP5_6; receptor expression-enhancing protein 5/6	188.83576	2.345289888	0.031821	Cellular Processes
KO:K13293	PDE4; cAMP-specific phosphodiesterase 4	188.48215	2.090159706	0.000185	Human Diseases
KO:K08867	WNK, PRKWNK; WNK lysine deficient protein kinase	188.23418	2.353718891	0.000334	Metabolism

Table 4.6. Continued

KO_number	KO_name	base mean	log fold change	padj[a]	group_1[b]
KO:K11718	HUGT; UDP-glucose:glycoprotein glucosyltransferase	174.50770	2.056813634	0.030307	Genetic Information Processing
KO:K07641	*creC*; two-component system, OmpR family, sensor histidine kinase CreC	159.19735	2.304558842	0.000451	Metabolism
KO:K13752	SLC24A4, NCKX4; solute carrier family 24 (sodium/potassium/calcium exchanger), member	149.38637	2.647367745	0.024864	Organismal Systems
KO:K05218	P2RX4; P2X purinoceptor 4	147.18105	1.989812849	0.026047	Environmental Information Processing
KO:K14826	FPR3_4; FK506-binding nuclear protein	111.94241	3.276453381	0.001825	Genetic Information Processing
KO:K17616	CTDSPL2; CTD small phosphatase-like protein	108.16453	2.930705338	0.001751	Metabolism
KO:K03083	GSK3B; glycogen synthase kinase 3 beta	99.776803	2.326985018	0.031544	Environmental Information Processing
KO:K02905	RP-L29e, RPL29; large subunit ribosomal protein L29e	92.054017	2.217898405	0.013910	Genetic Information Processing
KO:K13329	*spnR*; dTDP-4-dehydro-2,3,6-trideoxy-D-glucose 4-aminotransferase	88.314976	2.017374251	0.002962	Metabolism
KO:K03122	TFIIA1, GTF2A1, TOA1; transcription initiation factor TFIIA large subunit	82.125314	2.045574269	0.022021	Genetic Information Processing
KO:K18732	SARNP, CIP29, THO1; SAP domain-containing ribonucleoprotein	80.743436	3.397535727	0.039467	Genetic Information Processing
KO:K17800	LETM1, MDM38; LETM1 and EF-hand domain-containing protein 1, mitochondrial	56.647818	2.199127268	0.038716	Environmental Information Processing
KO:K19678	IFT80; intraflagellar transport protein 80	53.298847	2.345623609	0.015419	Genetic Information Processing
KO:K11087	SNRPD1, SMD1; small nuclear ribonucleoprotein D1	47.680653	2.553006276	0.000598	Genetic Information Processing
KO:K10710	*frlD*; fructoselysine 6-kinase	39.618977	8.975960869	0.000242	Unclassified
KO:K08515	VAMP7; vesicle-associated membrane protein 7	38.684968	7.641374745	6.78E-07	Genetic Information Processing
KO:K15306	RANBP1; Ran-binding protein 1	38.465727	2.253097081	0.030307	Human Diseases
KO:K01099	INPP5B_F; inositol polyphosphate 5-phosphatase INPP5B/F	36.331142	3.09509765	0.021827	Environmental Information Processing
KO:K05304	SAS; sialic acid synthase	21.943933	2.666127756	0.023363	Metabolism

Table 4.6. Continued

KO_number	KO_name	base mean	log fold change	padj[a]	group_1[b]
KO:K01275	CTSC; cathepsin C	21.193157	3.422299998	0.038716	Cellular Processes
KO:K08059	IFI30, GILT; interferon, gamma-inducible protein 30	17.825167	4.507986588	0.040621	Organismal Systems
KO:K09669	FUT10; alpha-1,3-fucosyltransferase 10	15.051164	22.52686386	3.84E-11	Metabolism
KO:K19679	IFT74; intraflagellar transport protein 74	14.168770	3.783283833	0.020603	Genetic Information Processing
KO:K06099	CSDA, ZONAB; cold shock domain protein A	13.714774	7.444086611	4.95E-06	Genetic Information Processing
KO:K02257	COX10; protoheme IX farnesyltransferase	11.921387	3.963550968	0.004735	Metabolism
KO:K11971	RNF14, ARA54; E3 ubiquitin-protein ligase RNF14	11.011917	5.154536387	0.009593	Genetic Information Processing
KO:K13131	DDX20, GEMIN3; ATP-dependent RNA helicase DDX20	10.301321	5.84176821	0.016598	Genetic Information Processing
KO:K01164	POP1; ribonuclease P/MRP protein subunit POP1	9.9993267	4.523296796	0.004800	Genetic Information Processing
KO:K00083	E1.1.1.195; cinnamyl-alcohol dehydrogenase	9.312677	6.887655586	0.002532	Metabolism

[a]padj is the Benjamini-Hochberg corrected p-value associated with the log-fold change between tidal cycles.

[b]group_1is a hierarchical functional category into which KO numbers are sorted. Group_1 represents the broadest functional category.

IX. APPENDIX: FIGURES

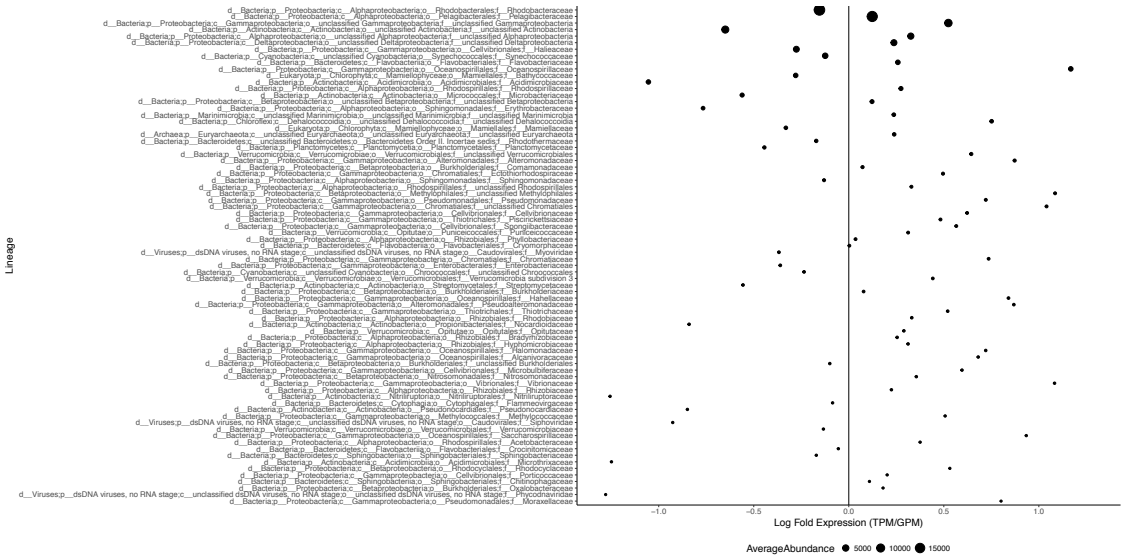

Figure 4.1. Most active families in the marsh at high tide.

Families which had an average of 50 genes per million (GPM) at high tide. Log-fold expression was calculated by dividing the average transcripts per million (TPM) by the average GPM per tidal stage. The size of each point represents the abundance of that family in the marsh community in GPM according to the legend.

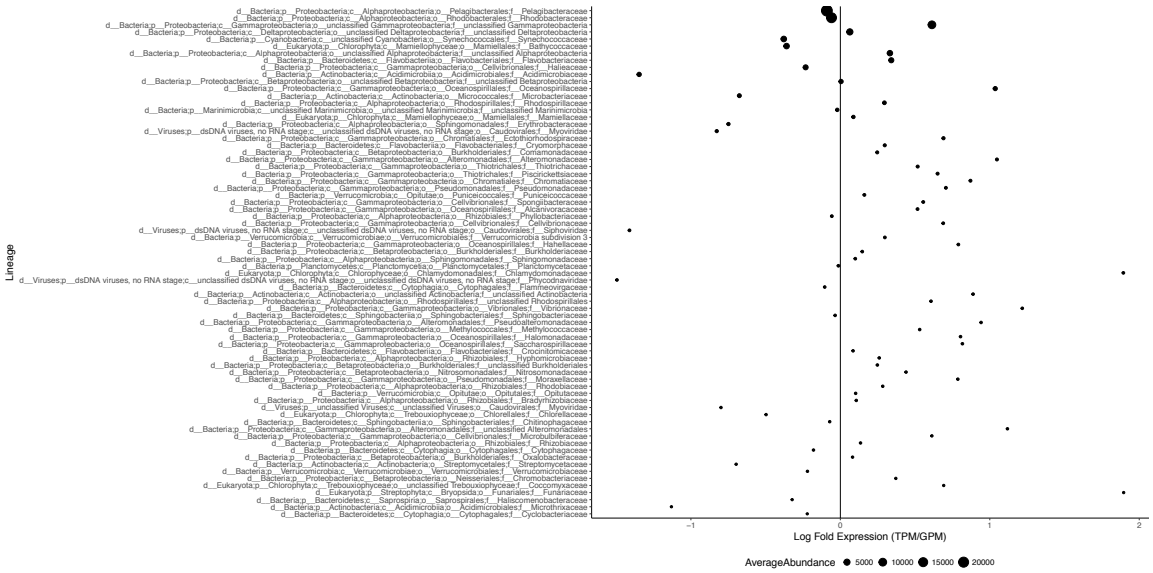

Figure 4.2. Most active families in the marsh at low tide.

Families which had an average of 50 genes per million (GPM) at low tide. Log-fold expression was calculated by dividing the average transcripts per million (TPM) by the average GPM per tidal stage. The size of each point represents the abundance of that family in the marsh community in GPM according to the legend.

Figure 4.3. Taxonomic tree of the archaeal and bacterial orders present in the 16S rRNA libraries, metagenomes, and metatranscriptomes.

Color represents the log fold change between tidal cycles. Orange represents lineages more abundant at high tide; purple are more abundant at low tide. Trees on the left are archaeal taxonomic trees while those on the right are bacterial taxonomic trees. Nodes with lineage names on them represent lineages that are significantly more abundant during a given tide (Wilcox rank-sum test followed by a Benjamini-Hochberg [FDR] correction for multiple comparisons). Light blue nodes represent lineages for which there were no reads. A guide tree with all nodes labeled is available in the supplemental material.

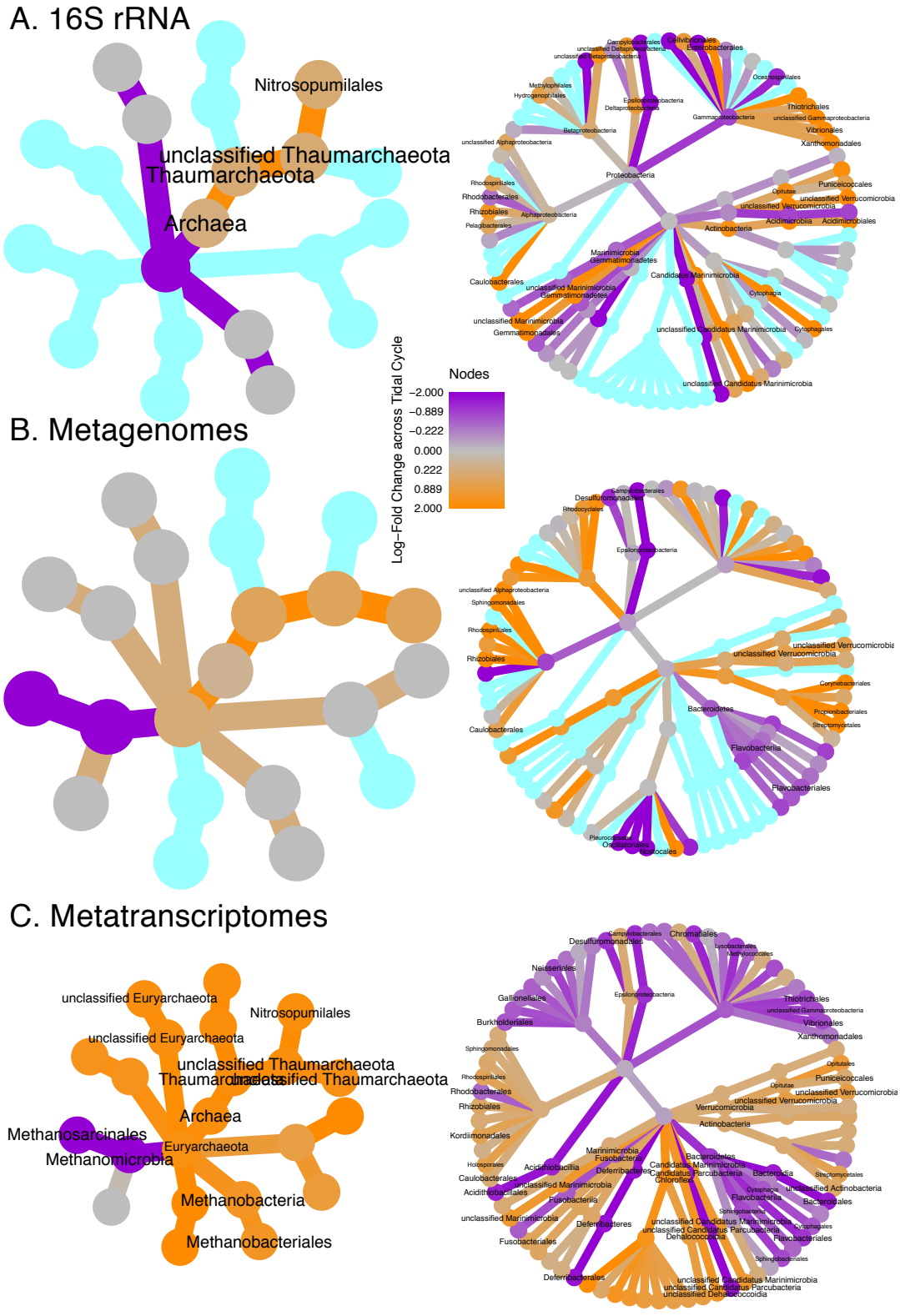

Figure 4.3. Continued

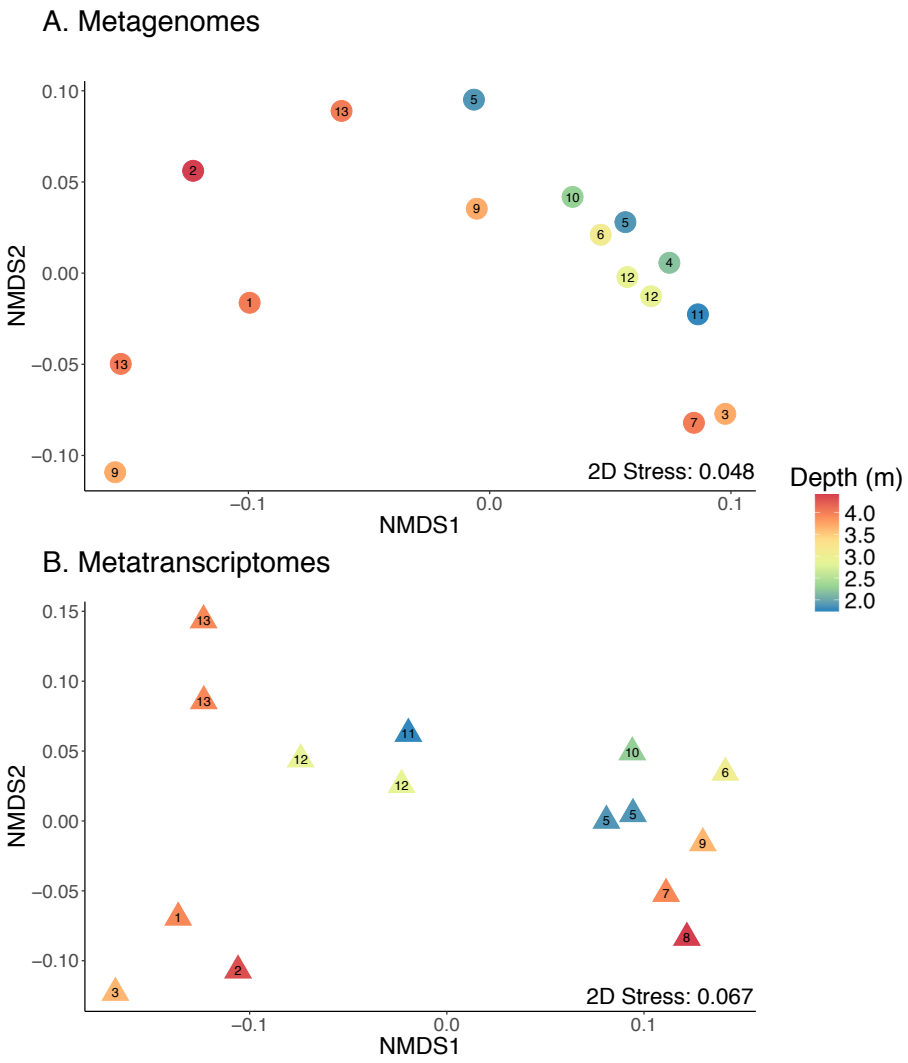

Figure 4.4. NMDS ordination of microbial community functioning as described by KEGG ontology annotation in the metagenomes and metatranscriptomes across the tidal cycle.

The ordination in both panels is statistically significant (PERMANOVA, $p < 0.05$) Time point is indicated on each symbol with a number according to Table 4.1. Symbol color indicates the water depth in the marsh at the time of sampling according to the legend, a proxy for tidal stage.

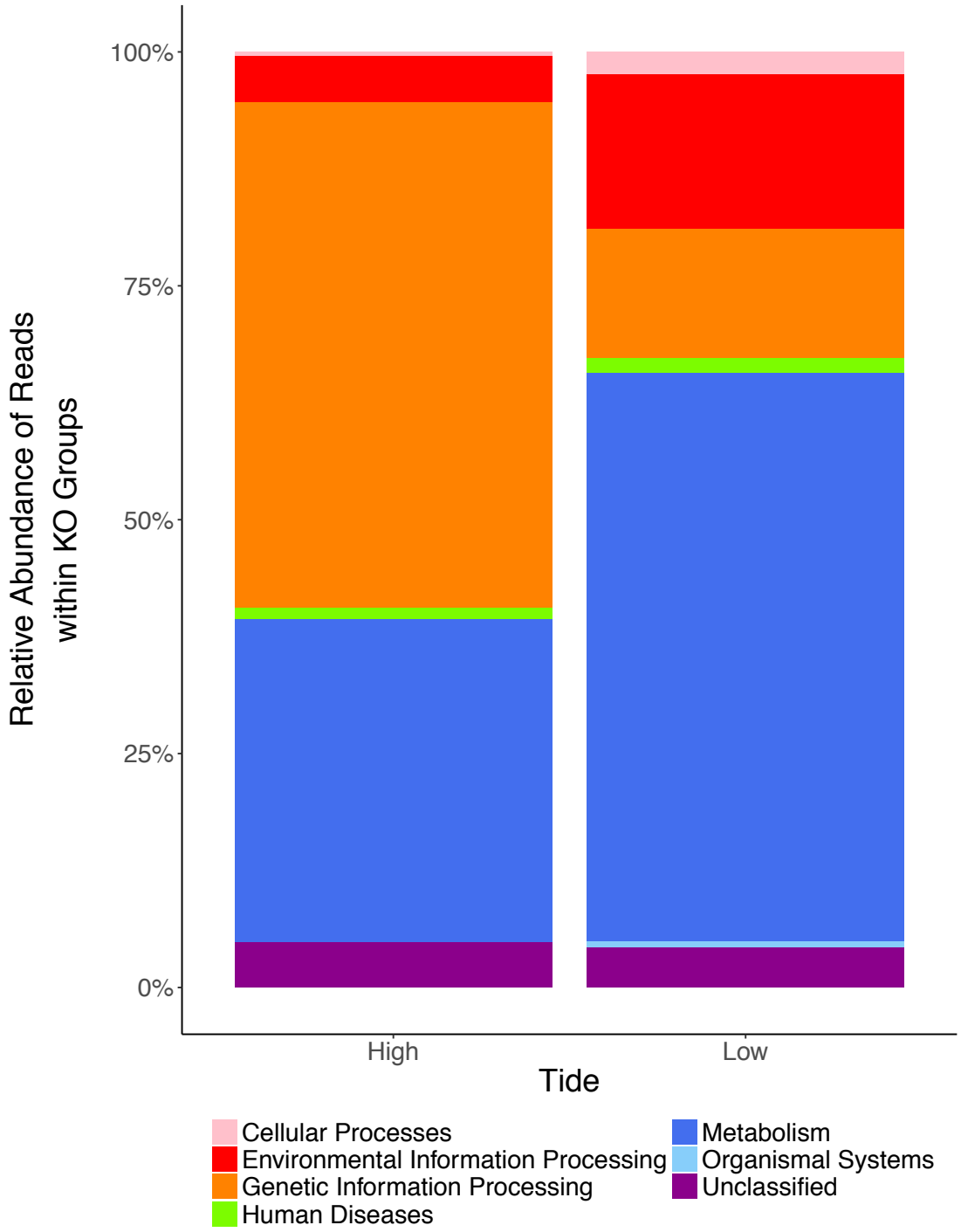

Figure 4.5. Relative abundance of reads which were significantly different between tidal cycles annotated to KO numbers within KO Groups.

Only reads for transcripts that were above a log-fold difference between tidal cycles were included in this plot.

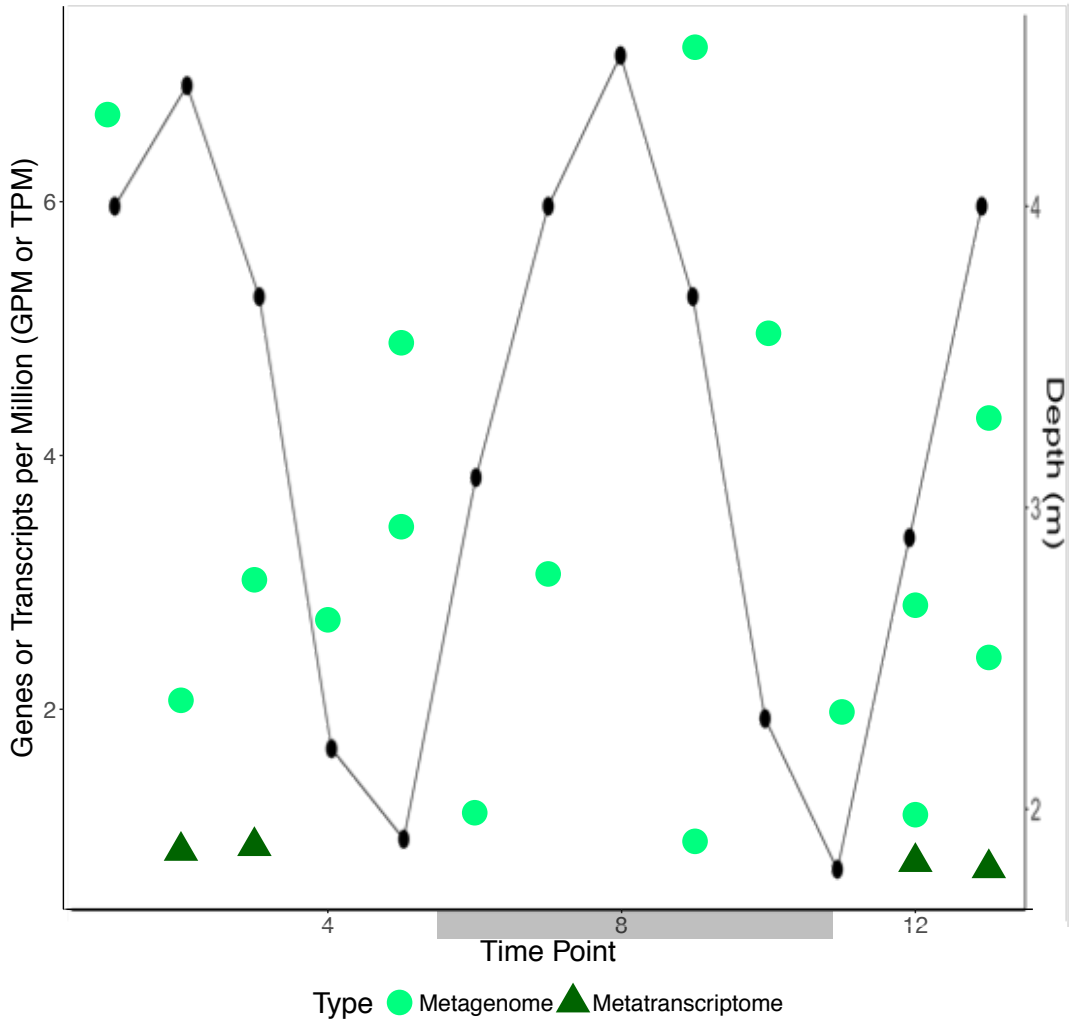

Figure 4.6. Genes and transcripts per million of dye-decolorizing peroxidases (KO:K15733; EC 1.11.1.19) across the tidal cycle.

The black box on the x-axis represents samples which were collected at night.

Figure 4.7. Genes and transcripts per million (GPM or TPM) and community composition of ring-cleaving genes from the benzoyl-CoA, catechol, gentisate, and protocatechuate pathways.

Chemical structures of the aromatic carbon compound subject to ring cleavage are displayed on the left. The gene and transcript abundance for the ring-cleaving genes of each pathway (A. *boxB*, B. *catA*, C. *genA* D. *pcaH*) are displayed in the middle and right panels. Color represents families providing genes and transcripts for the specific ring-cleaving genes. Axes are held consistent between gene and transcript abundance of a particular gene, but each horizontal panel has its own y-axis. The black boxes on the x-axis represent samples which were collected at night.

A. Benzoyl-CoA

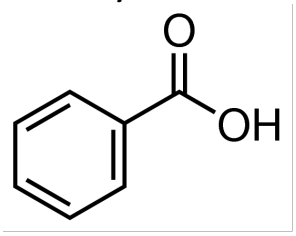

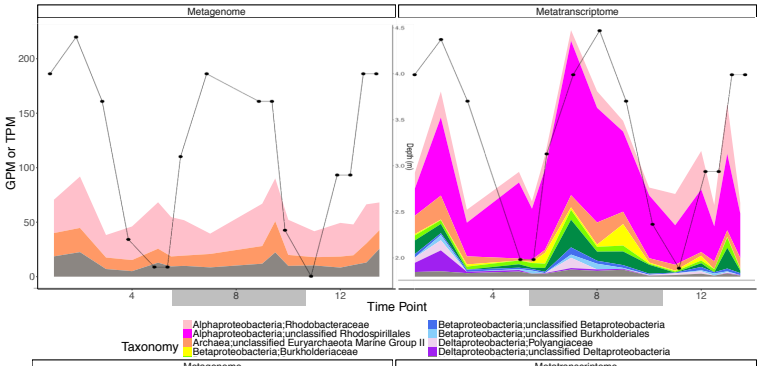

B. Catechol

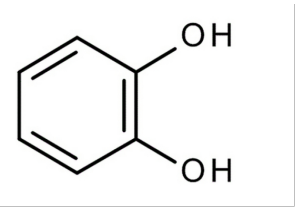

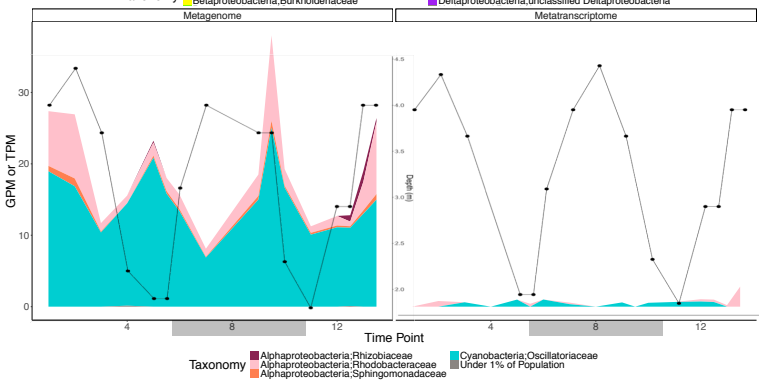

C. Gentisate

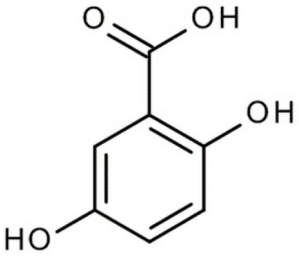

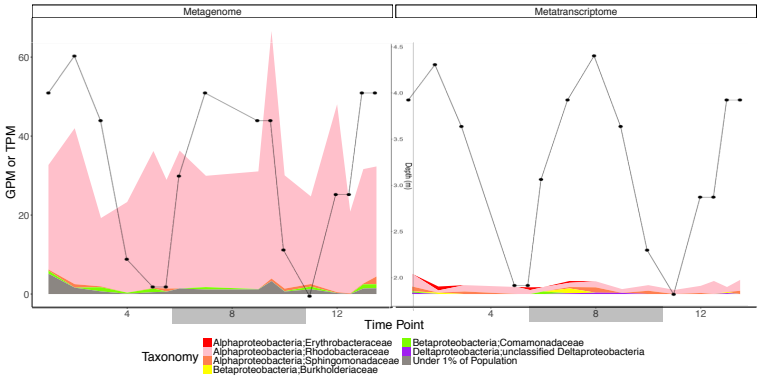

D. Protocatechuate

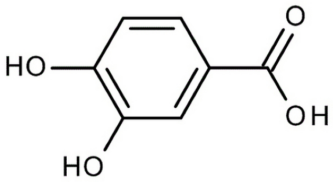

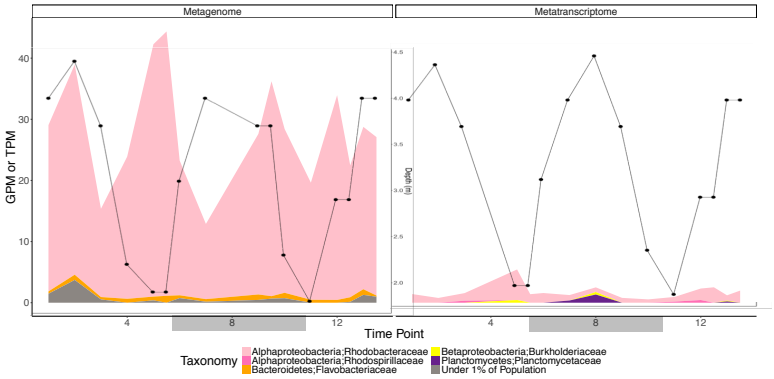

Figure 4.7. Continued

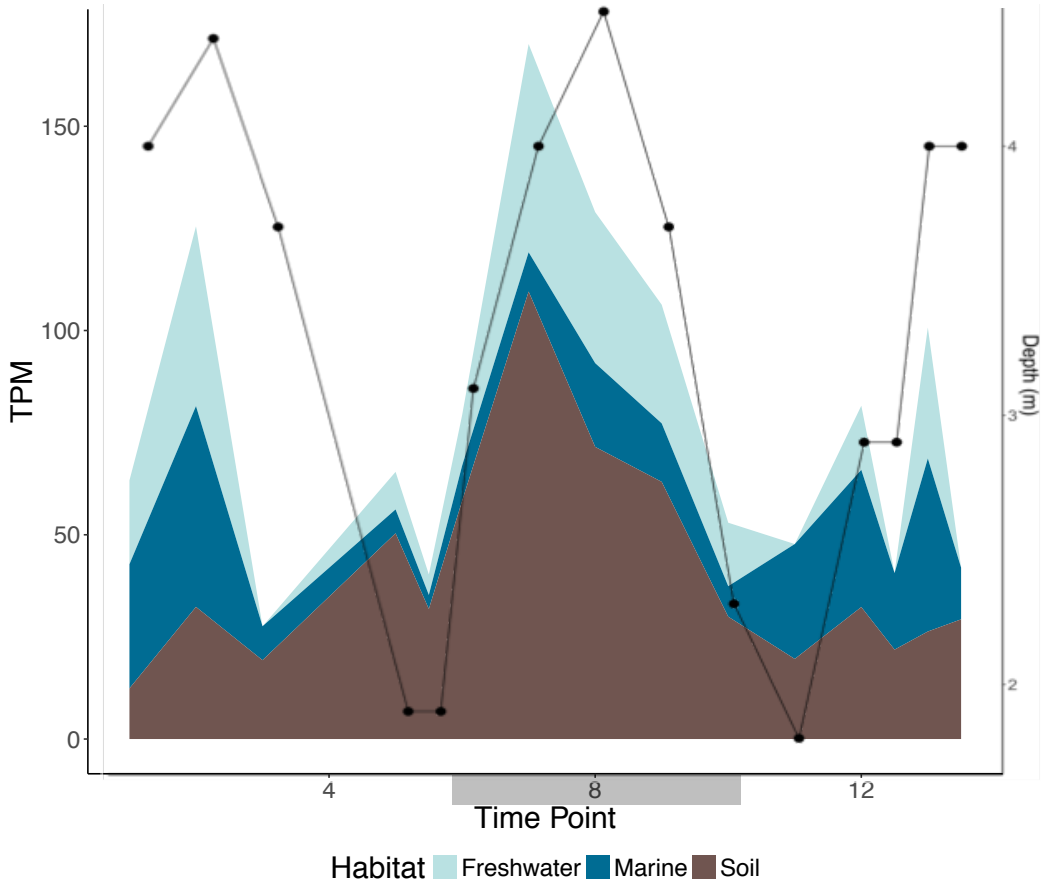

Figure 4.8. Habitats from which organisms expressing *boxB* were isolated.

boxB transcripts presented as transcripts per million (TPM) displayed by environmental origin of organisms with the greatest homology to those possessing *boxB* in the metatranscriptomes. The black box on the x-axis represents samples which were collected at night.

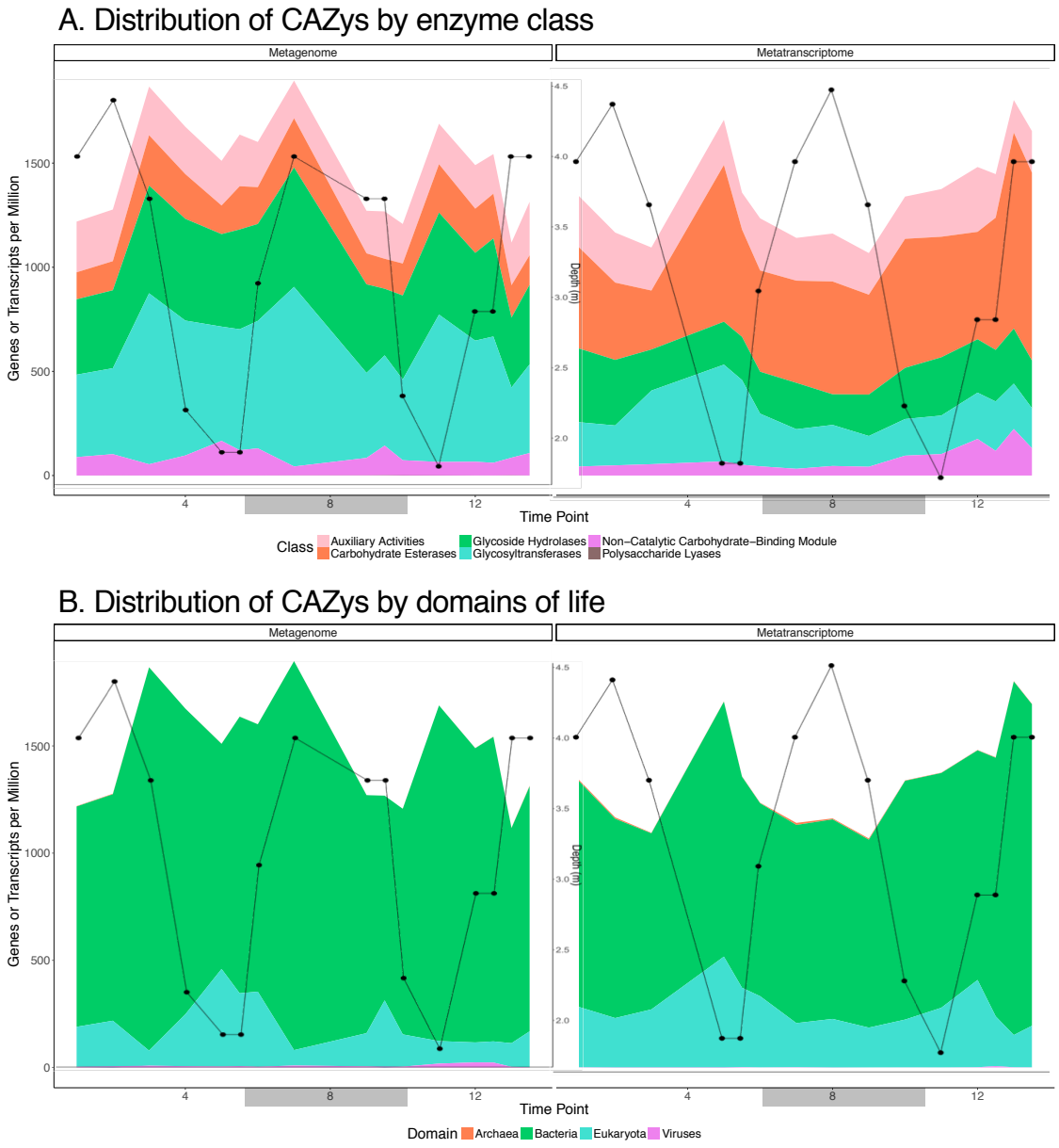

Figure 4.9. Distribution of CAZys by enzyme class and community composition.

Black boxes on the x-axis represent samples which were collected at night.

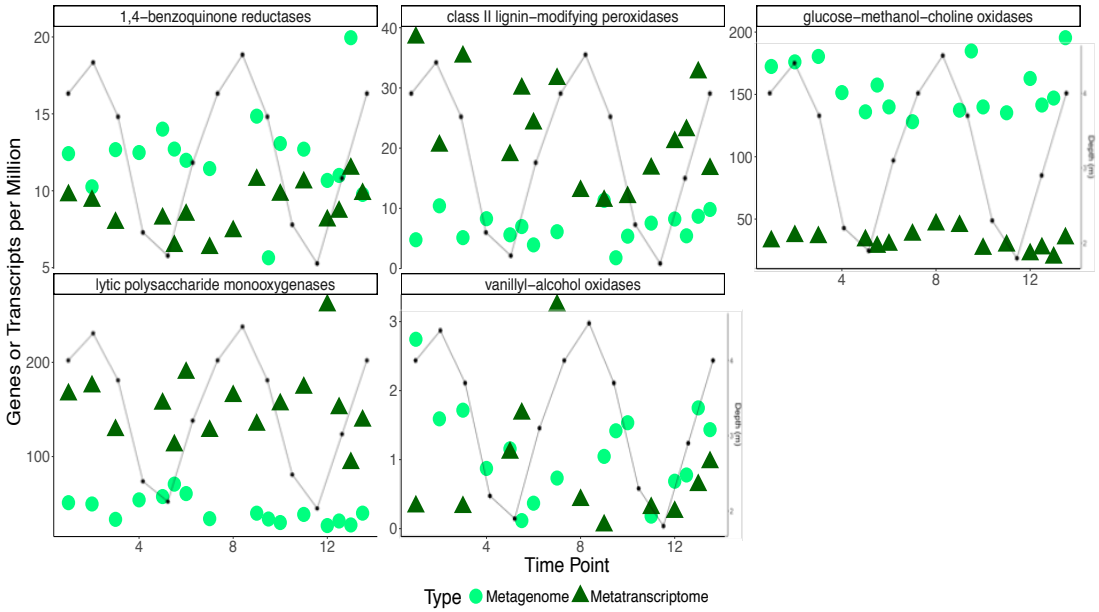

Figure 4.10. Genes and transcripts of AA enzymes.

Black boxes on the x-axis represent samples which were collected at night.

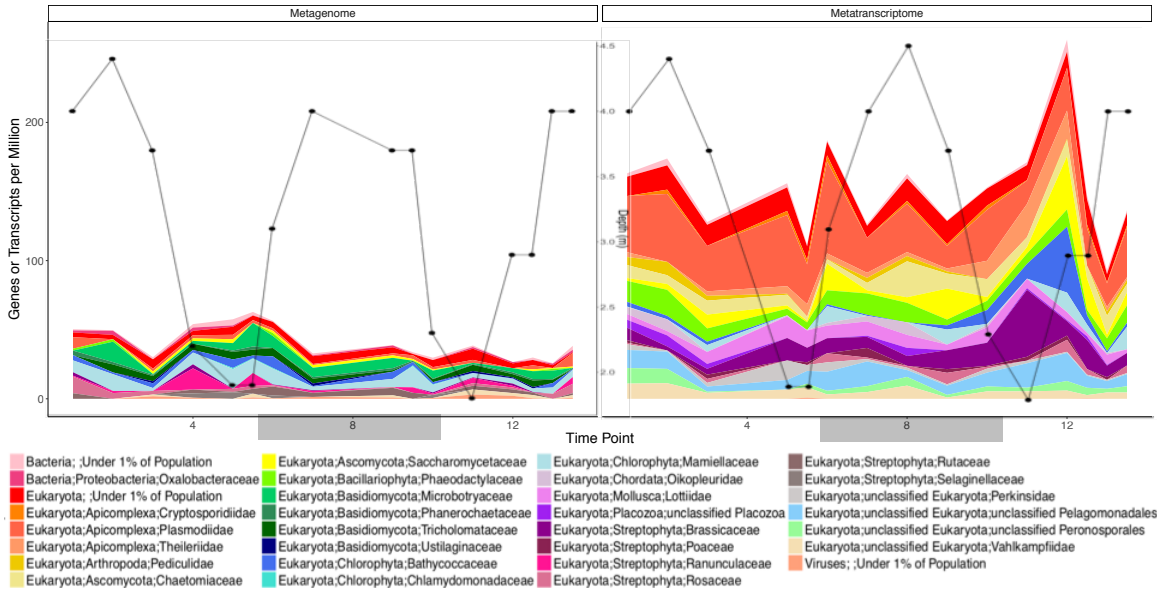

Figure 4.11. Community composition of lytic polysaccharide monooxygenases in the metagenomes and metatranscriptomes.

Black boxes on the x-axis represent samples which were collected at night.

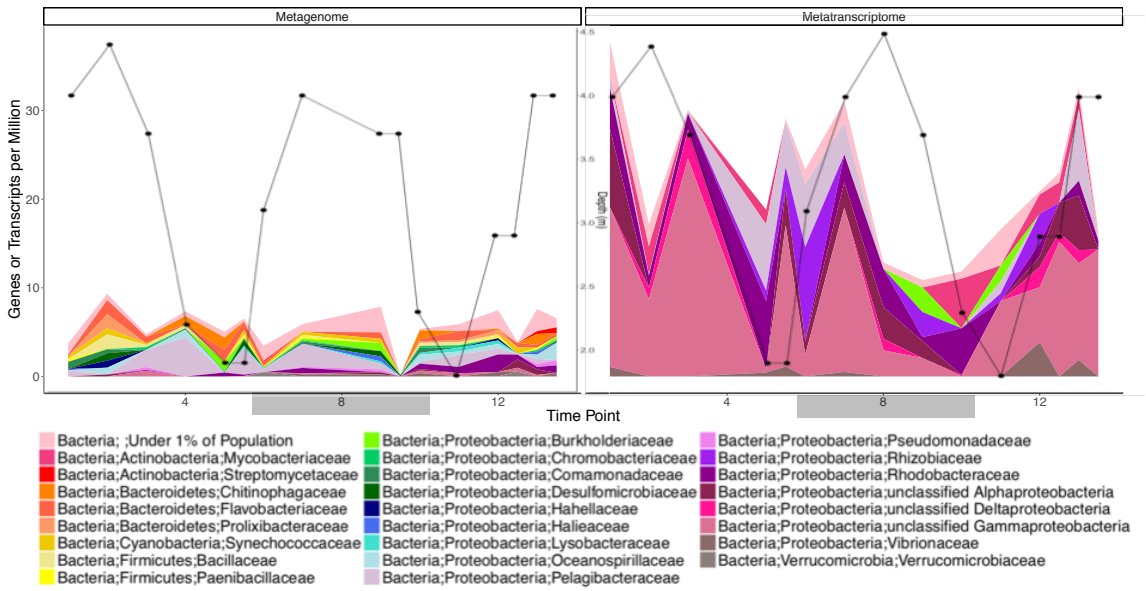

Figure 4.12. Community composition of class II lignin-modifying peroxidases in the metagenomes and metatranscriptomes.

Black boxes on the x-axis represent samples which were collected at night.

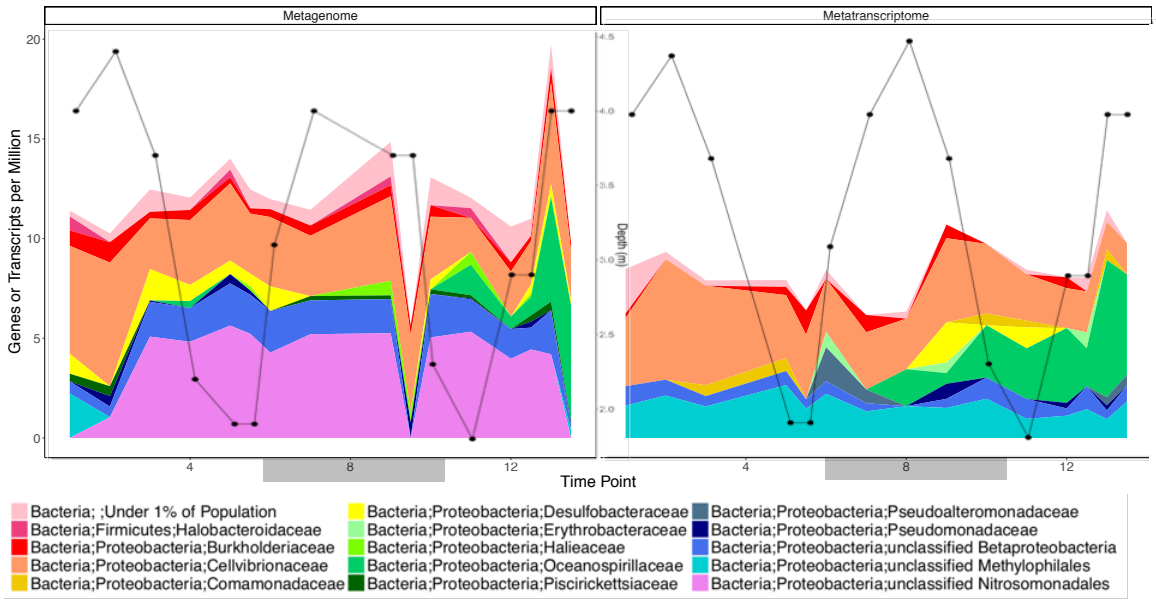

Figure 4.13. Community composition of the benzoquinone reductases in the metagenomes and metatranscriptomes.

Black boxes on the x-axis represent samples which were collected at night.

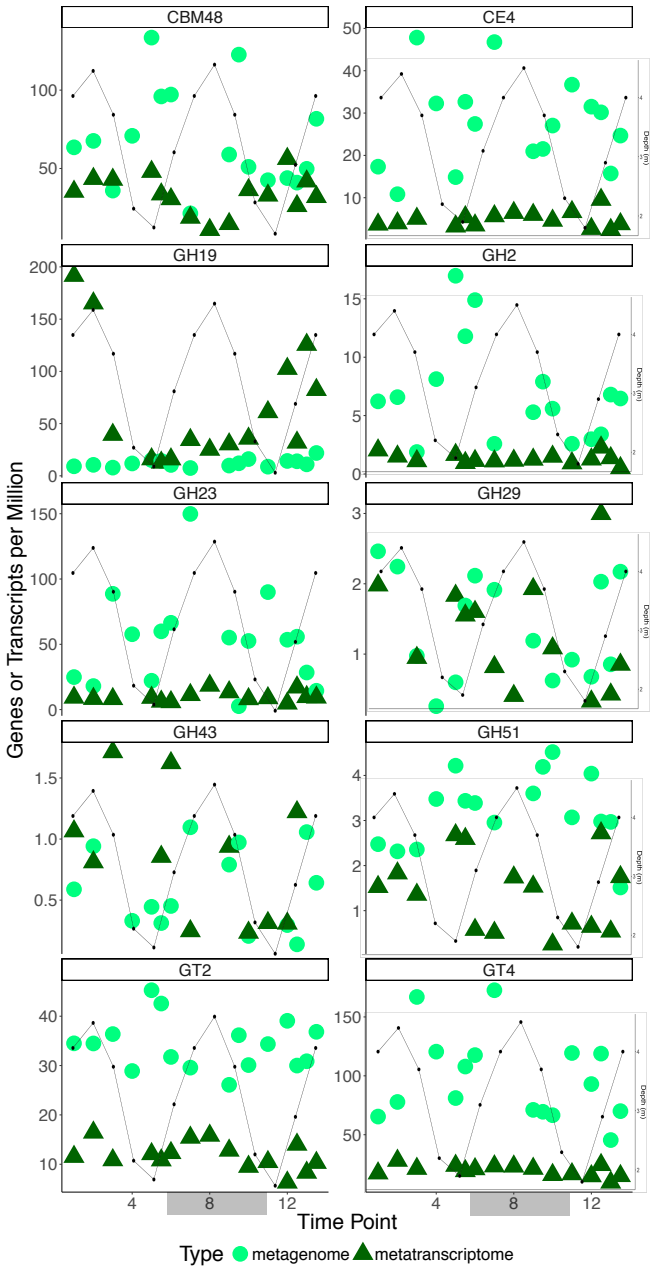

Figure 4.14. Genes and transcripts of CAZys active against plant and algal-derived carbohydrates across the tidal cycle.

The predicted substrates for the following CAZy families are: CBM48 – glycogen, CE4 – acetyl xylan and chitin, GH19 – chitin, GH 2 – galactose and mannitol, GH 23 – peptidoglycan, GH29 – fucose, GH43 – xylan, GH51 – cellulose, GT2 – cellulose, GT4 – sucrose. Black boxes represent samples which were collected at night.

CHAPTER FIVE – THE INFLUENCE OF PROCESSING TIME ON METATRANSCRIPTOMES GENERATED FROM SURFACE WATER OF A COASTAL SALT MARSH

AUTHOR CONTRIBUTIONS

Five individuals significantly contributed to this chapter: Lauren Quigley, Megan Thompson, Aron Stubbins, Andrew D. Steen, and Alison Buchan. Conceived the experiment: LQ, AB. Collected samples: LQ, MT, AS, ADS. Extracted nucleic acids and analyzed community sequencing data: LQ. Wrote the manuscript: LQ, AB.

I. ABSTRACT

Metatranscriptomic sequencing has greatly enhanced our understanding of microbial community function but given both the potential for microbes to rapidly respond to altered environmental conditions and the rapid half-life of mRNA (~ two minutes) these datasets have the potential to be greatly influenced by collection and processing times. While it is widely accepted that RNA collection should happen as quickly as possible, there is limited data to demonstrate the influence of processing time on metatranscriptomic analyses. To fill this gap, we compared metatranscriptomes collected from a Southeastern US salt marsh that were processed within either 15 minutes or an hour. To capture variability in microbial composition, samples were collected from three timepoints during a tidal cycle. We found that processing time significantly influences transcription profiles. For instance, community composition, assessed by taxonomic identification of coding sequences, was altered in 35-45% of the bacterial orders, compared to only 2.0-9.6% in true biological replicates. Processing time also influenced the transcriptional profile of the community. However, neither the differences between the community composition nor function were consistent across the three time points from which the differential processing time metatranscriptomes were generated. These data support the widely held assumption that samples being collected for metatranscriptomic analyses should be processed as quickly as possible.

II. INTRODUCTION

Metatranscriptomics are a powerful tool enabling scientists to analyze the mRNA transcripts within a community. Analyzing transcripts allows us to understand how microbial communities respond to perturbations, such as the Deepwater Horizon oil spill or treatment with a broad spectrum antibiotic (*1, 2*), in addition to understanding the mechanisms by which microbial communities mediate biogeochemical cycling and how they interact with symbiotic hosts, such as plants and humans, and each other (*3–5*).

Coastal salt marshes are detritus-based ecosystems and are critically important to biogeochemical cycling (*6–8*). The salt marshes that fringe the coast of the Southeastern United States have some of the highest rates of net primary productivity on Earth, ranging from 0.2 to 2.25 kg C m^{-2} yr^{-1} (*8, 9*), thus serving as an important sink for atmospheric CO_2. Salt marshes also have the highest rates of dimethyl sulfide (DMS) production (*10*), an important sulfur volatile compound, which stimulates cloud condensation nuclei and results in a negative feedback to global warming (*11*). In addition to mediating biogeochemical cycling with important ramifications to global climate change, salt marsh systems are very dynamic with a 2-3 m tidal amplitude (*12*). Given how dynamic these ecosystems are, metatranscriptomics provide a powerful tool in order to understand how the microbial communities of these systems mediate biogeochemical cycling across strong environmental gradients.

While metatranscriptomics have greatly expanded our knowledge of microbial community functioning. High-quality samples for metatranscriptomic analyses are difficult to obtain due to the limited amount of mRNA in the overall RNA pool and the short half-lives of mRNA (*13, 14*). The median half-lives of mRNA from *Vibrio* sp. S14 and *Prochlorococcus* MED4 are 1.7 and 2.4 minutes, respectively (*15, 16*); these organisms are both members of the marine microbial community and their mRNA half-lives should be reflective of the natural community (*17–19*). Due to the short half-lives of mRNA and rapid biological response times, metatranscriptomic analyses are thought to be particularly vulnerable to

increases in processing time (*20*). While it is a widely held belief that sample collection for metatranscriptomes must occur as quickly as possible in order to be a representative snapshot of the potential functions within a community, there is limited data to show how increased processing time changes the resultant metatranscriptomes. To this end, we generated six metatranscriptomes that were collected at three different time points. For each time point two metatranscriptomes were generated with varying degrees of processing time (15 and 60 minutes). These datasets enable us to quantify the effect of increased processing time on changes in community structure and function.

III. MATERIALS AND METHODS

Sample collection

On April 23-24 and July 16-17 2014 microbial communities from Groves Creek, a temperate salt marsh fringing Skidaway Island, GA (31.972, -81.028), were collected by vacuum filtration. All samples were collected from the surface water by pumping water into a 20 L carboy. Two filtration methods were used in April. For the first method whole marsh water was pre-filtered through a 3 μm filter and 375 mL of the resultant filtrate was passed through a 0.22 μm pore size, 47 mm diameter filter (Millipore, Burlington, MA). These filters were processed within 15 minutes of sample collection and are referred to as early processing. The second set of filters was prefiltered in the same manner. One liter of water was collected on a 0.22 μm pore size, 142 mm diameter filter (Millipore, Burlington, MA). These filters were processed within an hour of sample collection and are referred to as late processing. For July collection, water was first filtered through a GF/D glass fiber filter (~2.7 μm pore size, Whatman, GE Healthcare Life Sciences, Marlborough, MA); 500 mL of the filtrate was passed through a 0.22 μm pore size, 47 mm diameter filter (Millipore, Burlington, MA). Filtration was completed within 15 min of sample collection. After filtration all filters were placed in cryovials and flash frozen in liquid nitrogen. The samples were stored at -80 C until processing. A summary of the filtration schemes is provided in Table 5.1.

Sample processing

For all samples, the filters were thawed and placed in a 2 mL tube with 0.3 g glass and zirconia beads (0.2 g glass and 0.1 g zirconia), 0.75 mL CTAB extraction buffer, 0.75 mL phenol:chloroform:isoamyl alcohol (25:24:1, pH 8), internal standards (Satinsky et al. 2013), proteinase K, and 10% SDS. Samples were vortexed for 10 min to lyse the cells. then centrifuged for 10 min at 10,000 rpm and 4° C. The lysates were transferred to a sterile 1.5 mL microcentrifuge tube and mixed with 0.75 mL chloroform:isoamyl alcohol (24:1). The aqueous phase was added to a sterile 1.5 mL microcentrifuge with $MgCl_2$, sodium acetate, and isopropanol. This solution was incubated at -80° C for 1.5 hrs and then centrifuged at 4° C for 45 min at 10,000 rpm. The supernatant was discarded, and the RNA was washed with 70% EtOH twice. Following RNA extraction Turbo DNase was used to remove residual DNA.

All sequencing, assembly, and annotation was performed by DOE JGI. A plate-based RNA sample preparation was performed on the PerkinElmer Sciclone NGS robotic liquid handling system using the Illumina Ribo-Zero rRNA Removal Kit (Bacteria) and the TruSeq Stranded Total RNA HT sample prep kit following the protocol outlined by Illumina. Total RNA starting material consisted of 100 ng per sample and included 10 cycles of PCR for library amplification. Illumina sequencing was performed as described for metagenome samples.

Quality filtered metatranscriptomic sequences for each sample were assembled with Megahit (version 1.10.6) (*21*), and all contigs > 200 bp were annotated by the Integrated Microbial Genomes (IMG) pipeline (*22*). Resultant assemblies were combined with coding sequences (CDS) using bedtools2 (*23*) in order to generate an assembly with CDS embedded. Quality controlled raw reads were mapped to the assembly with gene features using bowtie2 (version 2.2.9) (*24*). Coverage information on the number of reads mapping to each contig was generated using pileup in the BBmap suite of tools. The coverage information was used to normalize read counts to account for the length of reads and the length of CDS. Read counts within KEGG ortholog groups (KO) were summed and

normalized as read counts per million mapped to KO-annotated contigs (transcripts per million [TPM]) (*25, 26*). TPM were also used in taxonomic analyses. Details on the assembly and annotation of each sample are available in Tables 5.2 and 5.3.

Data analysis

Data analysis and visualization was performed using the R statistical platform (*27, 28*). Metacoder was used to plot taxonomic trees showing changes in community composition between early and late processing samples and replicates (*29*). Only bacterial orders that had an average of 50 TPM per sample were used in the metacoder analyses. All multivariate statistics and ordination were performed with Vegan (*30*). Taxonomic lineages and KEGG ortholog groups that appeared at only a single time point were removed from analyses, and only those annotations which were a 75% or greater match to the reference were used in analyses. Raw data and scripts are posted at http://github.com/lnmquigley.

IV. RESULTS

Community composition

CDS within the metatranscriptome were annotated for both taxonomy and function within JGI's Genomes OnLine Database (GOLD)(*31*); those taxonomic identifications of CDS were used for all community composition analyses. Bacterial communities in the April metatranscriptomes early processing samples are made up of 190 orders, but only 18 of them account for more than 1% of the community. Metatranscriptomes in April were generated at three timepoints, named A-1, A-2, and A-3. All three time points occurred within 14 hours of each other with samples for A-2 and A-3 being collected 12 and 14 hours after A-1 respectively. While the overall structure of the community is similar, A-1 is enriched in γ-Proteobacteria and depleted in Cyanobacteria compared to A-2 and A-3 (Figure 5.1). In order to determine how much processing time influences the bacterial community composition the log-fold change between orders with an average of 50 TPM was calculated for each time point. Of the 56 orders with an average of 50 transcripts per million (TPM) per sample 19, 27, and 20 orders in A-1, A-2, and A-3, respectively, had a log-fold or greater change in bacterial order due to processing time (Figures 5.2 and 5.3).

The orders that change as a result of processing time are not consistent between the three time points with the one exception of the order Nitrosomonadales, the abundance of which decreased with increased processing time. However, the greatest enrichment in the late samples occurs in γ-Proteobacteria, which accounts for 30,231, 13,989, and 17,961 TPM in the early processed samples and 49,161, 16,090, and 31,742 TPM in the late processed samples from A-1, A-2, and A-3, respectively. The five most abundant orders in the April bacterial communities are Rhodobacterales (12.5%), Flavobacteriales (9.67%), Nostocales (8.82%), Synechococcales (7.93%), and Oscillatoriales (6.58%). Of these orders only Synechococcales changes more than a log-fold in all three April time points, with an enrichment in the late processed samples at A-1 and A-3 and a depletion at A-2, while Nostocales and Oscillatoriales were both depleted in the late A-2 and A-3 samples and Flavobacteriales was depleted in A-1. Rhodobacterales did not vary more than a log-fold change between processing times at any of the three time points. For all three time points the effective number of bacterial orders in the sample increases with processing time, though the magnitude of change is different for all time points. A-1 increases less than a percent from the initial number of orders (33.98 in the early sample and 34.24 in the late sample, while the effective number of orders nearly doubles with increased processing time at A-2 (22.64 to 41.28). A-3 increases from 28.49 orders to 33.42.

In order to understand how great the magnitude of change due is to processing time, true replicates collected in July were analyzed as well. These samples were collected at the same time and processed in an identical manner at two time points, named J-1 and J-2. Log-fold changes between the replicates were calculated for the 62 orders with an average of 50 TPM per sample. Of those, 62 orders only two changed at J-1 and six at J-2. The two orders that are greater than a log-fold change for the J-1 replicates are Geodermatophilales and Chroococcidiopsidales (Figures 5.4 and 5.5). These two orders represent 0.118% and 0.013% of the community in one replicate and less than 0.001% and 0.004% in the other. The orders that have greater than a log-fold difference in J-2 are Bacteroidales, Gloeoemargaritales, Spirulinales, Gemmatimonadales, Pelagibacterales, and Opitutales (Figures 5.4 and 5.5). Of these six orders the Pelagibacterales makes up the greatest portion

of the community, 7.6% and 17.1% in the two replicates. Of the remaining five orders with a log-fold change the next closest in relative abundance is Gleoemargaritales at 0.28% and 0.13% of the community in the two replicates. The effective number of orders for the J-1 samples is 20.449 and 21.335 and 22.32 and 19.1 for J-2. The difference in the effective number of orders between the July replicates is smaller than the difference between the April samples with different processing time, with the exception of A-1. These data indicate that the differences in bacterial community composition between biological replicates that are processed quickly and identically are minor compared to the differences between bacterial community composition in metatranscriptomic samples that are processed an hour after collection.

Community functioning

Processing time and month significantly structure the clustering of the metatranscriptomes based on KEGG ontology (PERMANOVA processing time R^2=0.185, p <0.039, month R^2=0.388, p < 0.003; Figure 5.6). It is unsurprising that the metatranscriptomes collected in July would cluster away from the April metatranscriptomes, but for both months the metatranscriptomes that were processed early cluster closely, while those in April that were processed later form a looser cluster around the samples that were processed early in April and show no definitive pattern. In order to determine which functions were driving the difference between the early metatranscriptomes average, TPM per KO number within KEGG groups was calculated. The KEGG groups for which there was the greatest difference for the early processed TPM in April were cell growth and death, signaling molecules and interactions, and glycan biosynthesis and metabolism (Figure 5.7). The July replicates had more similar average TPM per KO number across all the KEGG groups (Figure 5.7). Log-fold change between average TPM per KO within KEGG group was calculated for the late metatranscriptomes compared to the early and the true replicates collected in July. The KEGG groups for which the late samples differed the most from the early samples were cell growth and death, replication and repair, and xenobiotics degradation and metabolism, while the true replicates showed very little difference in

average TPM per KEGG group between replicates (all less than 0.25 log-fold change; Figure 5.8).

V. DISCUSSION

Processing time greatly influences the accuracy of metatranscriptomic analyses. Increased processing time leads to large shifts in both transcriptional profiles both functionally and taxonomically, obscuring the original community structure and gene expression. On average, natural communities from marine and riverine environments possess 200 transcripts per cell with a half-life of close to two minutes (*4, 14, 32–36*). This means that roughly one transcript in a billion was present in the sample when it was collected by the time it was flash frozen for the samples that took an hour to process, while samples that were processed in 10 minutes had one transcript in every 32 that was present at the time of collection. The remaining transcripts were transcribed during processing and are thus less representative of the transcriptional activity in the marsh.

Processing time drastically changes the community composition and function, but it does not do so in a consistent manner, possibly due to underlying differences in the community composition and functional profile of the community at each individual time point. The metatranscriptomes processed early for all three time points shared very similar community structure and function profiles; however, the metatranscriptomes processed late show very little overlap between the taxa that are enriched with the exception of γ-Proteobacteria and show the most similar functional response for transcription. γ-Proteobacteria have been shown to bloom when seawater undergoes a bottle effect, particularly members of the order Altermonadales and Vibrionales (*37–41*). At A-1 and A-3 both Altermonadales and Vibrionales bloom during the increased processing time as well as Nevskiales, while none of these orders bloom at A-2. Most of the late processed samples have an increased number of TPM for all KO groups that we looked at possibly as a result of increased cell density, which has been demonstrated to occur when marine communities undergo a bottle effect (*42*); therefore it is unsurprising that each time point had a relatively similar increase in the

number of TPM annotated to transcription. The late processed metatranscriptomes demonstrate inconsistencies in how the microbial community responds to increased residence time in a bottle. These data underscore the necessity of collecting and preserving samples for metatranscriptomic analyses as quickly as possible. Caution should be used when interpreting metatranscriptomic analyses from samples that were not preserved within an hour of sampling.

We analyzed true biological replicate metatranscriptomes collected from the same site three months later in order to establish how much variation should be expected between metatranscriptome replicates. Metatranscriptomes collected at the same time but with different processing time are much more different in both community structure and function than true replicates. The true biological replicates have very similar community structures with only two and six bacterial orders changing by an order of magnitude between the replicates for the two time points analyzed. Additionally, the log-fold change of average TPM per KO number within a KEGG group for both replicates is always less them 0.25, indicating very similar functionality between the two replicates. Taken together these data suggest that while increased processing time greatly affects transcriptional profiles, replicates processed quickly and at the same time display a high degree of similarity.

VI. ACKNOWLEDGEMENTS

We would like to thank Drs. Mary Ann Moran and Alexey Vorobev for their RNA extraction protocol without which we would have been unable to complete this work. We also acknowledge and thank Drs. Byron Crump and Jérôme Payet for their bioinformatics pipeline and help with its implementation.

This work was supported by a grant from the National Science Foundation [OCE-1357242] awarded to AB, ADS, and AS and sequencing was conducted by the U.S. Department of Energy Joint Genome Institute, a DOE Office of Science User Facility, is supported by the Office of Science of the U.S. Department of Energy under Contract No. DE-AC02-05CH11231 through a community sequencing project awarded to AB, ADS, and AS.

VII. REFERENCES

1. A. R. Rivers *et al.*, Transcriptional response of bathypelagic marine bacterioplankton to the Deepwater Horizon oil spill. *ISME J.* **7**, 2315–2329 (2013).
2. L. K. Ursell, R. Knight, Xenobiotics and the human gut microbiome: Metatranscriptomics reveal the active players. *Cell Metab.* **17**, 317–318 (2013).
3. L. Moitinho-Silva *et al.*, Integrated metabolism in sponge-microbe symbiosis revealed by genome-centered metatranscriptomics. *ISME J.* **11**, 1651–1666 (2017).
4. B. M. Satinsky *et al.*, Expression patterns of elemental cycling genes in the Amazon River Plume. *ISME J.* **11**, 1852–1864 (2017).
5. C. N. Hesse *et al.*, Forest floor community metatranscriptomes identify fungal and bacterial responses to N deposition in two maple forests. *Front. Microbiol.* **6** (2015), doi:10.3389/fmicb.2015.00337.
6. S. C. Pennings, M. D. Bertness, in *Marine Community Ecology* (2001; http://www.sillimanlab.com/pdf/Bertness_Chapter11.pdf), pp. 289–316.
7. R. G. Wiegert, L. R. Pomeroy, W. J. Wiebe, in *The Ecology of a Salt Marsh* (1981), pp. 3–20.
8. R. G. Wiegart, B. J. Freeman, Tidal marshes of the southeastern Atlantic coast: a community profile. *U.S. Fish Wildl. Serv.* **85**, 1–80 (1990).
9. G. A. Hyndes *et al.*, Mechanisms and ecological role of carbon transfer within coastal seascapes. *Biol. Rev.* **89**, 232–254 (2014).
10. P. A. Steudler, B. J. Peterson, Contribution of gaseous sulphur from salt marshes to the global sulphur cycle. *Nature*. **311**, 455–457 (1984).
11. L. Bopp, O. Aumont, S. Belviso, P. Monfray, Potential impact of climate change on marine dimethyl sulfide emissions. *Tellus Ser. B-Chemical Phys. Meteorol.* **55** (2003), pp. 11–22.
12. R. G. Wiegert *et al.*, The Georgia Rivers Land Margin Ecosystem Research Program. *Limnologica*. **29**, 286–292 (1999).
13. S. He *et al.*, Validation of two ribosomal RNA removal methods for microbial metatranscriptomics. *Nat. Methods*. **7**, 807–812 (2010).

14. M. P. Deutscher, Degradation of RNA in bacteria: Comparison of mRNA and stable RNA. *Nucleic Acids Res.* **34**, 659–666 (2006).
15. N. H. Albertson, T. Nyström, S. Kjelleberg, Functional mRNA half-lives in the marine Vibrio sp. S14 during starvation and recovery. *J. Gen. Microbiol.* **136**, 2195–2199 (1990).
16. C. Steglich *et al.*, Short RNA half-lives in the slow-growing marine cyanobacterium Prochlorococcus. *Genome Biol.* **11** (2010), doi:10.1186/gb-2010-11-5-r54.
17. P. Flombaum *et al.*, Present and future global distributions of the marine Cyanobacteria Prochlorococcus and Synechococcus. *Proc. Natl. Acad. Sci.* **110**, 9824–9829 (2013).
18. J. D. Oliver, R. A. Warner, D. R. Cleland, Distribution and ecology of Vibrio vulnificus and other lactose-fermenting marine vibrios in coastal waters of the Southeastern United States. *Appl. Environ. Microbiol.* **44**, 1404–1414 (1982).
19. J. R. Westrich *et al.*, Saharan dust nutrients promote Vibrio bloom formation in marine surface waters. *Proc. Natl. Acad. Sci. U. S. A.* **113**, 5964–5969 (2016).
20. S. Bikel *et al.*, Combining metagenomics, metatranscriptomics and viromics to explore novel microbial interactions: Towards a systems-level understanding of human microbiome. *Comput. Struct. Biotechnol. J.* **13** (2015), pp. 390–401.
21. D. Li, C. M. Liu, R. Luo, K. Sadakane, T. W. Lam, MEGAHIT: An ultra-fast single-node solution for large and complex metagenomics assembly via succinct de Bruijn graph. *Bioinformatics*. **31**, 1674–1676 (2015).
22. M. Huntemann *et al.*, The standard operating procedure of the DOE-JGI Metagenome Annotation Pipeline (MAP v.4). *Stand. Genomic Sci.* **11** (2016), doi:10.1186/s40793-016-0138-x.
23. A. R. Quinlan, I. M. Hall, BEDTools: A flexible suite of utilities for comparing genomic features. *Bioinformatics*. **26**, 841–842 (2010).
24. B. Langmead, S. L. Salzberg, Fast gapped-read alignment with Bowtie 2. *Nat. Methods*. **9**, 357–359 (2012).
25. G. P. Wagner, K. Kin, V. J. Lynch, Measurement of mRNA abundance using RNA-seq data: RPKM measure is inconsistent among samples. *Theory Biosci.* **131**, 281–

285 (2012).

26. M. R. Gradoville, B. C. Crump, R. M. Letelier, M. J. Church, A. E. White, Microbiome of Trichodesmium colonies from the North Pacific Subtropical Gyre. *Front. Microbiol.* **8** (2017), doi:10.3389/fmicb.2017.01122.
27. R Core team, R Core Team. *R A Lang. Environ. Stat. Comput. R Found. Stat. Comput. , Vienna, Austria. ISBN 3-900051-07-0, URL http//www.R-project.org/.* **55** (2015), pp. 275–286.
28. H. Wickham, ggplot 2 Version 1. *Media*. **35**, 211 (2009).
29. Z. S. L. Foster, T. J. Sharpton, N. J. Grünwald, Metacoder: An R package for visualization and manipulation of community taxonomic diversity data. *PLoS Comput. Biol.* **13** (2017), doi:10.1371/journal.pcbi.1005404.
30. J. Oksanen *et al.*, vegan: Community Ecology Package. *R Packag. ver. 2.4–3* (2017), p. 282.
31. M. A. Moran *et al.*, Sizing up metatranscriptomics. *ISME J.* **7** (2013), pp. 237–243.
32. S. M. Gifford, S. Sharma, M. Booth, M. A. Moran, Expression patterns reveal niche diversification in a marine microbial assemblage. *ISME J.* **7**, 281–298 (2013).
33. S. M. Gifford, S. Sharma, J. M. Rinta-Kanto, M. A. Moran, Quantitative analysis of a deeply sequenced marine microbial metatranscriptome. *ISME J.* **5141**, 461–472 (2011).
34. S. H. Lee, P. F. Kemp, Single‐cell RNA content of natural marine planktonic bacteria measured by hybridization with multiple 16S rRNA‐targeted fluorescent probes. *Limnol. Oceanogr.* **39**, 869–879 (1994).
35. M. Simon, F. Azam, Protein content and protein synthesis rates of planktonic marine bacteria. *Mar. Ecol. Prog. Ser.* **51**, 201–213 (1989).
36. M. Landa, M. T. Cottrell, D. L. Kirchman, S. Blain, I. Obernosterer, Changes in bacterial diversity in response to dissolved organic matter supply in a continuous culture experiment. *Aquat. Microb. Ecol.* **69**, 157–168 (2013).
37. J. Dinasquet, T. Kragh, M. L. Schrøter, M. Søndergaard, L. Riemann, Functional and compositional succession of bacterioplankton in response to a gradient in

bioavailable dissolved organic carbon. *Environ. Microbiol.* **15**, 2616–2628 (2013).

38. H. Eilers, J. Pernthaler, F. O. Glöckner, R. Amann, Culturability and in situ abundance of pelagic Bacteria from the North Sea. *Appl. Environ. Microbiol.* **66**, 3044–3051 (2000).
39. C. E. Nelson, C. A. Carlson, Tracking differential incorporation of dissolved organic carbon types among diverse lineages of Sargasso Sea bacterioplankton. *Environ. Microbiol.* (2012), doi:10.1111/j.1462-2920.2012.02738.x.
40. J. Pinhassi, T. Berman, Differential growth response of colony-forming alpha- and gamma-proteobacteria in dilution culture and nutrient addition experiments from Lake Kinneret (Israel), the eastern Mediterranean Sea, and the Gulf of Eilat. *Appl. Environ. Microbiol.* **69**, 199–211 (2003).
41. R. L. Ferguson, E. N. Buckley, A. V. Palumbo, Response of marine bacterioplankton to differential filtration and confinement. *Appl. Environ. Microbiol.* **47**, 49–55 (1984).

VIII. APPENDIX: TABLES

Table 5.1. Summary of filtration schemes.

Sample	Replicate	Time	Processing Time (min)	Depth (m)	Water collected (mL)	RNA extracted (ng)
A-1	1	04/23/14 22:45	15	1.5	375	357
A-1	2	04/23/14 22:45	60	1.5	500	124.25
A-2	1	04/24/14 11:00	15	1.4	375	301
A-2	2	04/24/14 11:00	60	1.4	500	297.5
A-3	1	04/24/14 13:15	15	2.3	375	406
A-3	2	04/24/14 13:15	60	2.3	500	378
J-1	1	07/16/14 19:00	15	1.9	500	609
J-1	2	07/16/14 19:00	15	1.9	500	1,449
J-2	1	07/17/14 9:30	15	2.9	500	1,386
J-2	2	07/17/14 9:30	15	2.9	500	2,674

Table 5.2. Sequencing Statistics.

Sample	Replicate	Illumina paired-end reads	Paired-end reads remaining after QC	Contigs assembled	Weighted-average contig length (N50)	Reads aligning to assembly[a]
A-1	1	86214786	31917534	308,057	660 bp	27,541,146 (86.29)
A-1	2	84,381,964	61,151,218	184,049	571 bp	52,924,587 (86.55)
A-2	1	99,413,892	62,726,168	103,214	579 bp	56,964,038 (90.81)
A-2	2	89,223,254	84,466,300	937,878	893 bp	75,728,547 (89.66)
A-3	1	100,410,934	61,065,488	106,106	606 bp	54,855,868 (89.83)
A-3	2	109,889,748	72,418,130	510,459	643 bp	66,820,329 (92.27)
J-1	1	99,310,818	59,698,470	554,002	608 bp	53,777,322 (90.08)
J-1	2	102,593,816	64,047,020	610,658	639 bp	57,868,041 (90.35)
J-2	1	134,676,690	91,790,984	798,201	602 bp	84,559,059 (92.12)
J-2	2	104,172,002	68,547,096	659,468	611 bp	62,701,910 (91.47)

a. Values in parentheses represent percentages

Table 5.3. Annotation Statistics.

Sample	Replicate	CDS	CDS annotated to KO[a]	CDS without KO annotation[a]	Number of CDS annotated to KO with greater than 75% ID to reference[a]	Number of reads mapped to annotated CDS[a]	Number of reads mapped to CDS with greater than 75% ID to reference[a]	Number of reads mapped to CDS without annotation[a]
A-1	1	381,289	196,247 (51.47)	185,042 (48.53)	116,028 (30.43)	12,352,335 (44.85)	8,596,147 (31.21)	15,188,811 (55.15)
A-1	2	215,139	116,241 (54.03)	98,898 (45.97)	73,811 (34.31)	21,678,929 (40.96)	15,899,516 (30.04)	31,245,658 (59.04)
A-2	1	506,067	267,931 (52.94)	238,136 (47.06)	164,310 (32.47)	33,118,661 (58.14)	27,251,972 (47.84)	23,845,377 (41.86)
A-2	2	1,339,782	651,975 (48.65)	687,987 (51.35)	328,347 (24.51)	42,439,272 (56.04)	24,433,070 (32.26)	33,289,275 (43.96)
A-3	1	535,535	264,769 (49.44)	270,766 (50.56)	154,900 (28.92)	28,549,976 (52.05)	22,560,501 (41.13)	26,305,892 (47.95)
A-3	2	629,725	334,856 (53.17)	294,869 (46.83)	205,420 (32.62)	37,078,184 (55.49)	29,742,145 (44.51)	29,098,626 (43.55)
J-1	1	688,853	361,173 (52.43)	327,680 (47.57)	195,064 (28.32)	24,495,371 (45.55)	15,793,331 (29.37)	29,281,951 (54.45)
J-1	2	771,864	415,898 (53.88)	355,966 (46.12)	228,458 (29.60)	30,278,422 (52.32)	19,731,530 (34.1)	27,589,619 (47.68)
J-2	1	822,283	453,692 (55.17)	368,591 (44.83)	260,451 (31.67)	36,336,439 (42.97)	25,483,271 (30.14)	48,222,620 (57.03)
J-2	2	816,902	416,195 (50.95)	400,707 (49.05)	227,296 (27.82)	30,090,818 (48)	19,875,133 (31.7)	32,611,092 (52)

a. Values in parentheses are percentages

IX. APPENDIX: FIGURES

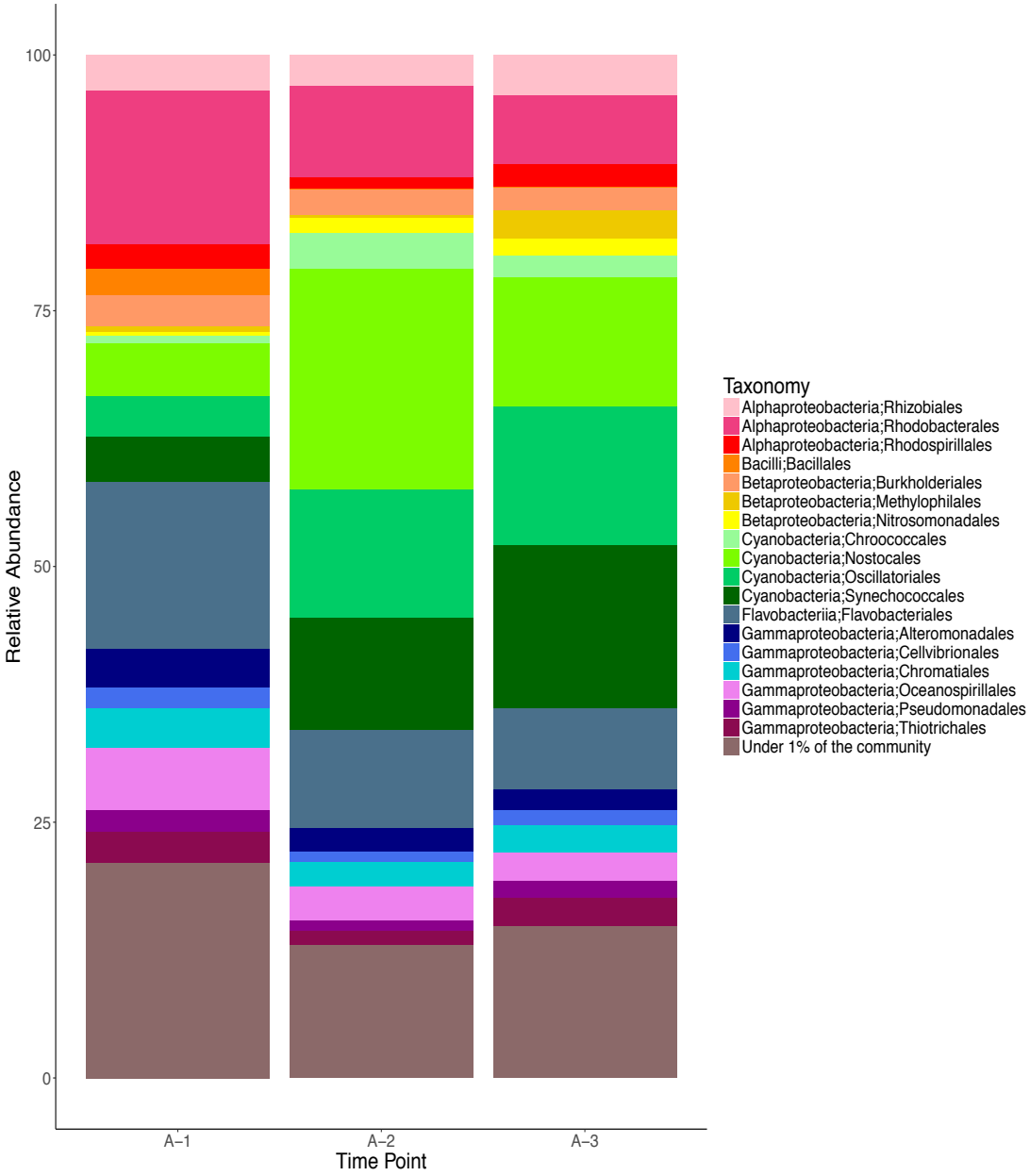

Figure 5.1. Order-level taxonomic distributions from read length corrected coding sequences in the early-processed April metatranscriptomes.

Figure 5.2. Taxonomic tree comparing log-fold change of bacterial orders between samples processed early and those processed late for three timepoints collected in April 2014.

A-1, A-2, and A-3 are the time points at which the metatranscriptomes were generated. Orange nodes represent those lineages, which are more abundant in the samples that were processed early while grey nodes represent lineages, which are more abundant in samples that were processed late. Blue Nodes are lineages for which there are zero reads at that time point. Nodes labeled are taxonomic lineages with greater than a log fold change between the two processing times. Figure 5.3 is guide tree with all of the nodes labeled.

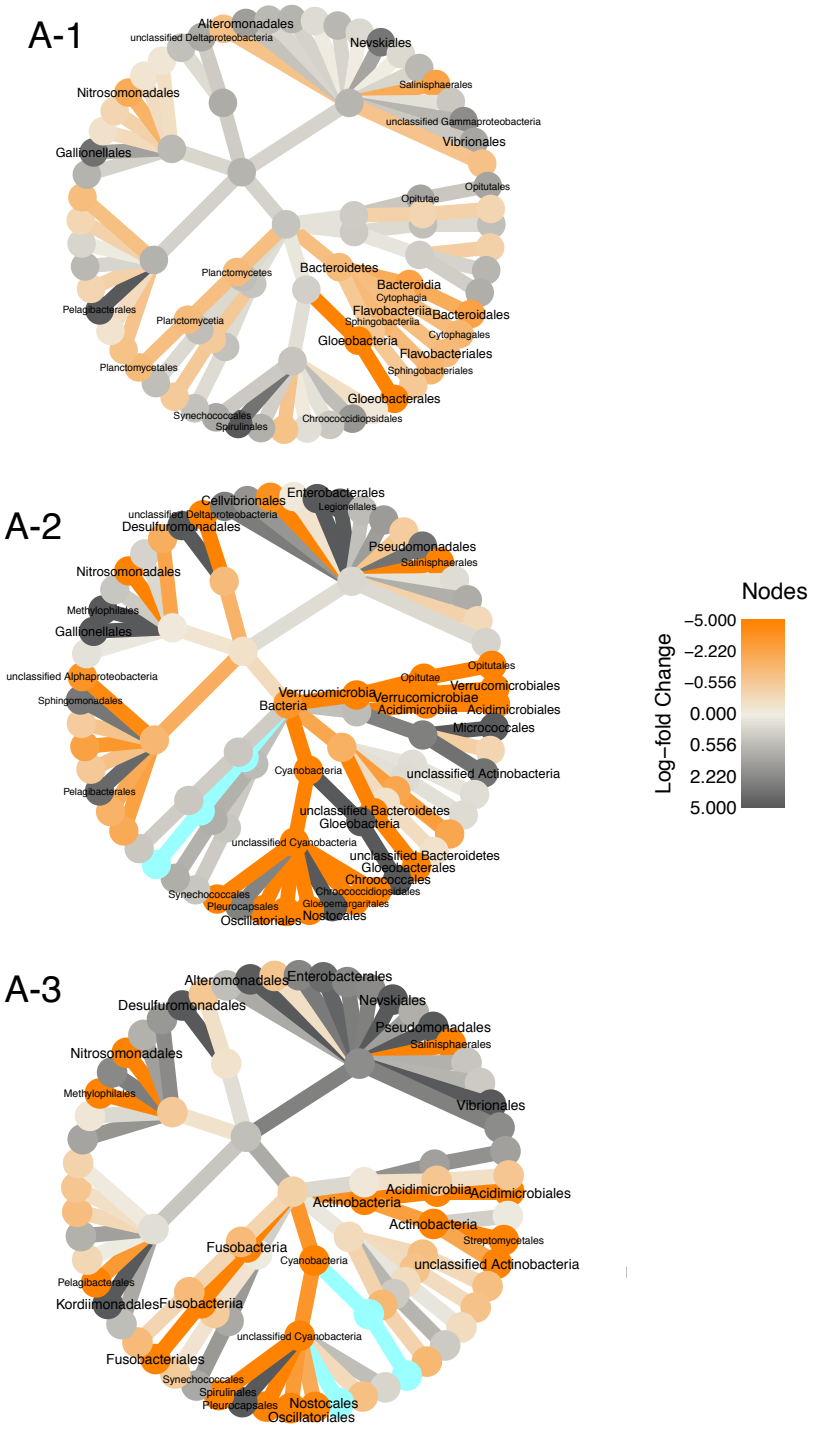

Figure 5.2. Continued

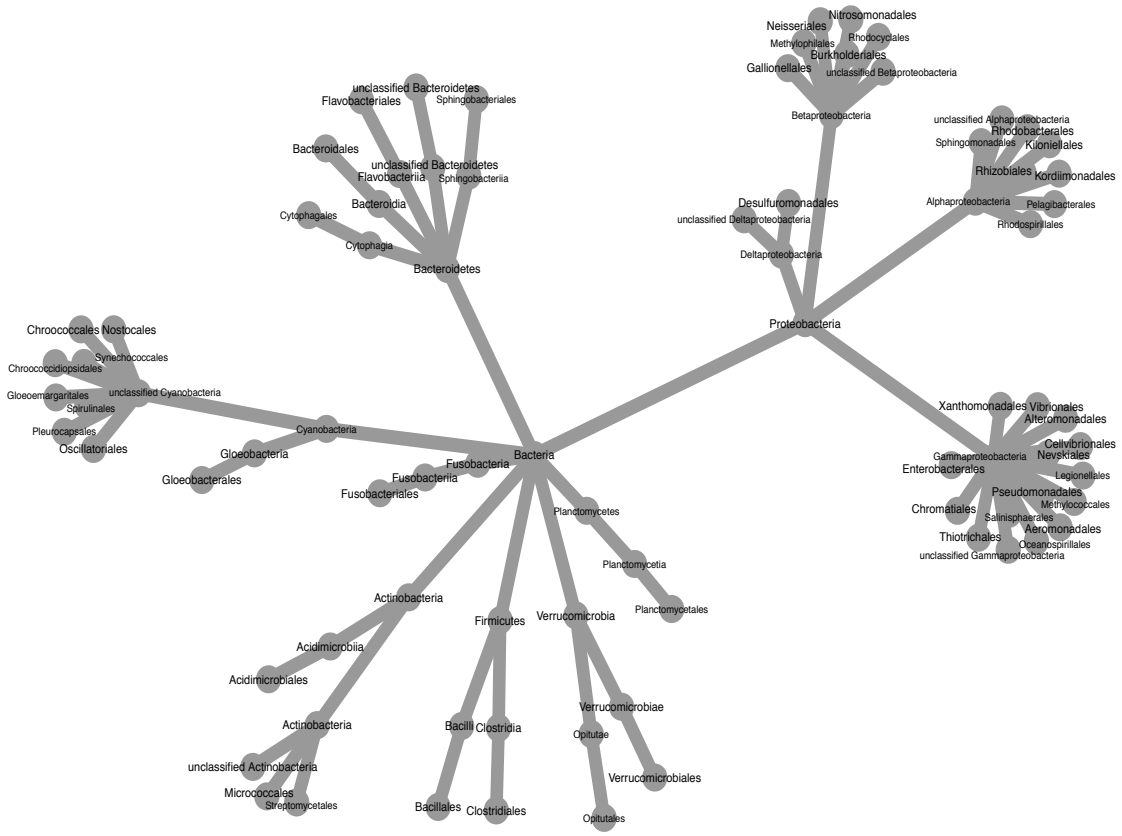

Figure 5.3. Guide tree for April metatranscriptomes with all of the nodes present in Figure 5.2 labeled.

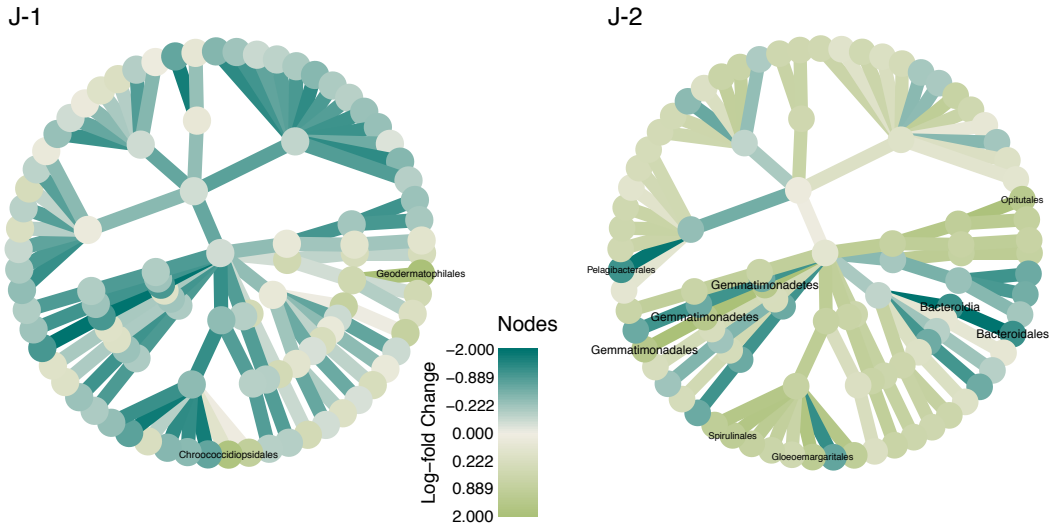

Figure 5.4:.Taxonomic tree comparing log-fold change of bacterial orders in replicates for two time points collected in July 2014.

J-1 and J-2 are the time points at which the metatranscriptomes were generated. Dark green nodes represent those lineages which are more abundant in replicate A while those in light green represent those lineages which are more abundant in replicate B. Nodes labeled are taxonomic lineages with greater than a log fold change between replicates. Figure 5.5 is guide tree with all of the nodes labeled.

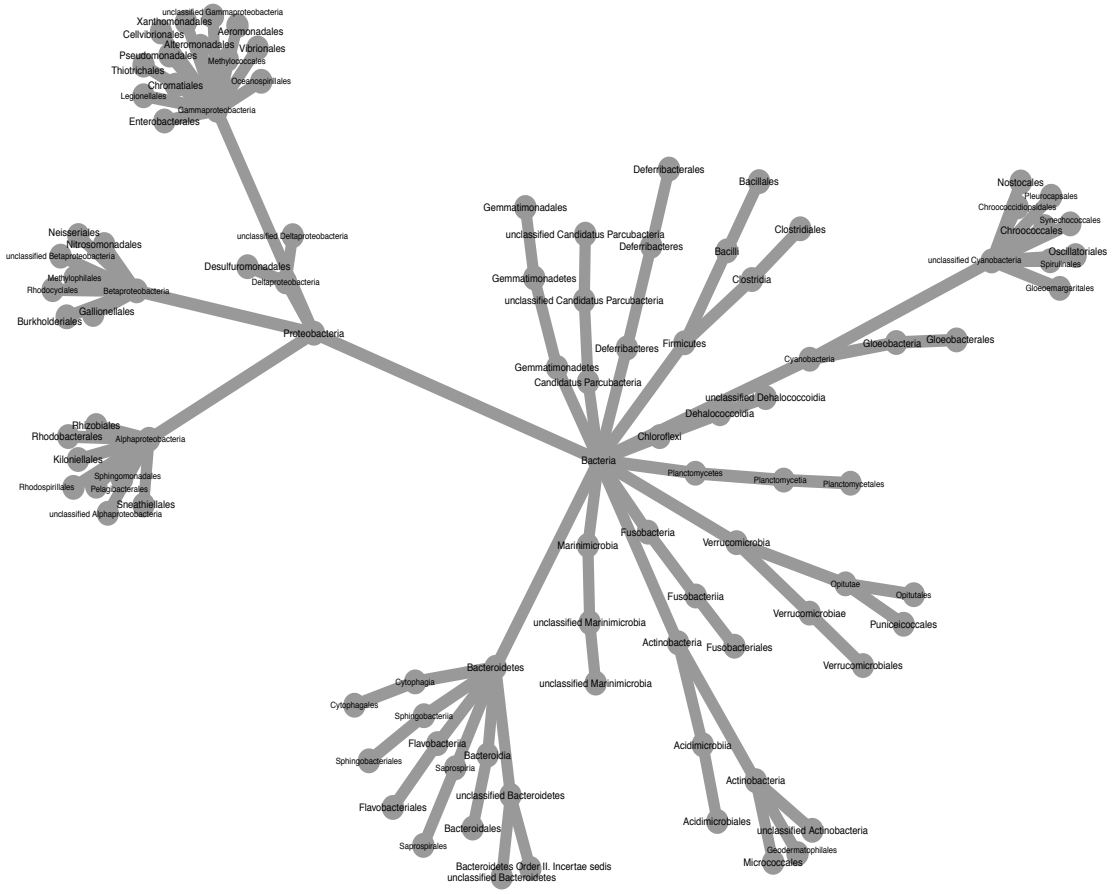

Figure 5.5. Guide tree for the July metatranscriptomes with all of the nodes present in Figure 5.4 labeled.

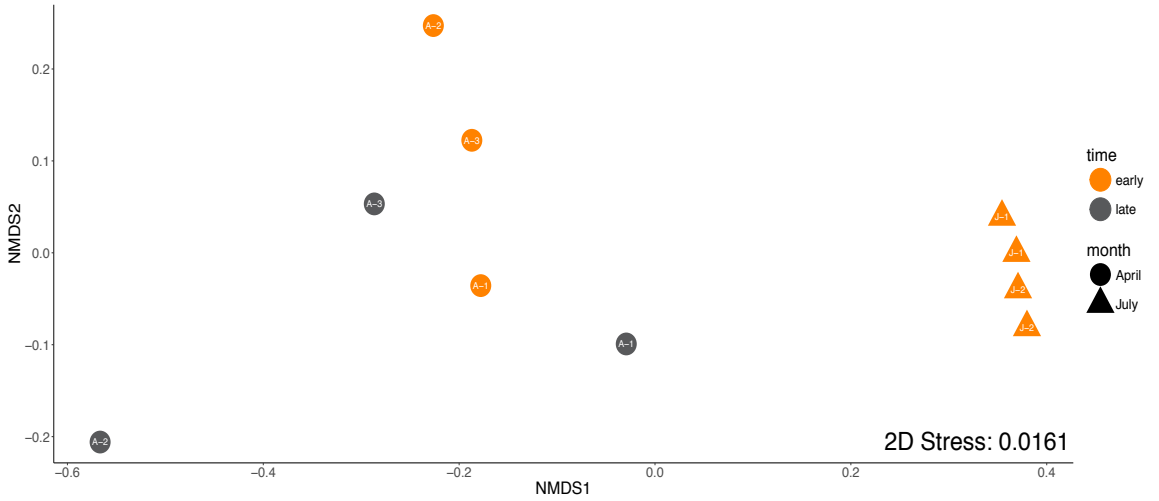

Figure 5.6. NMDS ordination of microbial community functioning as described by KEGG ontology annotation for the April and July samples.

Shape represents the month the samples were collected in. Orange shapes were processed early, while those in grey were processed late. The time point at which the metatranscriptome was collected is printed on the point.

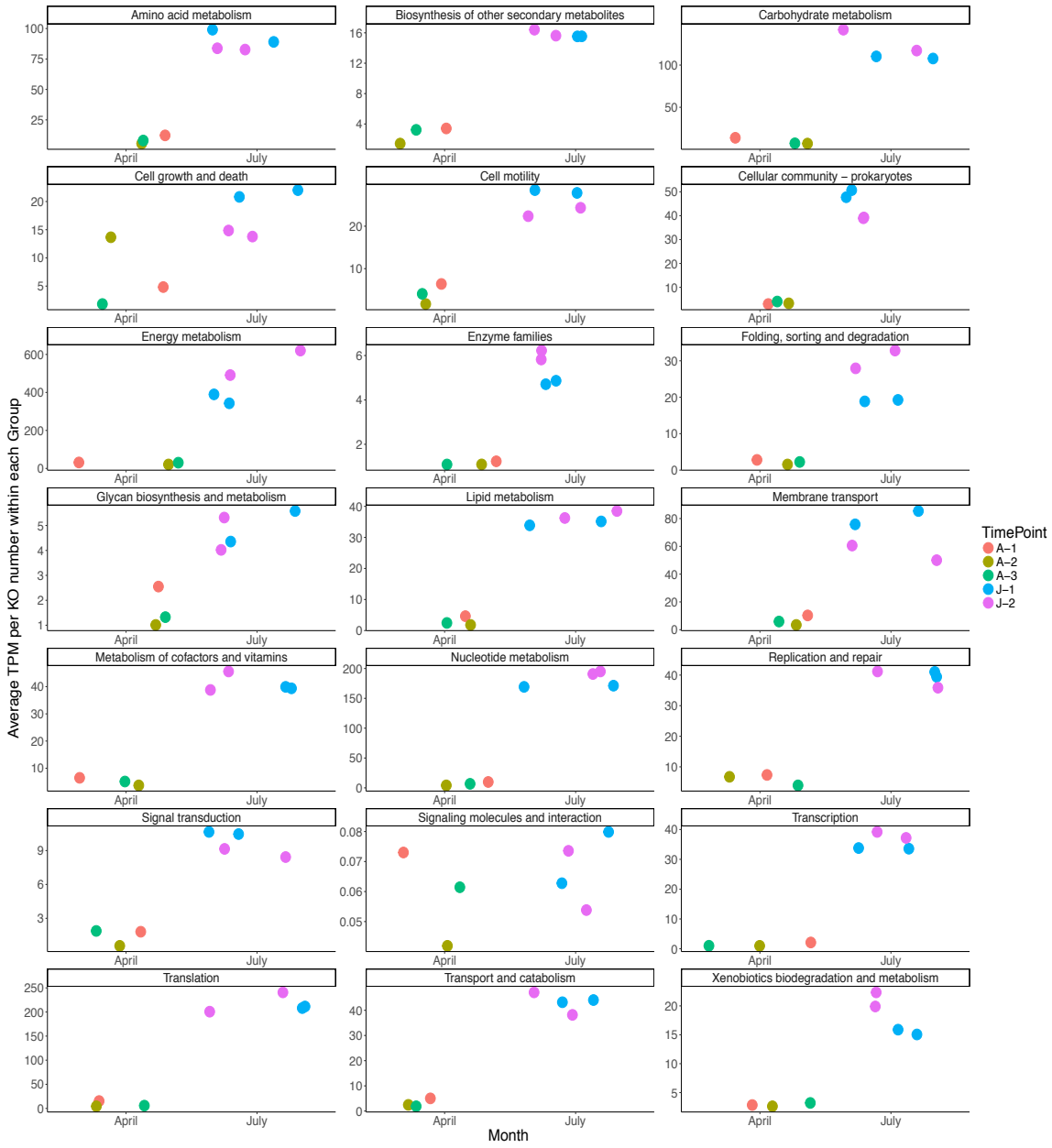

Figure 5.7. Average transcripts per million per KO number within a KEGG group for early processed metatranscriptomes.

Color represents the time point at which the metatranscriptome was collected.

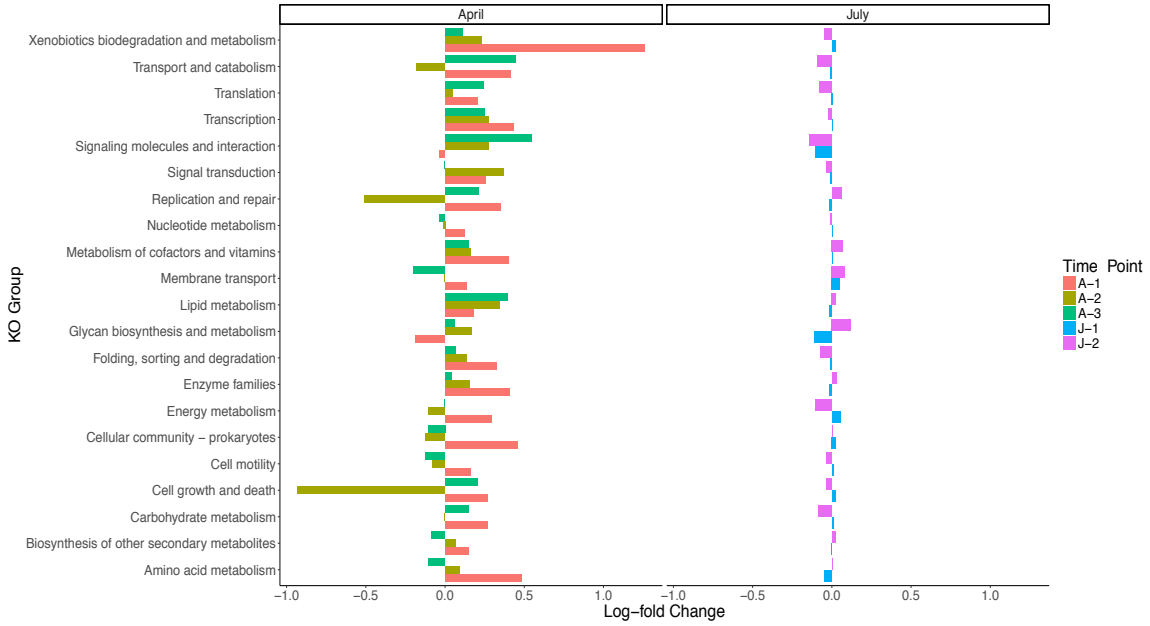

Figure 5.8. Log-fold change in the late processed samples compared to samples that were processed early as well as log-fold change for July samples that were processed at the same time.

Colors represent the time point at which the metatranscriptome was collected.

CHAPTER SIX – CONCLUSIONS AND FUTURE DIRECTIONS

Terrestrially-derived, dissolved organic matter (t-DOM) represents one of the largest pools of reduced carbon (*1*). This pool of carbon is resistant to biodegradation because it is largely comprised of fulvic and humic acids, the degradation products of vascular plant decay which are enriched in aromatic moieties (*2*, *3*). Microbial communities in the coastal margins transform t-DOM, as there are only small amounts of conservative chemical tracers for t-DOM (e.g. lignin phenols) in the open oceans (*4*). While abiotic mechanisms such as photodegradation and burial contribute to the degradation of t-DOM, biodegradation is thought to be the primary process by which t-DOM is removed from these systems (*2*). The primary goal of this dissertation was to gain a more mechanistic understanding of how coastal microbial communities degrade t-DOM, which was achieved using a combination of manipulative laboratory experiments with a natural estuarine microbial community and cultured estuarine isolates and also observational studies employing paired metagenomics and metatranscriptomics to understand how estuarine microbial communities responds to t-DOM *in situ*.

The coastal systems in which t-DOM is being degraded are typically characterized by autochthonous inputs of labile carbon from both plant biomass and phytoplankton. These systems represent transition zones where marine and riverine systems meet, and it is postulated that the estuarine microbial community is better able to degrade recalcitrant t-DOM in the presence of labile marine DOM. Interactions between organic matter of differing bioavailability, or priming effects, have been well studied in soil systems (*5*, *6*) and are receiving increased interest in aquatic ecosystems (*7*, *8*). However, priming effects in aquatic systems are not well characterized and there are inconsistencies in the literature about whether they occur or not. The first half of this dissertation uses the priming effect as a framework for investigating interactions between recalcitrant and labile organic matter to see if these interactions lead to increased biodegradation of t-DOM.

The first step to determining whether not organic matter interactions contribute to the degradation of t-DOM was to assess whether or not an estuarine community was capable of undergoing a priming effect. This experiment was performed by incubating a natural

estuarine community in the presence of a ^{14}C-enriched, recalcitrant carbon source and four treatments of labile carbon and/or nutrients and revealed that labile carbon can either enhance or repress the ability of the estuarine community to remineralize recalcitrant carbon. Bovine serum albumin (BSA) and potassium phosphate resulted in a 100% increase in recalcitrant carbon respiration, while acetate repressed respiration of recalcitrant carbon. This study provided definitive evidence that labile organic matter influences the bioavailability of recalcitrant carbon to an estuarine community. Additionally, this study demonstrated that aquatic priming effects are far more transient than those in soil systems, with priming lasting only through the first week of the incubation before the primed treatment became statistically indistinguishable from the control Many aquatic priming studies that have reported no priming effects have had sampling regimes with temporal resolution on the order of month (*9*), while studies reporting positive priming often have temporal resolution of the order of days (*10*, *11*). However, the factors that mediate the increased bioavailability of recalcitrant organic matter in the presence of labile carbon remain unknown.

Priming studies in soil suggest that the concentration and chemical structure of the labile carbon influence the ability of the microbial community to degrade recalcitrant carbon (*12*). The work described in Chapter 3 assessed if these factors are relevant in estuarine systems using single isolates and a constructed community of model marine heterotrophs from the Roseobacter clade. A fully factorial experiment employing four different concentrations of four different sources of labile organic matter with three inocula, *Sagittula stellata* E-37, *Citreicella* sp. SE45, and a constructed community of estuarine bacterial isolates was used to determine the influence of concentration and source of labile organic matter and microbial species identity on the degradation of t-DOM which was inferred through viable counts and respiration. This study demonstrated that while all inocula responded best to treatments with the highest concentration of labile carbon in the presence of t-DOM they all had unique conditions under which growth and respiration on t-DOM and labile carbon was greater than the additive effect of control treatments.

The chapters 2 and 3 of this dissertation provided evidence that estuarine microbial communities are likely better able to degrade recalcitrant carbon in the presence of labile carbon and identified factors influencing the interactive effects of two carbon sources on microbial metabolism. However, a molecular mechanism for how these interactive effects occur are still lacking and thus a next step towards identifying a molecular mechanism would be to select certain conditions and repeat them to take samples for transcriptomic characterization. Identifying the metabolic pathways upregulated during positive interactive effects would provide genetic signatures of increased t-DOM degradation. These genetic signatures could then be used to mine publicly available metagenomic and metatranscriptomic datasets generated from coastal systems and salinity chases to find hotspots of interactive effects to degrade t-DOM and the organisms responsible for them.

The last two research chapters of this dissertation leveraged community sequencing techniques to understand how microbial communities in a coastal salt marsh interact with recalcitrant t-DOM (Chapter 4) and the efficacy of metatranscriptomics (Chapter 5). Chapter 4 of this dissertation used paired metagenomes and metatranscriptomes to infer how the tidal cycle may influences the degradation of t-DOM. The salt marshes fringing the coastline of the Southeastern United States have a tidal amplitude of 2-3 m, leading to a dynamic system where the microbial community and DOM composition are more marine influenced at high tide and terrestrial or riverine influence at low tide (*13–15*). This dichotomy between high and low tide may be important in understanding the degradation of t-DOM in these systems. Ring-cleaving genes and transcripts for aromatic monomers are significantly more abundant at high tide and are mostly provided by members of the class α-Proteobacteria. The most active aromatic carbon catabolism pathway in the marsh is the benzoyl-CoA pathway. Lignin peroxidases and lytic polysaccharide monooxygenases (LPMO), which degrade cellulose and hemicellulose, were both actively expressed in the marsh community and showed temporal variation which was not statistically explained by tidal cycle. The lignin peroxidase genes and transcripts were provided exclusively by bacteria, the majority of which belonged to the phyla Actinobacteria and Proteobacteria. These data confirm earlier research which showed that

bacteria are the primary lignin degraders in these systems (*16*), but provided information on the specific pathways that may be invoked in the degradation of this material in coastal marshes. Furthermore, eukaryotes were almost exclusively responsible for the genes and transcripts of the LPMOs, suggesting that they actively degrade the carbohydrates found in association with lignin. These data demonstrate that there are functional niches for degradation of t-DOM in the marsh which are occupied by communities that are conserved at the domain level across tidal cycles.

As a whole this dissertation demonstrates that bacterial isolates and natural communities actively degrade t-DOM in both laboratory and field studies. I have shown conditions which can stimulate bacterial transformation of t-DOM and that functional niches exist within a microbial community for the degradation of t-DOM with prokaryotes responsible for lignin and aromatic monomer ring-cleavage and eukaryotes degrading carbohydrates associated with lignin. However, with the exception of Chapter 2, my dissertation does not address how the microbial community degradation influences the composition of t-DOM. A next step in understanding the degradation dynamics of t-DOM is linking the presence of functional genes and transcripts with disappearance of chemical signatures within t-DOM. This marriage of geochemistry and molecular microbial ecology is possible given both the high resolution of metatranscriptomics and Fourier transform ion cyclotron resonance mass spectrometry and will provide a more holistic understanding of recalcitrant organic matter turnover.

REFERENCES

1. J. I. Hedges, R. G. Keil, R. Benner, in *Organic Geochemistry* (1997), vol. 27, pp. 195–212.
2. N. D. Ward *et al.*, Degradation of terrestrially derived macromolecules in the Amazon River. *Nat. Geosci.* **6** (2013), doi:10.1038/ngeo1817.
3. X. Cao *et al.*, Evidence for major input of riverine organic matter into the ocean. *Org. Geochem.* **116**, 62–76 (2018).
4. C. L. Osburn *et al.*, Optical Proxies for Terrestrial Dissolved Organic Matter in Estuaries and Coastal Waters. *Front. Mar. Sci.* **2** (2016), doi:10.3389/fmars.2015.00127.
5. E. Blagodatskaya, Y. Kuzyakov, Mechanisms of real and apparent priming effects and their dependence on soil microbial biomass and community structure: Critical review. *Biol. Fertil. Soils*. **45** (2008), pp. 115–131.
6. Y. Kuzyakov, J. K. Friedel, K. Stahr, Review of mechanisms and quantification of priming effects. *Soil Biol. Biochem.* **32** (2000), pp. 1485–1498.
7. T. S. Bianchi, The role of terrestrially derived organic carbon in the coastal ocean: a changing paradigm and the priming effect. *Proc. Natl. Acad. Sci. U. S. A.* **108**, 19473–81 (2011).
8. B. Guenet, M. Danger, L. Abbadie, G. Lacroix, Priming effect: Bridging the gap between terrestrial and aquatic ecology. *Ecology*. **91**, 2850–2861 (2010).
9. N. Catalán, A. M. Kellerman, H. Peter, F. Carmona, L. J. Tranvik, Absence of a priming effect on dissolved organic carbon degradation in lake water. *Limnol. Oceanogr.* **60**, 159–168 (2015).
10. T. S. Bianchi *et al.*, Positive priming of terrestrially derived dissolved organic matter in a freshwater microcosm system. *Geophys. Res. Lett.* (2015), doi:10.1002/2015GL064765.
11. A. D. Steen, L. N. Quigley, A. Buchan, Evidence for the Priming Effect in a Planktonic Estuarine Microbial Community Andrew. *Front. Mar. Sci.* (2016), doi:10.3389/fmars.2016.00006.

12. S. Blagodatsky, E. Blagodatskaya, T. Yuyukina, Y. Kuzyakov, Model of apparent and real priming effects: Linking microbial activity with soil organic matter decomposition. *Soil Biol. Biochem.* **42**, 1275–1283 (2010).
13. R. G. Wiegart, B. J. Freeman, Tidal marshes of the southeastern Atlantic coast: a community profile. *U.S. Fish Wildl. Serv.* **85**, 1–80 (1990).
14. A. Chauhan, J. Cherrier, H. N. Williams, Impact of sideways and bottom-up control factors on bacterial community succession over a tidal cycle. *Proc. Natl. Acad. Sci.* **106**, 4301–4306 (2009).
15. M. A. Goñi, M. J. Teixeira, D. W. Perkeya, Sources and distribution of organic matter in a river-dominated estuary (Winyah Bay, SC, USA). *Estuar. Coast. Shelf Sci.* **57**, 1023–1048 (2003).
16. R. Benner, M. A. Moran, R. E. Hodson, Biogeochemical cycling of lignocellulosic carbon in marine and freshwater ecosystems: Relative contributions of procaryotes and eucaryotes. *Limnol. Oceanogr.* **31**, 89–100 (1986).

VITA

Lauren N. M. Quigley was born in Dayton, OH to Kim and Tim Mach. Growing up, Quigley's passion for science began at a young age with her love of dinosaurs and prehistoric marine reptiles. When asked what her favorite animal was she would reply, a plesiosaur, an answer that often lead to consternation on both sides; with the person asking the question not knowing what a plesiosaur was and a young Lauren in shock that people could be unaware of the magical creatures that were plesiosaurs. She also began her career as an experimentalist at a young age when she unsuccessfully attempted to watch a caterpillar metamorphose into a moth; however, she did learn in the process that she has a severe skin allergy to caterpillars.

Quigley graduated from Centerville High School in Centerville, OH in 2008, where she took every science class offered with the exception of A.P. Physics. She would later do so poorly on a physics test on projectile motion that her physics professor told Quigley that she had brought dishonor on her family, specifically her great, great, great, great, great, great grandfather, "who make speed of sound, and you do this!!". It is unclear whether or not Ernst Mach actually is Lauren Quigley's great, great, great, great, great, great grandfather. She continued undaunted by her physics professor's disappointment, and even took physical chemistry on a dare. Quigley received a B+ in physical chemistry, and she is sure Chancellor Angela Merkel who has a PhD in physical chemistry would be very proud of her accomplishment. Lauren Quigley graduated with a Bachelor of Science in Biological Sciences from the University of Notre Dame in 2012.

As an undergraduate she had the privilege of working in the Museum of Biodiversity with Ron and Barb Hellenthal. While working there, Quigley organized the museum's bird collection in phylogenetic order, and was responsible for creating a display on the history of microscopy with the museum's collection of antique microscopes, which remains on display to this day. While visiting, the museum in 2014, Quigley was afforded the privilege of holding the dome of a *Pachycephalosaurus*, her favorite dinosaur, not to be confused

with her favorite marine reptile, the plesiosaur. This experience remains the highlight of Quigley's scientific career.

Her senior year Quigley left the Museum of Biodiversity to work in the laboratory of Dr. Maria Pia Miglietta, who's research focuses on understanding the drivers of different ecotypes of the hydrozoan, *Turritopsis dohrnii*, famously dubbed the Immortal Jellyfish. Quigley's first project in Miglietta's lab was attempting to start a culture collection of the hydrozoan, which are notoriously difficult to culture even under the best conditions. Needless to say a windowless laboratory in South Bend, IN almost 1,000 miles away from the Gulf of Mexico was a non-ideal environment. Quigley spent roughly 10 hours a week attempting to pipet brine shrimp larvae into the tentacles of the anemic hydrozoan polyps. She successfully had one culture produce a single medusa, however, the attempt to begin a culture collection ultimately failed despite Quigley and Miglietta's best efforts. Additionally, Quigley performed hundreds of DNA extractions from the tissue of *Turritopsis dohrnii* in order to help elucidate whether or not a temperate ecotype with fewer tentacles than the tropical ecotype was in fact a speciation event or a result of environmental factors.

Lauren Quigley started graduate school at the University of Tennessee in January 2013, and eventually joined the lab of Alison Buchan in the summer of the same year. The work outlined in this dissertation began on June 10, 2013. For the past five years Quigley has lived her childhood dream of being a marine biologist, although five-year-old Lauren undoubtedly dreamed of studying whales and was blissfully unaware of humic acids. That being said Quigley thoroughly enjoyed her time as a PhD student in Buchan's lab during which she traveled to Savannah, GA five times to conduct field work, Atlanta, GA and New Orleans, LA for conferences, and Honolulu HI for a workshop. The past five years and 32 days as a PhD student in Buchan's lab have been invaluable in shaping Quigley as both a scientist and a person, and the products of her graduate career are available for your perusal in the previous pages.

Quigley will continue her scientific career as a postdoctoral fellow in the laboratory of Dr. Katherine Lemon at the Forsyth Institute in Cambridge, MA beginning late August – early September of 2018. There she will study the microbial interactions within the nasal microbiome that inhibit *Streptococcus pneumoniae* and *Staphylococcus aureus* infections.